CHEMICAL ENGINEERING SCIENCE
GENIE CHIMIQUE

VOL. I APRIL 1952 NO. 3

Spray drying

Theoretical considerations on the movement and evaporation of liquid droplets, the use of various drying gases, and the application of the concept of transfer units to a rational evaluation of the process

F. SJENITZER

Koninklijke/Shell-Laboratorium, Amsterdam

(Received 5 June 1951)

Summary—Some essential parts of the spray drying process are treated, *viz.*

1. The evaporation of liquid drops, both during the first period after formation when they are decelerated by air resistance, and during the second period when they fall at a constant settling rate.
2. The humidity and temperature of the drying air during the process with reference to the humidity chart.

The transfer units-concept is introduced and a rational evaluation of the spray drying process is suggested.

Zusammenfassung—Es werden einige essentielle Teile der Zerstäubungstrocknung besprochen und zwar:

1. Die Verdampfung von Tropfen, sowohl während der ersten Periode nach ihrer Formierung, wenn sie durch Luftwiderstand gehemmt werden, als in der zweiten Periode wenn sie mit konstanter Endgeschwindigkeit fallen.
2. Feuchtigkeitsgrad und Temperatur der Trocknungsluft während des Prozesses in bezug auf das Feuchtigkeitsdiagramm.

Der Begriff der "transfer units" wird eingeführt und eine rationelle Methode zur Beurteilung der Zerstäubungstrocknung wird vorgeschlagen.

1. Introduction

The object of spray drying is to recover a solid material, dissolved or suspended in a liquid, from this liquid in the form of a dry powder, without damaging it thermically during the operation. This entails that the operation in general is of short duration (a few seconds) and that it must be carried out at moderate temperatures.

The process as such consists in the contacting of a dry, hot gas with drops produced by atomization from the solution or suspension in a thermally insulated space, the drying chamber. During the contacting the liquid of the drops evaporates, while the gas becomes moister and colder. The mixture leaving the drying chamber consists of a powder and a gas, which are separated by means of a cyclone and/or filters. The contacting process of drops and gas is often carried out under concurrent conditions.

There are many aspects to the spray drying process. The following subjects will not be treated in the present article: the air heater; the drying chamber; the droplet-formation; the dropsize-distribution; a comparison with other drying processes; economical considerations.

We shall, however, contribute some theoretical views on some of the essential parts of the spray drying process.

These refer to the evaporation process of the drops in moving air. Primarily it is shown that there is a marked correlation between the heat and material transfer in the gas phase. A calculation can be made of the evaporation of the drop, both during the first period after formation when the drop is decelerated and during the second period when the drop falls at a constant rate.

Further, the change in condition of the gas during the process will be discussed with reference to the humidity chart. As in practice the liquid to be evaporated is very often water and the gas used is air several of the formulas given and of the conclusions arrived at apply to this combination.

2. The Evaporation of a Drop of Liquid in Air

The simplest case is that of a spherical drop of pure liquid of diameter D and temperature T in stationary air. The vapour tension of the liquid is $P(T)$, the partial vapour tension in the air, p, being smaller than $P(T)$.

As the vapour concentration at the surface of the sphere is higher than in the air atmosphere, there is molecular diffusion of vapour molecules outwards*. LANGMUIR [1] calculated the total diffusion current for this case, *viz.*

$$N = 2\pi D D_v \frac{\Delta p}{R T} \frac{\text{kmol}}{\text{sec}} . \qquad (1)$$

A more general problem is that of a drop which travels through the air at a certain velocity v. Vapour removal will then be promoted, because the vapour molecules only have to diffuse through a thin film of air round the drop.

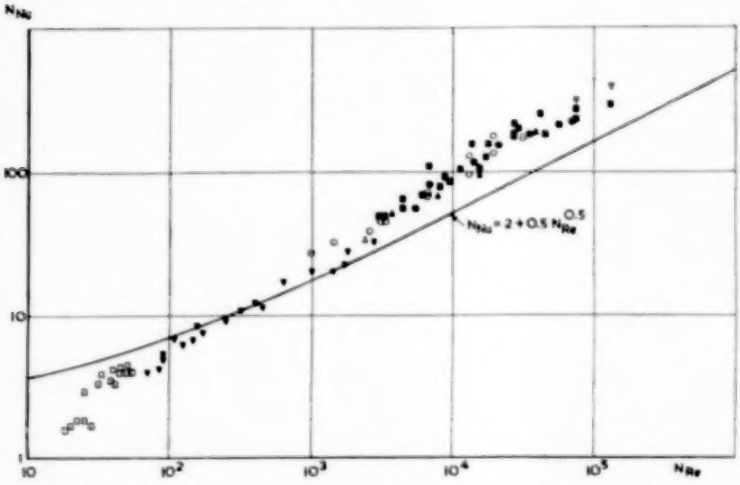

Fig. 1. Exp. data for heat transfer from air to spheres. Source: MCADAMS' "Heat Transmission." Theoretical line, derived from FRÖSSLING's data.

According to FRÖSSLING [2] the following empirical equation is valid for the evaporation of drops in moving air.

$$N = 2\pi D D_v \frac{\Delta p}{R T} \left(1 + 0{\cdot}276\, N_{Re}^{0.5}\, N_{Sc}^{0.33}\right) \frac{\text{kmol}}{\text{sec}} . \qquad (2)$$

FRÖSSLING used nitrobenzene, aniline, water and naphthalene (solid). The diameter of the drops was 0·2–2 mm, the relative air velocity 0 to 7 m/sec.

In eq. (2) N_{Re} represents the influence of the velocity on the condition of flow round the sphere, hence on the thickness of the film. SCHMIDT's number gives the influence of diffusion in the same way as does PRANDTL's number in the analogous problem of heat transfer.

Hence an additional justification of eq. (2) for the evaporation of a drop moving in air may be found by comparison with data on heat transfer to spheres.

* The case of natural convection was treated by P., MEYER; Trans. Inst. Chem. Eng. 1937 **15** 127.

In MCADAMS [3] these data are correlated as the relation between the dimensionless numbers of NUSSELT and REYNOLDS:

$$N_{Nu} = \frac{h D}{k_h} = f\left(\frac{v D \varrho}{\mu}\right) . \qquad (3)$$

FRÖSSLING's evaporation equation

$$N = 2\pi D D_v \frac{\Delta p}{R T} \left[1 + 0{\cdot}276\, N_{Re}^{0.5}\, N_{Sc}^{0.33}\right] \frac{\text{kmol}}{\text{sec}} \qquad (2)$$

can be replaced by the corresponding equation for heat transfer:

$$\frac{dW}{dt} = 2\pi D k_h \Delta T \left[1 + 0{\cdot}276\, N_{Re}^{0.5}\, N_{Pr}^{0.33}\right] \frac{\text{J}}{\text{sec}} . \qquad (4)$$

NUSSELT's number can be derived from (4). When at the same time the Pr-value for air is substituted the result is:

$$N_{Nu} = \frac{h D}{k_h} = 2\left[1 + 0{\cdot}25\, N_{Re}^{0.5}\right] . \qquad (5)$$

Eq. (5) is in good agreement with WILLIAMS' graph in MCADAMS' book mentioned above (Fig. 1). This proves the reliability of FRÖSSLING's equation.

For the case of evaporating drops of water in atmospheric air eq. (2) gives on substitution of the following values:

$$\left.\begin{aligned} &D_v = 3{\cdot}0 \,.\, 10^{-5}\ \text{m}^2/\text{sec}, \quad N_{Sc} = 0{\cdot}60, \\ &\varrho_G = 1{\cdot}28\ \text{kg/m}^3, \qquad M = 18 \\ &\text{and} \\ &\frac{\Delta p}{R T} = \Delta C_W \cong \Delta H \,.\, \frac{\varrho_G}{M} = \frac{\Delta H}{14{\cdot}1} \\ &\text{with } H^{\dagger} \text{ in } \frac{\text{kg H}_2\text{O}}{\text{kg dry air}} : \\ &N = 2\pi \,.\, 3{\cdot}0 \,.\, 10^{-5} D \frac{\Delta H}{14{\cdot}1} \times \\ &\qquad \times \left[1 + 0{\cdot}276\, N_{Re}^{0.5} \,.\, 0{\cdot}843\right] \frac{\text{kmol}}{\text{sec}} . \end{aligned}\right\} \qquad (6)$$

By multiplication by the molecular weight of water, $M = 18$:

$$L = 2{\cdot}4 \,.\, 10^{-4} D \Delta H \left[1 + 0{\cdot}23\, N_{Re}^{0.5}\right] \text{kg/sec} . \qquad (7)$$

Fractional evaporation follows from this by division by the weight of a drop, $W = \frac{\pi}{6} D^3 \,.\, 1000$.

$$\frac{dx_w}{dt} = 4{\cdot}6 \,.\, 10^{-7} \frac{\Delta H}{D^2} \left[1 + 0{\cdot}23\, N_{Re}^{0.5}\right] \text{sec}^{-1} . \qquad (8)$$

Though in a spray drying plant the movement of the drops is, admittedly, highly complicated and difficult to express in formulas, the *braking* of the high

† $H = 0{\cdot}001$ about corresponds to 1·2 mm Hg partial water vapour pressure.

VOL. 1 1952

initial velocity and then the *free fall* in relation to the moving air are two of its essential elements. Therefore, while bearing in mind this schematic picture we will

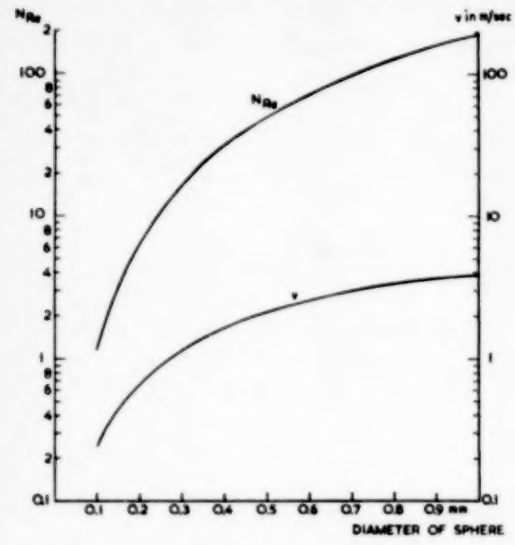

Fig. 2. Constant settling velocity and *Re*-Number of free falling water drop in air. $\varrho_{drop} = 1000$ kg/m³, $\varrho_{air} = 1$ kg/m³, $\mu_{air} = 2{\cdot}1 \cdot 10^{-5}$ kg/msec, $t = 83°$ C.

now deal with the evaporation of a drop during these two stages.

3. The Free Falling Drop of Liquid

We apply the equation found above (8) to a falling drop of water that has reached its final velocity v in air. This velocity greatly depends on its diameter (see Fig. 2).

The fractional evaporation per metre length of fall (relative to the air) follows by division by the relative velocity $= v$:

$$\left.\begin{aligned}\frac{dx_w}{dl} &= 4{\cdot}6 \times \\ &\times 10^{-7}\,\frac{\Delta H}{v D^2}\left[1 + 0{\cdot}23\,N_{Re}^{0{\cdot}5}\right].\end{aligned}\right\} \quad (9)$$

To apply eq. (9) at a given diameter D one has to find the corresponding values of v and N_{Re} and then substitute them in (9) at a certain value of ΔH, which follows from the temperature of the drop and the humidity of the air. In Fig. 3 the fractional evaporation for drop diameters between 1 and 0·1 mm is plotted at $\Delta H = 0{\cdot}06$. This ΔH is reached, for instance, in the case of water drops in dry air of 193° C, the water of its own accord assuming the wet bulb temperature of 43° C. This is further explained in section 7.

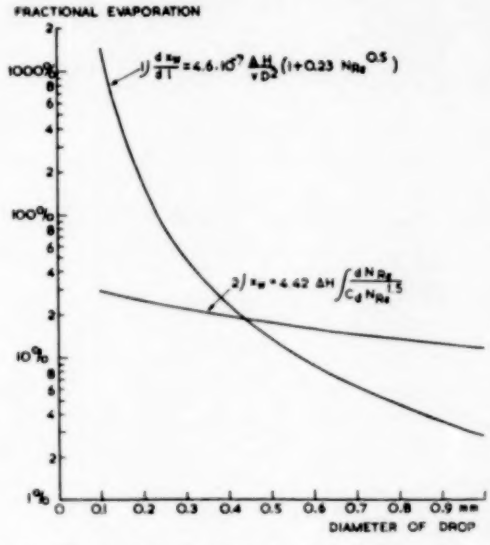

Fig. 3. Theoretical equations for fractional evaporation of water drops in air. 1) Free falling drop (per metre) $\Delta H = 0{\cdot}06$; 2) Brake-evaporation (total) $\Delta H = 0{\cdot}06$.

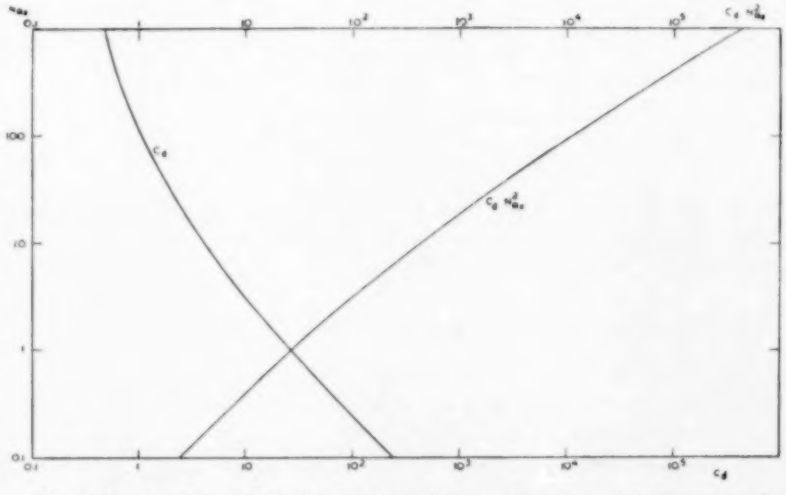

Fig. 4. Exper. values of the drag coefficient C_d as a function of the Reynolds' number N_{Re}, for spheres in a fluid.

Calculation of the constant settling speed of a falling sphere (compare Perry [4])

The resistance to the motion of a sphere in a fluid can be expressed as a dimensionless drag coefficient C_d, which is plotted against the Reynolds number (see Fig. 4). The drag coefficient C_d is defined by

$$F = C_d \cdot \pi \left(\frac{D}{2}\right)^2 \cdot \frac{1}{2}\,\varrho\, v^2. \quad (10)$$

For falling spheres also

$$F = g \frac{\pi}{6} D^3 (\varrho_s - \varrho). \tag{11}$$

For constant settling velocity, (10) is equal to (11), so

$$v^2 = \frac{4 g D(\varrho_s - \varrho)}{3 \varrho C_d},$$

or

$$C_d N_{Re}^2 = \frac{4 g D^3 \varrho(\varrho_s - \varrho)}{3 \mu^2}. \tag{12}$$

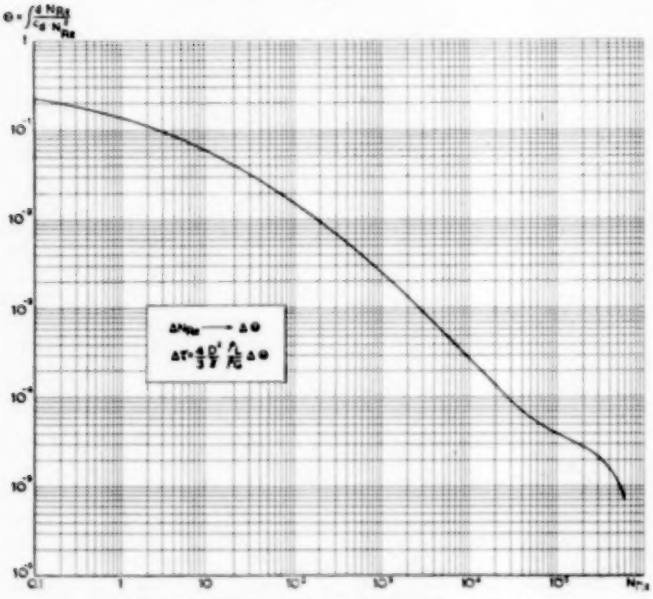

Fig. 5. Moving sphere, braked by a fluid. Graphical determination of reduced time Θ.

In Fig. 4, $C_d N_{Re}^2$ is plotted as a function of N_{Re}. For a given sphere, by eq. (12) we can calculate $C_d N_{Re}^2$. From Fig. 4 we find $N_{Re} = v D \varrho/\mu$, so v can be determined.

4. The Braked Drop of Liquid

Before the drops in a spray drying plant have reached their final velocity (discussed above) they have often had a much higher initial velocity. This happens, for instance with the much-used rotary disc atomizer, where the drops leave the disc at a very high horizontal velocity (say 150 m/sec). The drops are very soon slowed down by the air, but this is accompanied by considerable evaporation.

(a) *Path of the drop*

A precise method is now given for calculating the braking distance and braking time for any drop in any medium in any velocity interval.

A sphere is shot into a gas or liquid at a certain initial velocity. If the influence of gravity is left out of account, the velocity is braked by the fluid. If the final speed is given, calculation of the distance covered as well as of the braking time is required.

In retarded motion the kinetic energy of the sphere is partly consumed to overcome the resistance. This is expressed by the equation:

$$-\frac{d}{d\tau}\left(\frac{1}{2} m v^2\right) = F v \quad \text{or} \quad -m \frac{dv}{d\tau} = F. \tag{13}$$

Now

$$F = C_d \cdot \frac{1}{2} \varrho_G v^2 \cdot \frac{\pi}{4} D^2 \quad \text{and} \quad m = \frac{\pi}{6} D^3 \cdot \varrho_L.$$

Therefore:

$$\frac{1}{3} D^3 \cdot \varrho_L \frac{dv}{d\tau} = \frac{1}{4} \cdot C_d \cdot \varrho_G \cdot v^2 \cdot D^2. \tag{14}$$

Now introduce a dimensionless velocity and time:

$$N_{Re} = \frac{D \cdot v}{\nu} \quad \text{and} \quad \Theta = \frac{\tau}{\frac{4}{3}\frac{\varrho_L}{\varrho_G} \cdot \frac{D^2}{\nu}}.$$

Then the eq. (14) reduces to:

$$d\Theta = -\frac{d N_{Re}}{C_d \cdot N_{Re}^2}. \tag{15}$$

The time $\Delta\tau$ which elapses when the drop is slowed down from the velocity v_1 to v_2, *i.e.* for a change of *Re*-number from $(N_{Re})_1$ to $(N_{Re})_2$, is:

$$\Delta\tau = \frac{4}{3}\frac{\varrho_L}{\varrho_G} \cdot \frac{D^2}{\nu} \int_1^2 d\Theta = \frac{4}{3}\frac{\varrho_L}{\varrho_G} \cdot \frac{D^2}{\nu} \int_{(N_{Re})_2}^{(N_{Re})_1} \frac{d N_{Re}}{C_d \cdot N_{Re}^2}. \tag{16}$$

We call $\int d\Theta = \int \frac{d N_{Re}}{C_d \cdot N_{Re}^2}$ the reduced time Θ. It is plotted in Fig. 5.

The distance Δl covered during this time $\Delta\tau$ is given by:

$$\Delta l = \int_1^2 v \cdot d\tau.$$

We again introduce N_{Re} and Θ. Then:

$$\Delta l = \frac{4}{3} D \frac{\varrho_L}{\varrho_G} \int_1^2 N_{Re} \cdot d\Theta = \frac{4}{3} \cdot D \cdot \frac{\varrho_L}{\varrho_G} \cdot \int_{(N_{Re})_2}^{(N_{Re})_1} \frac{d N_{Re}}{C_d \cdot N_{Re}}. \tag{17}$$

We call $\int N_{Re} d\Theta = \int \frac{d N_{Re}}{C_d \cdot N_{Re}}$ the reduced distance σ. It is plotted in Fig. 6.

Special cases:

(a) *Case of* Newtons *law*, $C_d \cong 0{\cdot}44$, obtaining for $700 < N_{Re} < 200000$.

It is easy to calculate from eq. (16) and (17) that for this case

$$\Delta\tau = 3{\cdot}02 \frac{\varrho_L}{\varrho_G} D \left[\frac{1}{v_2} - \frac{1}{v_1}\right] \tag{18}$$

VOL. 1 1952

and

$$\Delta l = 3{\cdot}02\,\frac{\varrho_L}{\varrho_G}\,D \ln\left(\frac{v_1}{v_2}\right). \qquad (19)$$

(b) *Case of* STOKES' *law*, $C_d = 24/N_{Re}$, for $N_{Re} < 1\frac{1}{2}$.

For this case we find in a similar way from eq. (16) and (17):

$$\Delta\tau = 0{\cdot}0555\,\frac{D^2}{\nu}\,\frac{\varrho_L}{\varrho_G}\,[\ln v_1 - \ln v_2] \qquad (20)$$

and

$$\Delta l = 0{\cdot}0555\,\frac{D^2}{\nu}\,\frac{\varrho_L}{\varrho_G}\,[v_1 - v_2]. \qquad (21)$$

Example of the use of graphs 5 and 6 to determine the braking time and braking distance

Let us suppose that a drop of water with an initial velocity of 67 m/sec is braked by the air to a final velocity of 5 m/sec. The diameter of the drop is 100 μ. The densities of water and air are related as $\varrho_L/\varrho_G = 800$. The kinematic viscosity of air is $\nu = 1{\cdot}5 \,.\, 10^{-5}$ m²/sec.

We first calculate the initial and final values of

$$N_{Re} = \frac{D}{\nu} \,.\, v \quad \text{and find} \quad N_{Re_1} = 446 \quad \text{and} \quad N_{Re_2} = 33.$$

In graph Fig. 5 we find $\Delta\Theta = 0{\cdot}031 - 0{\cdot}005 = 0{\cdot}026$. Therefore

$$\Delta\tau = \frac{4}{3} \,.\, \frac{D^2}{\nu} \,.\, \frac{\varrho_L}{\varrho_G}\,\Delta\Theta = 0{\cdot}0185\,\text{sec}.$$

In graph Fig. 6 we find $\Delta\sigma = 33{\cdot}7 - 30{\cdot}3 = 3{\cdot}4$. Therefore

$$\Delta l = \frac{4}{3} \,.\, D \,.\, \frac{\varrho_L}{\varrho_G}\,\Delta\sigma = 0{\cdot}36\,\text{m}.$$

LAPPLE and SHEPHERD [5] give extensive calculations for four cases:

1. Two-dimensional motion in a gravitational field.
2. One-dimensional motion in absence of a gravitational field.
3. One-dimensional motion in the presence of a gravitational field.
4. Two-dimensional motion in a centrifugal field.

Of these, No. 2 partially covers the above-described case: the braking time integral (16) Fig. 5 is found, the braking distance integral (17) Fig. 6, is not, however.

(b) *The evaporation of the drop*

When a drop is shot into a gas at a high initial speed considerable evaporation takes place before this movement is entirely braked. It was discussed above how this braked movement exactly proceeds. With the aid of the equations developed and with FRÖSSLINGs evaporation equation it is possible to calculate this evaporation during braking. FRÖSSLINGs equation reads:

$$N = 2\pi\,D\,D_v\,\frac{\Delta p}{R\,T}\left(1 + 0{\cdot}276\,N_{Re}^{0{\cdot}5}\,N_{Sc}^{0{\cdot}33}\right)\frac{\text{kmol}}{\text{sec}}. \qquad (2)$$

In this equation the second term represents the extra evaporation because of the movement of the drop. Take D tp be constant.

Then the extra evaporation during the braking period is given by:

$$E_e = 2\pi\,D\,D_v\,\frac{\Delta p}{R\,T} \,.\, 0{\cdot}276\,N_{Sc}^{0{\cdot}33} \int_1^2 N_{Re}^{0{\cdot}5}\,d\tau. \qquad (22)$$

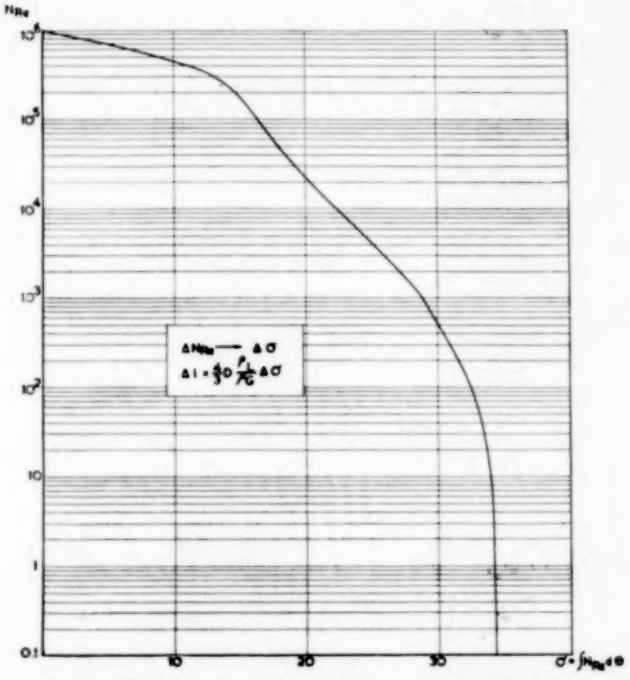

Fig. 6. Moving sphere, braked by a fluid. Graphical determination of reduced distance σ.

We again introduce the reduced time Θ. Then, using (15):

$$E_e = 0{\cdot}276 \,.\, \frac{8\pi}{3}\,D^3\,\frac{\varrho_L}{\varrho_G} \,.\, \frac{D_v}{\nu} \,.\, \frac{\Delta p}{R\,T} \,.\, N_{Sc}^{0{\cdot}33} \int_{(N_{Re})_2}^{(N_{Re})_1} \frac{d\,N_{Re}}{C_d \,.\, N_{Re}^{1{\cdot}5}}. \qquad (23)$$

The fractional evaporation is found by dividing

E_e by $\frac{\pi}{6}\,D^3\,\frac{\varrho_L}{M}$, and as $\frac{\Delta p}{R\,T} \cong \Delta H \,.\, \frac{\varrho_G}{M}$, so

$$x_w = 4{\cdot}42\,\Delta H \,.\, N_{Sc}^{-0{\cdot}67} \int_{(N_{Re})_2}^{(N_{Re})_1} \frac{d\,N_{Re}}{C_d \,.\, N_{Re}^{1{\cdot}5}}. \qquad (24)$$

It may be noted that the fractional evaporation is independent of the drop diameter and that, except for some material constants, it only depends on the initial and the final Re-number of the drop. For high initial Re-numbers the braking evaporation only depends on the final Re-numbers, as shown in Fig. 7. If the constant settling speed of the liquid sphere is taken as

an obvious final velocity of the braking by air, the final Re-number depends on the diameter of the sphere, as shown in Fig. 2. In Fig. 3 the total evaporation for this case is shown, calculated with eq. (24) and Fig. 7. It was assumed that the drop diameter is constant—so this applies when the fractional evaporation is small, *e.g.* because ΔH is small.

If, however, the diameter may not be assumed to be constant, the braked movement is different and the

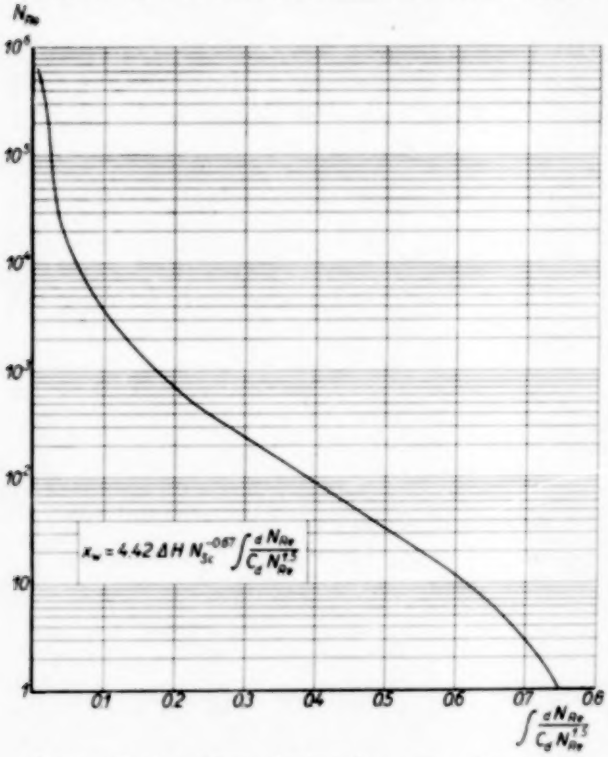

Fig. 7. Moving sphere, braked by a gas. Graphical determination of the extra evaporation.

extra evaporation must be ascertained step by step; with decreasing diameter it will become smaller than indicated by eq. (24).

This is evident, as eq. (24) indicates the fractional evaporation at every moment as referred to the drop mass if the diameter should not decrease after that moment. In reality the diameter does decrease, so the velocity decreases more rapidly than is indicated in eq. (14). So the *time* of evaporation becomes shorter than when the diameter is constant. Moreover, a smaller *area* is then available for evaporation than when the diameter is constant. Since the two factors, time and area, are smaller, the total evaporation as referred to the original weight of the drop, will be smaller than when the diameter is constant.

5. Some Conclusions from the Equations found for the free Falling and Braked Drop of Liquid

We shall draw some conclusions from the equations, as these apply in the first place to the evaporation of pure water.

Fig. 3 shows the fractional evaporation as a function of the drop diameter. The fractional evaporation per metre of height of fall greatly decreases with increasing diameter.

1. This means that even a comparatively slight inhomogeneity of drop sizes immediately results in the smaller drops drying too rapidly (with the chance of scorching) or the larger drops too slowly (with the chance of too great water content).

2. Another conclusion drawn from this curve is that moderate reduction of the drop size causes a great acceleration of the fractional evaporation, for which a much smaller height of fall is required. When, for instance, the required drop diameter is reduced from 0·9 to 0·4 mm the fractional evaporation rate is increased from 3·6 to 24%, so that the height of fall can also be decreased far below its original value.

3. It also follows from eq. (9), which describes the curve concerned, that for constant diameter drops the fractional evaporation is approximately in inverse ratio to the constant settling velocity when N_{Re} is small. Here the special advantage of *hollow* drops in the process becomes evident (moreover, a product consisting of hollow drops often has great advantages as regards easy solubility and slight bulk density). For instance, suppose that only a third of the volume of a hollow drop consists of a fluid, two thirds being gas. The rate of fall will then be about three times as low as in the case of a solid sphere of the same diameter. Moreover, evaporation on a weight basis will be equal, therefore on a fractional basis three times more rapid than in the case of a solid sphere of liquid at the same rate of fall. Therefore the "fractional" evaporation per metre of height of fall is about $3 \cdot 3 = 9$ times as great.

Fig. 7 shows, that the fractional evaporation during the total braking period is independent of the initial velocity (provided the latter is high) but is a function of the final Reynolds-number only.

From Fig. 3 the following conclusions can be drawn:

1. With small drops the "braking evaporation" is insignificant in comparison with free falling evaporation, but with larger drops the braking evaporation must certainly be taken into account. For instance, in

VOL. 1 1952

the case of a drop of 0·8 mm diameter the fractional evaporation per metre is 4·6%, the total braking evaporation being 13·6%, so the braking evaporation is here equivalent to 3 m free fall (of course, a certain distance is covered in braking evaporation—but this may be mainly horizontal, as with a rotary disc atomizer).

2. The fact that the braking evaporation is independent of the initial velocity (provided the latter is high as referred to the final velocity) has as its consequence that there is little point in choosing too rapid an initial velocity as, though this considerably increases the braking distance, it has little or no effect on the braking evaporation. Of course, it remains possible that the initial velocity should be very high for some other reason, for instance to increase the capacity of the atomizer or to obtain a suitable drop diameter.

6. The Source of the Evaporation Heat of the Drops

In theory, evaporation heat can be derived from three sources:

1. heat content of the drop,

2. radiation heat from the wall of the drying chamber,

3. sensible heat of the air.

Re 1—In the case of water the first source plays a minor part as its evaporation heat is very high (about 2250 kJ/kg) as compared with the heat content (specific heat is about 4·2 kJ/kg °C).

Re 2—In a technical plant radiation scarcely makes itself felt, as every drop is surrounded by others having about the same surface temperature. In a narrow tube this does not apply, however, and allowance can be made for this influence. It is not very great; for instance, for a 100% radiating wall of 227° C we find for water drops of 0·6 mm in air, also of 227° C, that the heat transfer is increased by about 4% by radiation effects. As the influence of radiation is so small, we shall now neglect this effect in our calculations.

Re 3—In practice, therefore, evaporation heat is derived from the sensible heat of the air, which is only transferred to the drop when this has obtained a sufficiently high difference of temperature from that of the surrounding air, by self-cooling. This self-cooling automatically adjusts itself in such a way that the difference in temperature becomes just sufficiently large to provide the necessary evaporation heat by heat flow to the drop, which is the result of molecular heat conduction through the air film round the drop. This means, therefore, that when air of a certain temperature and humidity is placed in contact with a drop of liquid, the latter will very rapidly assume a certain temperature (wet bulb temperature), which generally depends on the liquid chosen, the humidity and temperature of the air.

The air at the surface of the liquid is saturated, so here the air point is on the saturation curve. The accompanying temperature can be determined as follows, see Fig. 8. The heat flowing towards the surface of the drop must be = (liquid molecules diffusing away) × (evaporation heat):

$$A\,h\,\Delta t = A\,k_m\,\Delta H\,\lambda \quad \text{or} \quad \frac{\Delta H}{\Delta t} = \frac{h}{k_m\,\lambda}. \qquad (25)$$

On the other hand one can write an eq. (26) for the adiabatic cooling line as the condition that loss of sensible heat of air = evaporation heat of absorbed liquid vapour (both as referred to 1 kg dry air):

$$C_p\,dt = \lambda\,.\,dH \quad \text{or} \quad = \quad \frac{dH}{dt} = \frac{C_p}{\lambda}. \qquad (26)$$

$\frac{\Delta H}{\Delta t}$ and $\frac{dH}{dt}$ are equal when the "psychrometric ratio"

$$\frac{h}{C_p\,.\,k_m} = 1 \qquad (27)$$

and, according to Lewis [6], this happens to be the case almost exactly with air and water. This means that for this combination the wet bulb point is found from a certain air point L by passing along the adiabatic line until the saturation line is intersected. During the whole period of evaporation the wet bulb temperature remains practically constant, and equal to the adiabatic saturation temperature. For other liquid/gas combinations this simple method cannot be applied. For these it is necessary to determine separately the wet bulb point and the adiabatic saturation temperature, with the aid of eq. (25) and (26) respectively. Moreover, upon further wetting of the gas, the wet bulb point *changes* in the direction of the adiabatic saturation temperature, with which it eventually coincides.

Reverting to the water/air combination, it may be observed that the identity of (25) and (26) applies, independent of the value of the evaporation heat λ. This means that when the latter changes (for instance, in the case of a salt recrystallizing, λ must be reduced by the heat of crystallization released, see Williams [7], or, when almost dry material is used λ must be increased by the adsorption heat of the water), the

method for finding the wet bulb point remains valid all the same: draw a tangent in the point of the adiabatic line where the wet bulb temperature is required, and intersect this tangent by the vapour pressure line. It must be borne in mind, however, that an increase of λ entails a decrease of dH/dt, so of the slope of the adiabatic line. This is therefore

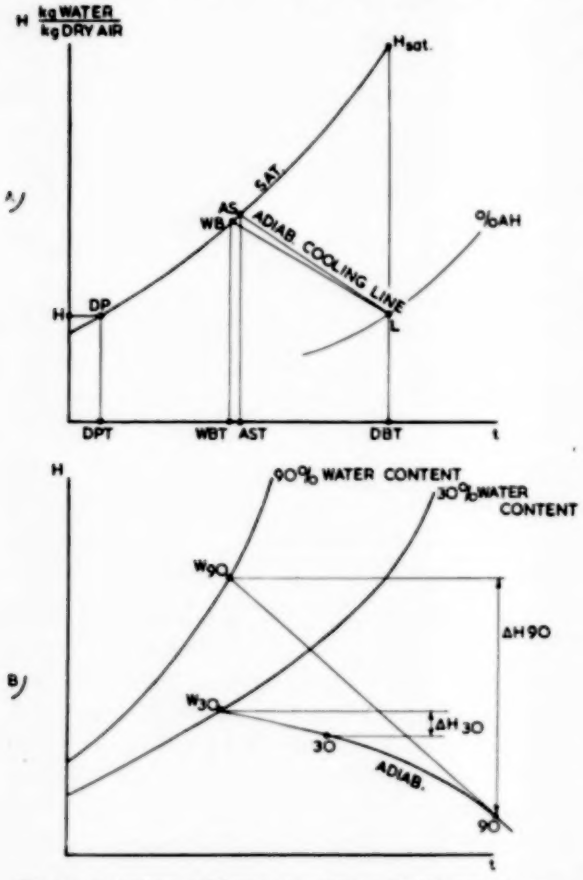

Fig. 8. A) Scheme of humidity, chart.; B) Scheme of graphical determination of the driving force ΔH at 90 and 30% water content.

accompanied by a simultaneous shifting of the wet bulb point along the vapour tension line, resulting in a lower wet bulb temperature. The reverse obtains when λ becomes smaller.

Another change generally occurs when solutions and suspensions are dried: the vapour tension is decreased upon progressive reduction of the humidity. This (lower) vapour tension line takes over the function of the vapour tension line of pure liquid in determining the wet bulb point. This of course affects the driving force (and hence the rate of evaporation). Generally this becomes smaller owing to the reduced vapour tension curve and with increasing evaporation heat. Fig. 8 illustrates this for a case in which the vapour tension curve is lower and the evaporation heat is higher for 30% water content than for 90% water content.

We emphasize the fact that this determination of the wet bulb point only applies to water and air, but that generally for other liquid/gas combinations the wet bulb point cannot be found with the aid of the adiabatic line, nor is it constant during the entire period of evaporation.

As we have already said, the wet bulb temperature is determined by molecular heat conduction on the one hand and molecular material diffusion (evaporation) on the other, through the same air film round the drop. The two processes are therefore fundamentally linked together, as one cannot occur without the other. The consequence of this is that we can test FRÖSSLINGS eq. (2) for the evaporation of moving drops of liquid by already familiar measurements of heat transfer of moving spheres in air. As was further explained in section 2, FRÖSSLINGS eq. (2) can be transformed to

$$N_{Nu} = 2\left(1 + 0{\cdot}25\, N_{Re}^{0{\cdot}5}\right). \qquad (5)$$

Another consequence of linking heat and material transfer is that the calculation of the spray cooling process can be carried out in a way almost identical to that for a spray drying process. Naturally, in spray cooling cold air is used, which withdraws heat from the drops (sensible heat, crystallization heat, solidification heat).

7. THE HUMIDITY CHART

The evaporation of *drops* having been discussed in the previous sections, we shall now ascertain what changes the drying *air* undergoes during the process. As the air changes both as regards temperature and humidity, the humidity chart (modified MOLLIER diagram) can obviously be used for the purpose; this gives us an air point by plotting against each other the absolute humidity H (lb H_2O per lb dry air) and the normal (dry bulb) temperature. See Fig. 9.

Various quantities can be found in this humidity chart, such as dew point temperature, the saturation line, the percentage absolute humidity, the percentage relative humidity, the adiabatic cooling line and the adiabatic saturation temperature. The reader is referred to PERRY [4].

Fig. 10 gives a schematic diagram of the course of the evaporation process. The saturation pressure of

VOL. 1 1952

water is shown by the line Sat. If the condition of the inflowing air may be represented by point L, then, during the evaporation of the water, the condition of the air changes along a known line (the adiabatic cooling line) which is given by the condition that the evaporation heat is supplied entirely by the sensible heat of the air. This line is almost straight and has a slope of dH/dt = about 1/2300° C. This is valid for all the adiabatic lines of this chart.

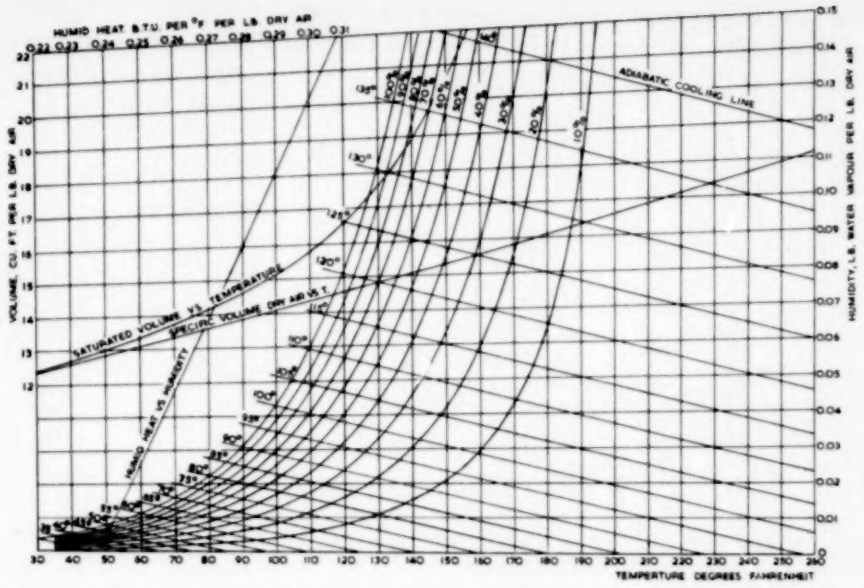

Fig. 9. Humidity chart for low temperature range. The adiabatic cooling lines on this chart are straight and parallel. From "Elements of chemical engineering," 2nd ed., by BADGER and MCCABE. Copyright, 1936. Courtesy of McGraw-Hill Book Co., New York.

As already shown (see section 6) the adiabatic line can also be used (at least in the case of the air/water system) to find the wet bulb temperature; for this is given by the point of intersection W of the adiabatic line and the line of saturated vapour tension. We see, therefore, that in this system the wet bulb temperature of pure water does not change in accordance with the condition of the air. The driving force, expressed either as ΔH or as Δt, decreases, however, as the air point shifts along the adiabatic cooling line towards the wet bulb point W. The rate at which the air point shifts is, at a given weight of evaporated water, in inverse ratio to the quantity of drying air.

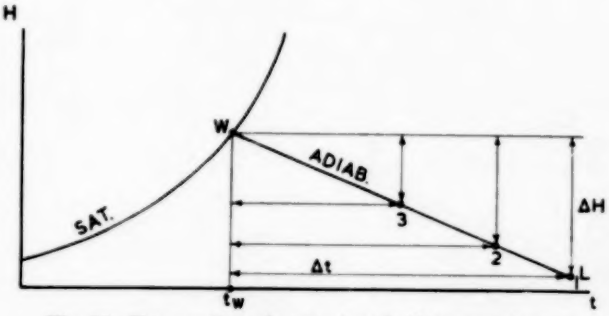

Fig. 10. Evaporation of water (wet bulb temperature constant).

Decreasing vapour tensions occur when solutions or suspensions are dried; not with pure water. According as the water content of the drop decreases, the vapour tension (at the same temperature) drops. When this dependence is represented schematically, as in Fig. 11, we see that as the air point rises along the adiabatic line, the wet bulb point descends along the adiabatic line (contrary to what happens with pure water, see Fig. 10). Consequently, the wet bulb temperature is no longer constant, but rises.

The relation of the shifts of the air and wet bulb points is in direct ratio to the weight relation of the currents of liquid and air.

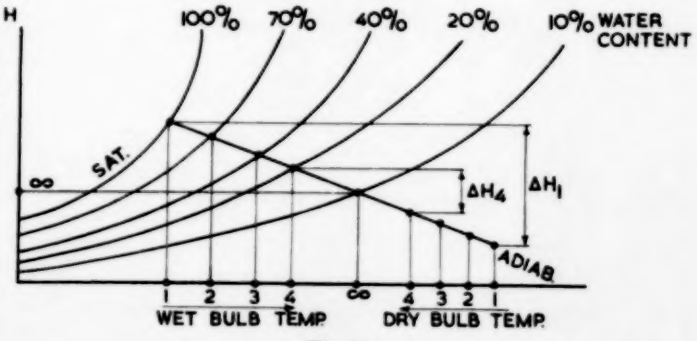

Fig. 11.
Drying of a wet material (increasing wet bulb temperature).

The second consequence of the shifting of the wet bulb point is that the driving force (ΔH or Δt) decreases much more rapidly than when pure water is evaporated. When the point of equilibrium has been reached (in an adiabatic process of infinite length), the moisture content of the drop becomes so small

that the vapour tension is equal to the partial water vapour tension of the air. The driving force has then become nil.

Conclusions

The humidity chart is an aid by which we may predict the course of the spray drying process, when only the

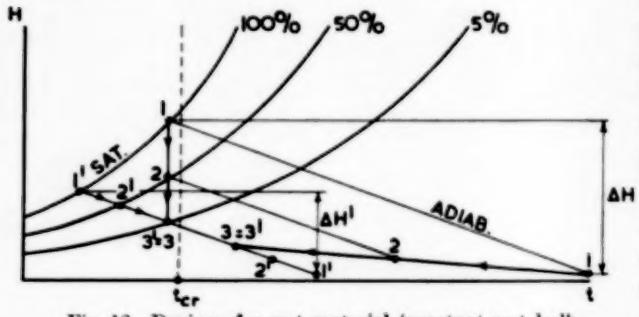

Fig. 12. Drying of a wet material (constant wet bulb temperature).

vapour tension curves of the material as functions of temperature and humidity have been measured. This has already been done for some materials, for instance for powdered egg by GREENE *et al.* [8].

The process can be accurately worked out by means of the vapour tensions, according to the example of

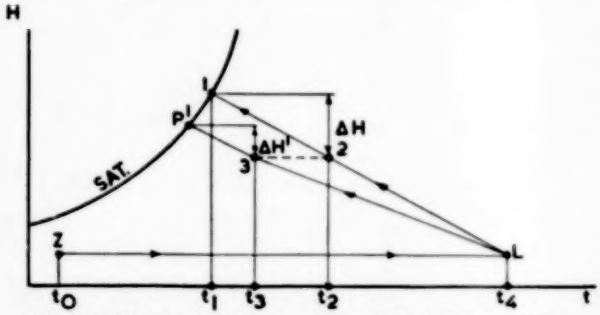

Fig. 13. Efficiencies of 3 processes: *ZL* 1, *ZL* 2 and *ZL* 3.

Fig. 11, if the temperature and humidity of the incoming air are known. At each point of the process the driving force ΔH is then directly read off, and then, with the aid of the equation already derived, *viz.*

$$\frac{d x_w}{dl} = 4{\cdot}6 \,.\, 10^{-7} \frac{\Delta H}{v D^2} \left(1 + 0{\cdot}23 N_{Re}^{0{\cdot}5}\right) \qquad (9)$$

the fractional evaporation velocity per metre of height of fall of the drop at this point can be calculated. The diameter of the drop must be known and it must be remembered that (9) is the evaporated fraction of the whole drop when this has the same density as water.

The above eq. (9) is correct, also for the evaporation of wet, drying spheres, if the rate of drying is controlled by the resistance to diffusion in the air film round the drop. It is not until the moisture transfer *within* the drop starts to control the rate of evaporation that (9) loses its validity.

Drying at constant wet bulb temperature

Another conclusion is concerning the fact (depicted in Fig. 11) that during drying the wet bulb temperature rises according as drying proceeds. When a thermolabile material is dried care will have to be taken that the highest wet bulb temperature (which the dry particles have at the end of the process) remains below a certain critical temperature. This means that at the start of the process the wet bulb temperature is unavoidably low, so that the driving force is small and the process proceeds too slowly. It would be ideal if the wet bulb temperature could be kept constant just below the critical temperature. This can be achieved by starting the process with very hot air, with the wet bulb temperature at its maximum. Then this temperature is kept constant artificially at the highest possible level, *i.e.* is prevented from rising by continuously admixing cold air along the entire length of the plant. The air point then does *not* intersect the adiabatic line, but shifts rapidly to the left, in such a manner that the wet bulb temperature remains constant (see Fig. 12). Apparently, therefore, particularly at the beginning of the process, advantage can be taken of a higher driving force than by the known (adiabatic) process; *cf.* ΔH with $\Delta H'$ in Fig. 12.

8. THERMAL EFFICIENCY AND EFFICIENCY RATIO

We shall first deal with the evaporation of pure water and consider this process in the humidity chart, see Fig. 13. Let us assume that the condition of the outer air is given by Z, and that after passing of the air heater condition L is reached. We shall consider three different processes:

(*1*) adiabatic process of infinite duration: *ZL* 1,
(*2*) adiabatic process of finite duration: *ZL* 2,
(*3*) non-adiabatic process of finite duration: *ZL* 3.

In (*1*), the air is entirely saturated with water vapour, so that the final temperature t_1 is reached. This is the ideal process, with maximum evaporation.

In (*2*), the air point passes along the adiabatic cooling line, without complete saturation being achieved. Final temperature t_2.

In (*3*), heat is lost by poor insulation of the plant. Consequently the final temperature t_3 is lower than t_2,

VOL. 1 1952

though the evaporation performance is equal to that of process (2).

The thermal efficiency is defined as

$$\eta = \frac{\text{heat of evaporation}}{\text{heat input}} . \qquad (28)$$

As the specific heat of the wet air is practically constant *, the ratio of the heats can be replaced by the ratio of the temperature changes, so that the following values are found in the three above-mentioned processes.

(1) $\eta = \frac{t_4 - t_1}{t_4 - t_0}$. (2) and (3) $\eta = \frac{t_4 - t_2}{t_4 - t_0}$ †.

These thermal efficiencies are still dependent on the non-essential temperature of the outer air t_0; therefore, they are not a correct indication of the quality of the process. It is possible to obtain an expression (efficiency ratio) which does not contain this temperature t_0 by referring the thermal efficiencies to the ideal process (1):

(1) $\eta_r = 1$. (2) and (3) $\eta_r = \frac{t_4 - t_2}{t_4 - t_1}$.

Process (3) differs from (2) in that the effluent air is colder and in that it requires a larger apparatus. The latter fact is evident if attention is paid to the driving force $\Delta H'$, which has become smaller than ΔH owing to the lower wet bulb point P', so that evaporation also proceeds more slowly.

It is clear that efficiencies are particularly high if (other temperatures being constant) the temperature of the inflowing hot air t_4 is kept as high as possible. This possibility is limited by the increasing difficulty and expense of air heating and by the highest permissible temperature of the drying drop. For, as the drop dries and the vapour tension becomes lower in consequence, the drop temperature will approach more and more closely that of the air passed off (*cf.* Fig. 11).

Recirculation of spent air

Recirculation of spent air makes it possible to increase the thermal efficiency by other means than those described above. This is shown in Fig. 14, where the same evaporation performance of the normal process $Z\,L\,E$ is obtained by the recirculation process $Z'L'E'$. The outer air Z is mixed with spent air E', forming the mixture Z'. When the two processes in Fig. 14 are compared it is found that the thermal efficiency has actually risen:

$$\frac{t_4 - t_3}{t_4 - t_0}, \quad > \frac{t_4 - t_3}{t_4 - t_0}.$$

All air humidities have increased considerably, however, and the driving force ΔH has therefore decreased everywhere, so that the length of the apparatus is to be enlarged.

Another disadvantage of recirculation of spent air is that the ventilation energy required soon becomes too large, making the plant uneconomical.

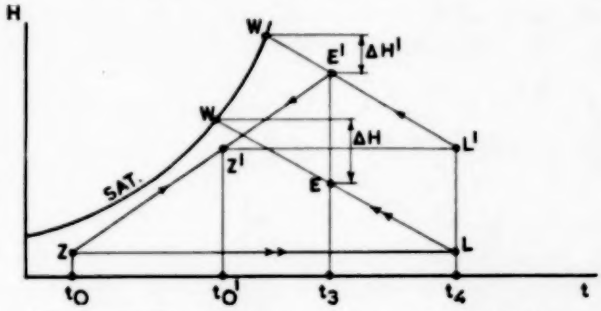

Fig. 14. Efficiencies of normal process: ZLE, and of recirculation process: $Z\,L'\,E'$.

Drying of solutions and suspensions

It was already shown in section 7 that when a suspension or solution is dried the wet bulb temperature is not constant, but rises, approaching the air temperature in a process of infinite length (see Fig. 11).

In an ideal process the position of this final temperature t_∞ depends on the position of the vapour tension curves of the dried material and on the ratio of air and liquid in the apparatus: the more air, the higher is t_∞ and the lower the final moisture content of the material.

If we compare this case with that for pure water (see Fig. 10) the situation is found to be distinctly less favourable: at equal H levels the driving force ΔH is greatly reduced; it is even impossible to get beyond H_∞. It is clear that the evaporation performance of the same plant has therefore become considerably lower in comparison with the evaporation of pure water. If these performances have to be compared, however, it is necessary to take into consideration the difference in driving force ΔH. This can be done with the aid of the transfer unit concept introduced by CHILTON and COLBURN [9], as explained in the next section.

* To be exact, the spec. heat is $(1 + 2H)$ kJ/kg °C for air with an absolute humidity of H.

† The useful evaporation heat is equal in processes (2) and (3).

9. TRANSFER UNITS

These dimensionless numbers were introduced by CHILTON and COLBURN [9] for processes of heat transfer and mass transfer (distillation, absorption, heat exchange, *etc.*). The difficulty of a diffusion process may be characterized by the number of transfer units, N_t. For instance, in heat transfer through an air film N_t is defined by:

$$N_t = \int_1^2 \frac{dt}{\Delta t}. \tag{29}$$

Let us first consider evaporating drops of water in air of which the surface temperature is the wet bulb temperature = adiabatic saturation temperature.

With adiabatic air wetting (*cf.* Fig. 13) from L to 2

$$\left.\begin{aligned} N_t &= \int_2^4 \frac{dt}{\Delta t} = \int_2^4 \frac{dt}{t - t_1} = \ln \frac{t_4 - t_1}{t_2 - t_1} = \ln \left[\frac{1}{1 - \dfrac{t_4 - t_2}{t_4 - t_1}} \right] \\ N_t &= \ln \frac{1}{1 - \eta_T} \quad \text{or} \quad \eta_T = 1 - e^{-N_t}. \end{aligned}\right\} \tag{30}$$

This simple relation [eq. (30)] between efficiency ratio and the number of transfer units only applies for adiabatic evaporation of a pure liquid.

Next, let us consider the case of the drying of drops of a solution or suspension. We have already seen (Fig. 11) that the vapour tension curves are lower in the humidity chart as the humidity is lower. It is now possible to draw full advantage from the special properties of the transfer unit concept. The definition eq. (29) remains perfectly valid, while Δt can be read off in the humidity chart step by step. As Δt decreases more rapidly, the number of transfer units will be much larger than in an equivalent evaporation (*i.e.* with equal increase of H) of pure water. A larger apparatus is therefore also needed.

Apparently the drying of a particular solution in a spray drier should be evaluated as follows:

1. Using pure water, the thermal efficiencies and the number of transfer units are determined as described in section 8 and with the aid of the above eq. (30).

2. The vapour tension curves of the material to be dried are determined as functions of temperature and humidity. If necessary, the maximum temperatures permissible to avoid thermal decomposition of the material are also determined.

3. The course of the process is plotted in the humidity chart. The ratio of air and liquid currents is adjusted so as to obtain the desired moist content of the product required with the same number of transfer units as determined under 1. Attention is also paid to the permissible temperature of dry air passed in.

When the drop distribution during the spraying of the solution is the same as during the spraying of pure water, the measured number of transfer units of the apparatus remains the same. When this is not the case, allowance must be made for the influence of particle size (see below).

Example of calculation

Water is sprayed in a spray drier. The following temperatures are measured:

a) outer air is 15° C (59° F) dry bulb thermometer,
b) outer air is 7° C (44° F) wet bulb thermometer,
c) air after heater 115½° C (240° F) dry bulb thermometer,
d) discharged air 57° C (135° F) dry bulb thermometer,
e) discharged air 32° C (89½° F) wet bulb thermometer.

The process can be easily followed on the humidity chart Fig. 9.

1. The *thermal efficiency* is $\eta = \dfrac{115\tfrac{1}{2} - 73\tfrac{1}{2}}{115\tfrac{1}{2} - 15} = 42\%$, the temperature of 73½° C (164° F) having been found as follows. From a) and b) it follows that the absolute humidity is $H = 0{\cdot}003$. From the air point ($H = 0{\cdot}003$ and $t = 115\tfrac{1}{2}$° C [240° F]) one follows a certain adiabatic cooling line, which ends at the wet bulb temperature of 35° C (95° F). But the measured wet bulb temperature of the spent air is 32° C (89½° F). In combination with the dry bulb temperature of 57° C (135° F) this points to an absolute humidity of $H = 0{\cdot}020$. We intersect the horizontal line $H = 0{\cdot}020$ by the adiabatic cooling line and find the temperature required to be 73½° C (164° F).

2. The *efficiency ratio* is $\eta_T = \dfrac{42\%}{80\%} = 52\tfrac{1}{2}\%$, the maximum value of the thermal efficiency of 80% having been found as follows. The above-mentioned adiabatic cooling line pointed to the wet bulb point of 35° C (95° F). The required maximum value is therefore

$$\frac{115\tfrac{1}{2} - 35}{115\tfrac{1}{2} - 15} = 80\%.$$

3. The *heat loss* follows from the fact that in an adiabatic process the final temperature, according to 1., might have been 73½° C (164° F). In fact, the temperature of the spent air is 57° C (135° F), so that $73\tfrac{1}{2} - 57 = 16\tfrac{1}{2}$° C was lost. Calculated on the total drop in temperature from 115½° C this is $\dfrac{73\tfrac{1}{2} - 57}{115 - 57} = 28\tfrac{1}{2}\%$.

4. The *number of transfer units.* Here we have a non-adiabatic process, so eq. (30) may not be applied. We therefore use the definition eq. (29):

$$N_t = \int_1^2 \frac{dt}{\Delta t} = \frac{115\tfrac{1}{2} - 73\tfrac{1}{2}}{\text{log mean } \Delta t}. \tag{31}$$

VOL. 1 1952

In (31) only the useful (evaporation) heat is, of course, considered, so that the drop in temperature to $73\frac{1}{2}$° C is taken (not to 57° C). The driving force varies from $(115\frac{1}{2} - 35)$ to (57–32). The logarithm mean of this is 46° C.

Therefore, $N_t = \dfrac{115\frac{1}{2} - 73\frac{1}{2}}{46} = 0{\cdot}91$ transfer unit.

Transfer units on a basis of concentration

It was said at the beginning of this section that the transfer units can also be calculated on a mass transfer basis. For spray drying the following definition is obvious:

$$N_{tm} = \int \frac{dH}{\Delta H} \,. \tag{32}$$

These transfer units are exactly proportional in number to those calculated on a temperature basis according to eq. (29) as

$$N_{tm} = \frac{k_m C_p}{h} N_t. \tag{33}$$

Proof—Use eq. (25) and (26) of section 6:

wet bulb line:

$$h \,.\, \Delta t = k_m \lambda \, \Delta H$$

adiabatic cooling line:

$$C_p \, dt = \lambda \, dH \,.$$

Hence,

$$\frac{\Delta H}{\Delta t} = \frac{h}{k_m \lambda} = \frac{h}{k_m C_p} \cdot \frac{C_p}{\lambda} = \frac{h}{k_m C_p} \cdot \frac{dH}{dt} \,. \tag{34}$$

Therefore

$$\int \frac{dH}{\Delta H} = \frac{k_m C_p}{h} \int \frac{dt}{\Delta t} \,, \tag{35}$$

from which follows the above-mentioned result, eq. (33).

For the special case in which LEWIS' equation applies, see eq. (27), $k_m C_p = h$, so that then

$$N_{tm} = N_t. \tag{36}$$

This obtains for the combination water/air, and for drying aqueous suspensions or solutions, regardless whether the adiabatic cooling line is straight or curved.

Calculation of the height of a transfer unit for falling drops

We shall now calculate the height required for a process of one transfer unit, for water drops falling in stagnant air, starting from the equation for fractional evaporation of a falling water drop per metre height of fall [see eq. (9)]:

$$\frac{dx_w}{dl} = 4{\cdot}6 \,.\, 10^{-7} \frac{\Delta H}{v D^2} \left(1 + 0{\cdot}23 \, N_{Re}^{0{\cdot}5}\right). \tag{37}$$

Suppose the flow of air through the tower to be V kg/sec and the flow of liquid at a given point L kg/sec. At that point the humidity of the air rises by

$$\frac{dH}{dl} = \frac{L}{V} \cdot \frac{dx_w}{dl} = 4{\cdot}6 \,.\, 10^{-7} \frac{L}{V} \frac{\Delta H}{v D^2} \left(1 + 0{\cdot}23 \, N_{Re}^{0{\cdot}5}\right). \tag{38}$$

Now, the height equivalent to one transfer unit is defined as

$$H_t = \frac{\text{length } dl}{\text{number of transfer units in } dl} \,. \tag{39}$$

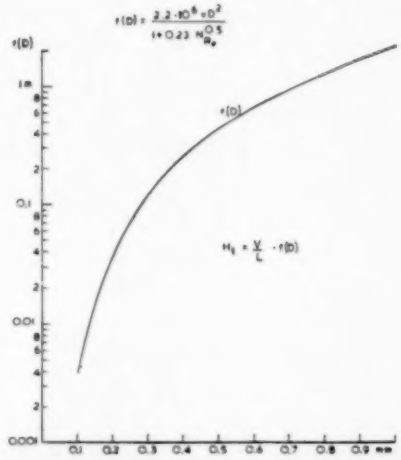

Fig. 15. Height equivalent to a transfer unit. Free falling water drops in stationary air (ϱ = 1 kg/m³).

From (38) we can find by means of (39) the value of H_t, as follows:

$$H_t = \frac{dl}{(N_t)_{dl}} = \frac{dl}{dH/\Delta H} = \frac{2{\cdot}2 \,.\, 10^6 \, v D^2}{1 + 0{\cdot}23 \, N_{Re}^{0{\cdot}5}} \cdot \frac{V}{L} \text{ m} \tag{40}$$

where L = kg water/sec at the given point.

Eq. (40) therefore obtains for every moving drop of water in air; hence also for drops falling at a constant settling speed. This speed was derived in section 3. When these speeds are substituted for water, the value of H_t for drop diameters between 0·1 and 1·0 mm follows as shown in Fig. 15.

This result can be interpreted as follows. If the job of humidifying air by a water spray is considered, it appears that the difficulty of this job (H_t) is in direct proportion to the ratio of air and liquid (V/L). Further, the smaller the drop size the more this difficulty decreases (Fig. 15).

Next we will treat H_t for falling drops of a solution or suspension. We suppose that the feed L at a given moment only contains a fraction B of water and $1-B$ of solid matter. For the fractional evaporation of the

falling drop we then get the modified equation:

$$\frac{dx'_w}{dl} = \frac{4{\cdot}6 \,.\, 10^{-7}}{R} \cdot \frac{\Delta H}{v\, D^2}\left(1 + 0{\cdot}23\, N_{Re}^{0{\cdot}5}\right) \qquad (37')$$

because the evaporation is taken to be equal to that of a drop of pure water.

At that moment the humidity of the air rises by

$$\left.\frac{dH}{dl} = \frac{B\,L}{V} \cdot \frac{dx'_w}{dl} = \frac{L}{V} \,.\, 4{\cdot}6 \,.\, 10^{-7}\, \frac{\Delta H}{v\, D^2} \times \right\} \qquad (38')$$
$$\left. \times \left(1 + 0{\cdot}23\, N_{Re}^{0{\cdot}5}\right)\right\}$$

which therefore tallies entirely with eq. (38) if L is taken to be kg feed/sec. The same also applies to H_t, represented by:

$$H_t = \frac{2{\cdot}2 \,.\, 10^{8}\, v\, D^2}{1 + 0{\cdot}23\, N_{Re}^{0{\cdot}5}} \cdot \frac{V}{L}\ \text{m} \qquad (40')$$

where again L = kg feed/sec at the given point.

The result, *viz.* that the H_t is the same regardless of the solids content of the drop, may be interpreted as follows: for the *wetting of air* it makes no difference at all whether the drop contains less or more solid matter (a difference in vapour tension, ΔH, is automatically accounted for in the concept of transfer units). On the other hand, for the *drying of the drop* it is of course advantageous if the solids content of the drop fed in is as high as possible.

Analogous considerations obtain in the drying of hollow drops as compared with solid drops of the same size (see section 5).

10. Hydrogen and Steam as Drying Gases

Although air is an obvious drying gas, there may be some other gas that has more advantages for this purpose.

Hydrogen possesses the advantage of having a higher rate of diffusion and heat conductivity. Careful analysis shows that the rate of evaporation of water in hydrogen is indeed three to six times as great as that in air (depending on the case under consideration). There are, however, considerable practical disadvantages, such as expense and inflammability, that make its use impracticable.

Superheated steam can also be employed as a drying gas. It is interesting to note that the evaporation rate of wet material in a steam atmosphere is only determined by the heat transfer of the drops. In the case of evaporation in air the material diffusion coefficient is also a determining factor. In the steam process there is, of course, no question of material diffusion in the gas phase.

Re hydrogen

The influence of the drying properties on the rate of evaporation is evident from Frössling's evaporation equation:

$$N = 2\,\pi\, D\, D_v\, \frac{\Delta p}{R\,T}\left(1 + 0{\cdot}276\, N_{Re}^{0{\cdot}5}\, N_{Sc}^{0{\cdot}33}\right) \frac{\text{kmol}}{\text{sec}}. \qquad (2)$$

The rate of evaporation depends on the following factors:

1. diffusion coefficient,
2. difference in concentration,
3. Reynolds' number and
4. Schmidt's number.

1. *The diffusion coefficient* D_v. This depends equally on the magnitude of the molecular weight of the evaporating material and of the gas. This is apparent from the equation (on an empirical basis) for molecules A and B:

$$D_v = 4{\cdot}3 \,.\, 10^{-2}\, \frac{T^{1{\cdot}5}}{P\left[(V_m)_A^{\frac{1}{3}} + (V_m)_B^{\frac{1}{3}}\right]^2} \sqrt{\frac{1}{M_A} + \frac{1}{M_B}}. \qquad (41)$$

Further particulars on this correlation eq. (41) are given by Gilliland [10].

If we compare the rate of diffusion of water ($M = 18$, $V_m = 15$) in air ($M = 29$, $V_m = 29{\cdot}9$) with that of water in hydrogen ($M = 2$, $V_m = 14{\cdot}33$), we find the value of D_v in hydrogen to be 3·2 times as high as in air.

No other gas has such a favourable rate of diffusion.

2. *The difference in concentration* $\Delta p/RT = \Delta C_w$ (kmol/m³) on either side of the gasfilm. This quantity depends on the difference in wet bulb and dry bulb temperature, as discussed in section 6. At a given gas temperature we now compare the wet bulb temperatures in hydrogen and in air; t_w is found from the gas point in the humidity chart by drawing a line with a slope according to eq. (25)

$$\frac{\Delta H}{\Delta t} = \frac{h}{k_m}\,\lambda. \qquad (42)$$

Now we can derive k_m and h from Frössling's equation for mass transfer [eq. (2)] and its analogon for heat transfer [eq. (4)]:

$$k_m = \frac{2\, D_v\, \varrho}{D}\left(1 + 0{\cdot}276\, N_{Re}^{0{\cdot}5}\, N_{Sc}^{0{\cdot}33}\right), \qquad (43)$$

$$h = \frac{2\, k_h}{D}\left(1 + 0{\cdot}276\, N_{Re}^{0{\cdot}5}\, N_{Pr}^{0{\cdot}33}\right). \qquad (44)$$

For low values of N_{Re}, when $1 \gg 0{\cdot}276\, N_{Re}^{0{\cdot}5}\, N_{Sc}^{0{\cdot}33}$, we find accordingly:

$$\frac{\Delta H}{\Delta t} = \frac{h}{k_m\,\lambda} = \frac{k_h}{D_v\,\varrho\,\lambda} = \frac{C_p}{\lambda}\, N_{Le} \qquad (45)$$

and for high values of N_{Re}, when $1 \ll 0{\cdot}276\, N_{Re}^{0{\cdot}5}\, N_{Sc}^{0{\cdot}33}$:

$$\frac{\Delta H}{\Delta t} = \frac{h}{k_m\,\lambda} = \frac{C_p}{\lambda}\, N_{Le}^{0{\cdot}67}. \qquad (46)$$

VOL. 1 1952

With eq. (45) and (46)* we may estimate how the slope $\Delta H/\Delta t$ will be affected, when hydrogen is used instead of air. For low values of N_{Re}, it follows from eq. (45) and the physical properties that

$$\frac{1}{\lambda_{\text{water}}} \cdot (C_p N_{Le})_{H_2} = \frac{1}{\lambda} (14{\cdot}5 \,.\, 2{\cdot}1) (C_p \,.\, N_{Le})_{\text{air}}.$$

Therefore, the slope $\Delta H/\Delta t$ will be 30 times steeper than in the case of air. For high values of N_{Re}, it follows from eq. (46) and the physical data that

$$\frac{1}{\lambda} (C_p N_{Le})_{H_2} = \frac{1}{\lambda} (14{\cdot}5 \,.\, (2{\cdot}1)^{0{\cdot}67}) (C_p \,.\, N_{Le}^{0{\cdot}67})_{\text{air}}.$$

Therefore, the slope will be 24 times steeper than for air.

It would now be possible to construct a new humidity chart for the combination water/hydrogen, for instance by the method indicated by BARTA and GARBER [11]. In this particular case, however, one can still make use of the known chart for water/air. For the humidity scale must be magnified 14·5 ×, in view of the fact that the density of air is 14·5 × greater than that of H_2. At the same time the slope of the adiabatic cooling line [eq. (26)] in this chart:

$$\frac{dH}{dt} = \frac{C_p}{\lambda} \qquad (47)$$

is also 14·5 × greater, as $(C_p)_{H_2} = 14{\cdot}5 (C_p)_{\text{air}}$.

Consequently, one can for practical purposes use the air/water chart for the case of H_2/water, including the adiabatic lines. The above-derived slopes for the wet bulb point, $\Delta H/\Delta t$ should also be divided by the same factor 14·5 before use in the air/water chart. We then find, that the slope should be multiplied by 2·1 for low values of N_{Re} and by 1·64 for high values of N_{Re}.

Example. Suppose N_{Re} has a low value. Suppose the gas point is $H = 0$, $t = 200°$ F. For air we find in Fig. 8: wet bulb point: $H = 0{\cdot}026$, $t = 85°$ F. Therefore the driving force $\Delta H = 0{\cdot}026$. For hydrogen, we construct a wet bulb point line with a slope of $2{\cdot}1 \,.\, \frac{0{\cdot}026}{200-85}$. The wet bulb point is $H = 0{\cdot}047$, $t = 103°$ F. So the driving force is 1·8 times larger than with air. Similarly, for a high value of N_{Re} we find a driving force 1·46 times larger than with air.

3. REYNOLDS' *number* $N_{Re} = vD\varrho/\mu$. When we consider falling drops, the constant settling velocity will, of course, be much higher in hydrogen than in air. Let us proceed with the case that STOKES' law obtains (that is for low N_{Re}). Then the practically unchanged drop weight is

$$3\pi\mu D v = \frac{\pi}{6} D^3 g \Delta\varrho. \qquad (48)$$

Therefore

$$N_{Re}^{0{\cdot}5} = \left(\frac{\varrho g D^3 \Delta\varrho}{18\mu^2}\right)^{0{\cdot}5}. \qquad (49)$$

So, comparing hydrogen with air, in STOKES' case $N_{Re}^{0{\cdot}5}$ is $\sqrt{\frac{0{\cdot}069}{0{\cdot}5^2}} = 0{\cdot}52$ times larger. A comparable factor will hold in the case of high values of N_{Re}.

4. SCHMIDT's *number* $N_{Sc} = \frac{\mu}{\varrho D_v}$. When the values are substituted for water in hydrogen we find $N_{Sc} = 1{\cdot}43$, as compared with 0·60 for water in air.

Summing up the four factors just discussed, we find that, according to FRÖSSLINGs eq. (2), when changing over from air to hydrogen as drying gas the following changes occur:

(a) At low values of N_{Re} : evaporation is effected according to the first term of eq. (2), in such a way that the rate is $3{\cdot}2 \,.\, 1{\cdot}8 = 5{\cdot}8$ times higher.

(b) At high values of N_{Re}: according to the second term of the FRÖSSLING equation, the rate is increased by a factor $3{\cdot}2 \,.\, 1{\cdot}46 \,.\, 0{\cdot}52 \,.\, \left(\frac{1{\cdot}43}{0{\cdot}60}\right)^{0{\cdot}33} = 3{\cdot}23$.

The required height of fall is affected less favourably, because the constant settling velocity in hydrogen will be higher than in air, as already mentioned above.

When hydrogen is used instead of air as a drying medium, a number of technical difficulties may be

Table 1

	Air	*Hydrogen*	*Steam*
Dyn. viscosity at 80° C, μ, in kg/m. sec	$2 \,.\, 10^{-5}$	$1{\cdot}2 \,.\, 10^{-5}$	$1{\cdot}2 \,.\, 10^{-5}$
Spec. heat, C_p, in kJ/kg °C	1.0	14·4	1·8
Heat conductivity, k_h in J/m. sec °C	0·03	0·21	0·02
Molecular weight, M, in kg/kmol	29	2	18
Diffusion coefficient with H_2O, D_v in m²/sec	$3 \,.\, 10^{-5}$	$9\frac{1}{2} \,.\, 10^{-5}$*	—
Molecular volume V_m [10]	29·9	14·3	15
Thermal diffusivity in m²/sec	$1{\cdot}8 \,.\, 10^{-5}$	$12{\cdot}9 \,.\, 10^{-5}$	$5{\cdot}2 \,.\, 10^{-5}$
Number of PRANDTL . . .	0·74	0·74	0·78
Number of SCHMIDT (with H_2O).	0·60	1·43	—
Number of LEWIS (with H_2O).	0·917	1·88	—

* By calculation, see above.

* If we try to check these equations for the case of water and air, we find for low N_{Re}: $\frac{h}{k_m C_p} = N_{Le}$ and for high N_{Re}: $\frac{h}{k_m C_p} = N_{Le}^{0{\cdot}67}$. As was mentioned in section 6, eq. (27), it is an experimental fact that $\frac{h}{k_m C_p} \cong 1$ for water and air. On the other hand, $N_{Le} = 0{\cdot}917$ according to JAKOB's "Heat Transfer," so that $N_{Le}^{0{\cdot}67} = 0{\cdot}94$.

The equation for the "psychrometric ratio" $\frac{h}{k_m C_p} = N_{Le}^{0{\cdot}67}$ checks quite well with a graph in GILLILAND [12].

expected, as, for instance, the recirculation of this comparatively expensive gas, necessitating the apparatus to be gas-tight and fire-proof. Although the use of hydrogen as a drying gas has been suggested by some authors [12], [13], so far these technical difficulties have prevented the realization of H_2-drying.

Some physical constants are cited of air, hydrogen and steam.

Re superheated steam

Another drying gas previously suggested [15], [16] is superheated steam. When a closed recirculation

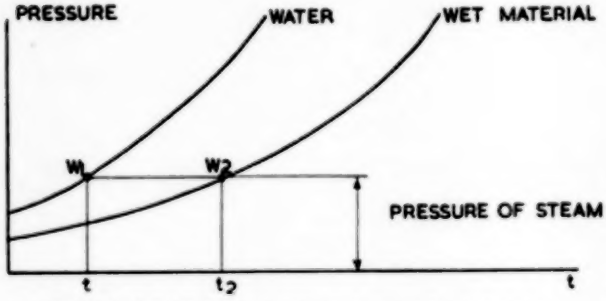

Fig. 16. Wet bulb temperature in superheated steam.

system is used, the consumption of heat will be a minimum, as only the evaporation heat of water has to be supplied (apart from heat losses).

Of course, in evaporation in overheated steam there is in the gas phase no material diffusion, but only heat transfer as a limiting factor. The surface temperature of a drop is determined entirely by the steam pressure (independent of the steam temperature): 1 ata corresponds to 100° C, $\frac{1}{2}$ ata to 81° C, etc. (to be found in the humidity chart or a vapour tension table). At equal temperatures wet material has a lower equilibrium vapour tension. Conversely, therefore, at a given steam pressure, the wet bulb temperature of wet material will be higher than of pure water. This is illustrated in Fig. 16.

If one wishes to compare the rate of evaporation with that in air, this can only be done if a reasonable basis of comparison is agreed on. This may be done as follows.

Drying in air—Using dry air of temperature t_a the corresponding wet bulb temperature is t_w; the driving force is then $t_a - t_w$.

Drying in superheated steam—Such a pressure is chosen that the corresponding temperature (according to the vapour pressure table of saturated steam) is t_w. Further the temperature of the steam is chosen $= t_a$; again the driving forces is $t_a - t_w$.

In order to compare the rate of heat transfer, eq. (44) should be used. In the case of low values of N_{Re}, only the first term is of interest. The value of the heat conductivity, k_h is for steam 2/3 times that for air, so that the rate of heat transfer is also decreased by a factor 2/3.

In the case of high values of N_{Re}, only the second term is of interest. Now N_{Re} and N_{Pr} also affect h. For steam, $N_{Pr}^{0.33}$ is nearly equal to the value for air. But N_{Re} should be calculated for a constant settling velocity in steam. Then we find

$$h_{\text{steam}} = h_{\text{air}} \cdot \frac{2}{3} \cdot \left[\frac{N_{Re} \text{ in steam}}{N_{Re} \text{ in air}} \right]^{0.5}. \qquad (50)$$

As in the case of hydrogen, the practical difficulties entailed by the recirculation of the gas are great. Moreover, the removal of the product from the steam atmosphere, without condensation of water, is another practical difficulty to be faced (see [15]).

Acknowledgements—I should like to thank the management of *N.V. De Bataafsche Petroleum Maatschappij* for their permission to publish this paper. I am also indebted to Ir. C. VAN DER POEL, Dr. Ir. A. KLINKENBERG and Dr. G. H. REMAN who have contributed to this work.

NOTATION

A = Surface area, m²
B = Fraction by weight of water in feed
C_d = Drag coefficient for sphere in fluid, dimensionless
C_p = Specific heat of gas at constant pressure, Joule/kg °C
C_w = Vapour concentration in air, kmol/m³
D_v = Diffusivity, m²/sec
D = Diameter of droplet, m
E = Energy, Joule
E_e = Extra evaporation in eq. (22)
F = Force, Newton
g = Acceleration of gravity, 9·8 m/sec²
H = Absolute humidity, kg water vapour/kg dry air
H_t = Height of a transfer unit, m
H_w = Absolute humidity for a given wet bulb temperature
H_∞ = Final humidity, reached after infinite time
h = Coefficient of heat transfer, Joule/m²sec °C
k_h = Heat conductivity Joule/msec °C
k_m = Coefficient of mass transfer, kg/m²sec (unit of ΔH)
l = Length, height or path, m
L = Liquid rate, kg/sec
M = Molecular weight, kg/mol

VOL. 1 1952

m = Mass, kg
N = Rate of transfer, kmoles/sec
N_{Nu} = Number of NUSSELT, dimensionless
N_{Pr} = Number of PRANDTL, dimensionles
N_{Le} = Number of LEWIS, dimensionless
N_{Re} = Number of REYNOLDS, dimensionless
N_{Sc} = Number of SCHMIDT, dimensionless
N_t = Number of transfer units, dimensionless
N_{tm} = Number of transfer units (mass basis), dimensionless
p = Partial pressure, N/m^2
P = Total pressure, N/m^2
q = Flow of heat, Joule/sec
R = Gas constant, $8{\cdot}3 \cdot 10^3$ Joule/kmol °K
T = Absolute temperature, °K
t = Temperature, °C
t_a = Temperature of air, °C
t_w = Wet bulb temperature, °C
t_∞ = Final temperature reached after infinite time, °C
V = Vapour rate, kg/sec
v = Velocity, m/sec
V_m = Molecular volume acc. KOPP-LE BAS, see eq. (41)
W = Weight of liquid, kg
x_w = Fraction by weight, dimensionless
Δ = Finite difference
δ = Thickness of film, m
η = Thermal efficiency, dimensionless
η_r = Efficiency ratio, defined in section 8.
Θ = Dimensionless time, defined in eq. (16)
λ = Heat of evaporation, Joule/kg
μ = Dynamic viscosity, kg/m sec
ν = Kinematic viscosity, m^2/sec
ϱ = Density, kg/m^3
ϱ_L = Density of liquid phase, kg/m^3
ϱ_G = Density of gas phase, kg/m^3
ϱ_s = Density of sphere, kg/m^3
σ = Dimensionless path, defined in eq. (17)
τ = Time, sec

LITERATURE

[1] LANGMUIR, I.; Phys. Rev. 1918 **12** 368. [2] FRÖSSLING, N.; Gerlands Beiträge Geophysik 1938 **52** 170. [3] MACADAMS, W. H.; Heat Transmission, 2nd ed. 1942, p. 236, fig. 122. [4] PERRY, J. H.; Chemical Engineers' Handbook, 2nd ed. 1941, p. 1850. [5] LAPPLE, C. E. and SHEPHERD, C. B.; Ind. Eng. Chem. 1940 **32** 605. [6] WALKER, W. H., LEWIS, W. K., MCADAMS, W. H. and GILLILAND, E. R.; Principles of Chemical Engineering. McGraw Hill, New York, p. 586ff. [7] WILLIAMS, G. C. and SCHMIDT, R. O.; Ind. Eng. Chem. 1946 **38** 967. [8] GREENE, R. M. *et al.*; Chem. Eng. Progr. 1948 **44** 591. [9] CHILTON, T. H. and COLBURN, A. P.; Ind. Eng. Chem. 1935 **27** 255. [10] GILLILAND, E. R.; Ind. Eng. Chem. 1934 **26** 681. [11] BARTA, E. J. and GARBER, H. J.; Chem. Metall. Eng. 1940 **47** 287. [12] GILLILAND, E. R.; Ind. Eng. Chem. 1938 **30** 506. [13] ANTONI, A.; Le Genie Civil, 1937, p. 417 and 433. [14] BADGER, W. L. and MCCABE, W. L.; Elements of Chemical Engineering. McGraw Hill, New York 1936. [15] HAUSBRAND, E.; Das Trocknen mit Luft und Dampf, 5th ed. 1920. [16] STUTZKE, R. W.; U.S. patents 1,215,889 and 1,350,428. FOGLER, B. and KLEINSCHMIDT, R. V.; Ind. Eng. Chem. 1938 **30** 1372. EDELING, C.; Verfahrenstechnik. Z. VDI-Beiheft 1942, No. 57. MARSHALL, W. R. and SELTZER, E.; Principles of spray drying. Chem. Eng. Prog. 1950 **46** 501 and 575. BÄR, P.; Über die physikalischen Grundlagen der Zerstäubungstrocknung, thesis 1935, Karlsruhe. SELTZER, E. and SETTELMEYER, J. T.; Advances in Food Research, Vol. II, p. 399, 1949.

The catalytic polymerisation of linseed oil with sulphur dioxide

C. BOELHOUWER, E. F. BOON, W. v. KLAVEREN, A. SIEDSMA, M. C. WAGEMAKER and H. I. WATERMAN *

(Received 14 November 1951)

Summary—The catalytic polymerisation of linseed oil with sulphur dioxide was investigated. The presence of small amounts of oxygen proved to be indispensable for this reaction, complete absence of oxygen resulting in an activation (conjugation) of oil without a marked increase in viscosity. Stand oil was continuously prepared on a small scale in a column at a relatively low temperature (approx. 300° C), using sulphur dioxide as a catalyst.

Résumé—On a examiné la polymérisation catalytique d'huile de lin avec du bioxyde de soufre. La présence de faibles quantités d'oxygène parut nécessaire à cette réaction parce qu'une absence totale de l'oxygène résulte à une activation (conjugaison) d'huile sans une augmentation considérable de la viscosité.

La préparation continue d'huile siccative fut effectuée à petite échelle dans un appareil à colonnes à une température relativement basse (300° C environ) en utilisant du bioxyde de soufre comme catalyseur.

INTRODUCTION

The polymerisation of linseed oil with sulphur dioxide as a catalyst has been the subject of extensive studies in this laboratory. The catalytic action of sulphur dioxide was first described by WATERMAN and VAN VLODROP [1] and was also applied on a technical scale. In later experiments [2] preparation of stand oil was performed continuously, using relatively high temperatures (360° C).

* This research work was carried out by the collaboration of the Chemical Engineering group (Prof. H. I. WATERMAN) and the Mechanical Engineering group (Prof. E. F. BOON) of the Department of Chemical Engineering, The University, Delft, Holland.

The action of the catalyst is based on an *activation* of the linseed oil molecules, bringing about a conjugation of the linoleic and linolenic acid groups, which, according to Kappelmeier [3], polymerise easily at higher temperatures, giving cyclic reaction products [4].

In accordance with this conception, the polymerisation of linseed oil activated beforehand (*e.g.* with sulphur dioxide at 180°–200° C and 60 atm [5] or with other catalysts [6] takes place rather easily; the polymerisation of tung oil, consisting for the greater part of conjugated acid glycerides, is not greatly affected by sulphur dioxide.

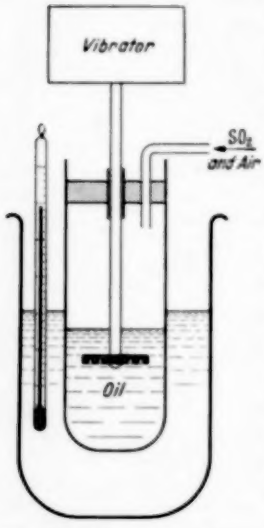

Fig. 1. Batch polymerisation of linseed oil.

In the catalytic manufacture of stand oil on a larger scale, difficulties arose in the mixing of oil and catalyst. A bell-stirrer, satisfactory in laboratory experiments, led to bad results in a semi-technical plant. Therefore another system was used for continuous stand oil preparation, using a packed column as the reactor.

As the influence of oxygen (air) on the polymerisation process cannot be neglected (this, of course, may be important when working in a closed apparatus), this problem was studied more closely in the following experiments.

Batch Experiments

Batch polymerisation experiments were made in a *Pyrex* reaction tube (contents approx. 1½ l), using 400 ml of a commercial bleached linseed oil in each experiment (Fig. 1). The tube was shut by means of a cork and heated in a metal bath. Stirring was performed by means of a vibrator [7], working as a churn and causing an intimate contact between oil and gas. Contact with the air was prevented as much as possible by using a fairly powerful stream of the gaseous catalyst and a narrow outlet-opening.

Two series of experiments were carried out, using different mixtures of sulphur dioxide and oxygen, at 300° C (45 min) and 330° C (15 min) respectively. The oil was heated to the desired temperature in 10–15 min, using carbon dioxide as an inert gas, which will have caused a fairly complete removal of peroxides present [5]; after the polymerisation the liquid was similarly cooled in a stream of carbon dioxide. The refractive indices (n_D^{20}), the viscosities (η) and the acid values of the reaction products were determined; the results are collected in Table 1 and Fig. 2.

Table 1. Batch polymerisation of linseed oil with sulphur dioxide and air. Amount of oil 400 ml in each experiment; oil preheated to the desired temperature in a CO_2-atmosphere

Catalyst		A) *Temp. 300° C, reaction time 45 min*			B) *Temp. 330° C, reaction time 15 min*		
SO_2 *l/hr*	*air l/hr*	n_D^{20}	η *(poise)*	*acid value*	n_D^{20}	η *(poise)*	*acid value*
12	0	1·4902	18	6	1·4885	16	10
12	1·8	1·4902	21	7	1·4891	18	8
12	3·6	1·4910	28	7	1·4905	21	9
12	5·4	1·4909	29	8	1·4905	32	13
12	7·2	1·4896	15	7	1·4894	18	10
0	10	1·4854	1·5	5	1·4837	1·5	6
Linseed oil (original)		1·4814	0·5	3			

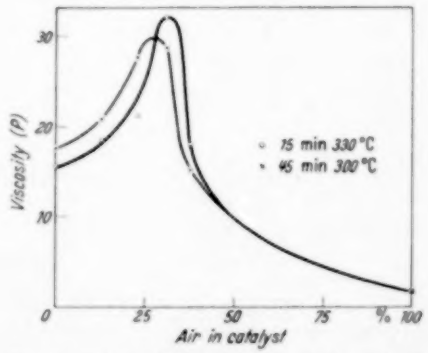

Fig. 2. Batch polymerisation of linseed oil with SO_2 and air.

It will be seen that air does influence the catalytic action of the sulphur dioxide, the most favourable composition of the catalyst containing approx. 30 vol.% of air. The total amount of oxygen used in the experiments was comparatively low; oxidation of the oil was therefore of little importance.

In some other experiments efficient precautions were taken to avoid any influence of traces of oxygen in the polymerisation experiments. The linseed oil was pre-treated with nitrogen (15 min at 290° C) in order to destroy any peroxides present in the

VOL. 1 1952

Table 2. Batch treatment of linseed oil with sulphur dioxide in the absence of oxygen. Amount of oil 50 ml.

Reaction conditions	Properties of reaction products						
	n_D^{20}	d_4^{20}	r_d^{20}	I. V. Wijs	acid value	Diene No. Ellis and Jones	Viscosity poises
A. Original oil	1·4808	0·9288	0·3063	178	4	1	0·5
1 hr 285° C, 8 l/hr SO_2	1·4861	0·9365	0·3066	155	—	14·5	2·5
1 hr 290° C, 8 l/hr SO_2	1·4879	0·9419	0·3058	142	—	15·5	5
1 hr 290° C, 12 l/hr SO_2	1·4874	0·9405	0·3060	143	5	15·5	4
B.* Original oil	1·4808	0·9283	0·3065	180	4	1	0·5
½ hr 300° C, 7 l/hr SO_2	1·4852	0·9363	0·3062	153	—	11·3	3
¼ hr 300° C, 7 l/hr SO_2	1·4867	0·9404	0·3057	146	—	12·0	4
¾ hr 300° C, 7 l/hr SO_2	1·4871	0·9391	0·3063	145	—	14·5	4
1 hr 300° C, 7 l/hr SO_2	1·4891	0·9474	0·3047	132	—	10·7	9

* In these experiments the sulphur dioxide was not treated with pyrogallol.

oil [5]; also, in some cases, the sulphur dioxide was distilled from solid pyrogallol [8].

These precautions had a remarkable influence on the results of the experiments, as is shown in Table 2. Although the refractive indices of the reaction products showed a considerable increase, the viscosity remained very low, and also the specific refraction did not alter very much. The diene values, on the other hand, were rather high. These observations may be compared with the results of the experiments of Waterman c.s. [5], in which linseed oil was "activated" by heating with sulphur dioxide at a temperature of about 200°C under a high SO_2 pressure, the activation being more marked, however, in the latter experiments.

From these results it may be concluded, in accordance with the views of Waterman, c. s. [1], [9] that the catalytic influence of the sulphur dioxide is restricted to the conjugation of the linseed oil fatty acid groups. Activation of linseed oil appears possible not only with high pressure sulphur dioxide, but also at atmospheric pressure, albeit at higher temperature. For the polymerisation of linseed oil small amounts of oxygen are indispensable. It may be advisable, therefore, to add a small percentage of oxygen to the catalyst in the catalytic (SO_2) manufacture of stand oil; in most cases, however, the oil to be heat bodied will contain a certain amount of oxygen as peroxides, which is sufficient for a normal course of the polymerisation process (compare Table 3).

Continuous Polymerisation of Linseed Oil

Continuous polymerisation of linseed oil with sulphur dioxide was performed in a packed column (40″ × 1″) of stainless steel, filled with aluminium turnings and externally heated by means of a Dowtherm system. Oil and gas were introduced into the bottom of the column and passed the reactor in concurrent flow (see Fig. 3). The oil was pre-heated in a metal bath *D*, the oil flow could be measured in *B* and was metered by means of a small gear pump *C* provided with a bypass valve *R*. The sulphur dioxide and air flow could be varied by means of the capillary tubes *K* and *L* and the heights of the mercury columns in the pressure regulators *M*; the gases were conveyed via the flow meters *I* in a mixing vessel *H* and introduced into the bottom of the column. The oil and

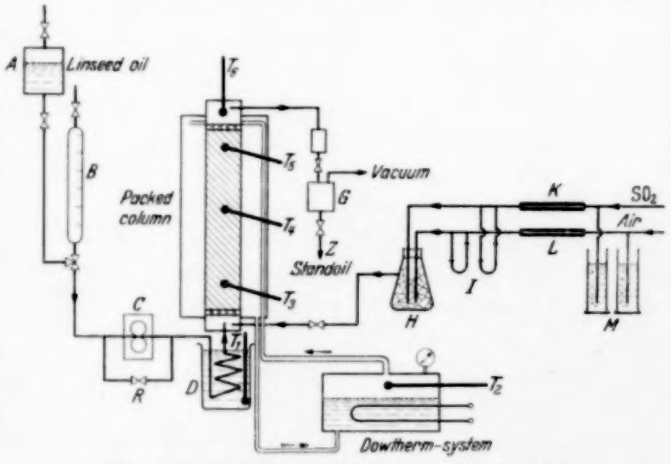

Fig. 3. Continuous polymerisation of linseed oil.

Table 3. Continuous polymerisation of linseed oil (non pretreated) with sulphur dioxide and air in a packed column. Volume of oil in the column 250 ml

Expt. No.	*Temp. °C*	*Catalyst* SO_2 *l/hr*	*Catalyst* *air l/hr*	*Linseed oil ml/min*	*Reaction time min*	n_D^{20}	*Viscosity in poises of the stand oil*	*Acid value*
1	290	1	0	5·8	43	—	13	14
2	290	1	0	5·0	50	1·4900	18[5]	14
3	290	1	0	3·9	64	1·4905	26	14
4	290	1	0	3·0	83	1·4910	33	16[5]
5	290	0·7	0·3	4·95	50	1·4889	16	14
6	290	0·7	0·3	3·8	66	1·4899	20	15
7	290	0·7	0·3	3·1	81	1·4903	28	17
8	300	0·7	0·3	5·0	50	1·4898	26	18
9	310	0·7	0·3	7·65	33	1·4900	22	20
10	320	0·7	0·3	8·1	31	1·4913	33	24
11	300	0·75	0	4·8	52	1·4907	28	18[5]
12	300	1·0	0	5	50	1·4907	27	17
13	300	1·25	0	5	50	1·4910	28[5]	18
14	300	1·50	0	4·9	51	1·4910	29	17
—		Linseed oil				1·4808	0·5	4

gas flow were adjusted in such a manner that good dispersion of gas in liquid was obtained; as was proved by preliminary experiments in a glass column small gas bubbles moved slowly upward in a regular stream, ensuring intimate contact between oil and catalyst. The reaction products, leaving the top of the column as a foam, flowed via the degasser *G* in the collecting vessel *Z*.

In some experiments the column was drained to measure the amount of oil in the reactor, in order to determine the contact time of the reaction and the rate of polymerisation. This amount appeared to be all but independent of the reaction conditions as used in our experiments, and was fixed at 250 ml of oil.

The application of the Dowtherm heating system made it possible during the experiments to maintain the temperature (thermometers T_3, T_4, T_5) along the column constant within 2°C.

Some of the results are collected in Table 3.

They show that continuous preparation of stand oil is possible at relatively low temperatures, using sulphur dioxide as a catalyst.

Varying the amount of catalyst (0·75–1·50 l/hr of SO_2, expts. 11–14) had no influence on the rate of viscosity increase. The addition of air appeared to be of no importance in these continuous experiments, the amount of oxygen in the non pretreated linseed oil apparently being sufficient for the polymerisation (expts. 2 and 5, 3 and 6, 4 and 7, 8 and 12).

The accumulation of free fatty acids is one of the main problems in continuous heat bodying of oils. Because of the relatively low temperatures which can be applied, the acid values of the polymerised oils, although rather high, can be kept within the Dutch standard specifications for zinc white stand oils [11].

When using temperatures above 300°C the formation of free fatty acids greatly increases, as follows from the experiments 8–10.

The results of the continuous heat bodying process of linseed oil, as regards the reaction time for preparation of stand oils of a certain viscosity, are in good agreement with batch experiments made at the same temperature and with the most favourable catalyst composition (Tables 1 and 3).

The packed column can easily be developed on a larger scale and be used for heat bodying of all types of drying oils, as temperature, flow of oil, amount of catalyst and eventually pressure can be widely varied.

The authors wish to express their gratitude to Ir. N. J. STENSTRA, Mr. W. A. KLAASSEN and Mr. J. A. BRENKMAN, for doing part of the experimental work.

REFERENCES

[1] WATERMAN, H. I. and VAN VLODROP, C.; J. Soc. Chem. Ind. 1936 **55** 333T; Brit. Pat. 480,677 (1936); U.S. Pat. 2,188,273 (1940). [2] WATERMAN, H. I., HAK, D. P. A. and PENNEKAMP, B.; J. Amer. Oil Chem. Soc. 1949 **26** 393. [3] KAPPELMEIER, C. P. A.; Farbenztg. 1933 **38** 1018 1077. [4] WATERMAN, H. I., CORDIA, J. P. and PENNEKAMP, B.; Research 1949 **2** 483. WATERMAN, H. I., KIPS, C. J. and STEENIS, J. v.; *ibid.* 1951 **4** 96. BOELHOUWER, C. and WATERMAN, H. I.; *ibid.* 1951 **4** 245. [5] WATERMAN, H. I., VLODROP, C. v. and PFAUTH, H. J.; Verfkroniek 1940 **13** 130; Research 1948 **1** 186. [6] WATERMAN, H. I. and VAN TUSSENBROEK, H. J.; Chemisch Weekblad 1929 **26** 566. WATERMAN, H. I. and VLODROP, C. v.; J. Soc. Chem. Ind. 1936 **55** 320T. RADLOVE, S. B., TEETER, H. M., BOND, W. H., COWAN, J. E. and KASS, J. P.; Ind. Eng. Chem. 1946 **38** 997. [7] A.G. für Chemie-Apparatebau, Zürich. [8] U.S.P. 2, 433, 270 (1948). [9] DE BOER, J. H., HOUTMAN, J. P. W. and WATERMAN, H. I.; Proc. Akad. Wetenschap, Amsterdam 1947 **50** 1181. [10] FONROBERT, E. and WACHHOLTZ, F.; Farbenztg. 1935 **40** 586. BOEKENOOGEN, H. A.; De Scheikunde der Oliën en Vetten, p. 382, Utrecht 1948. [11] Standard Specification N 598 of the Hoofdcommissie voor de Normalisatie in Nederland.

Distillation of multicomponent mixtures

W. R. VAN WIJK and H. A. C. THIJSSEN

Laboratorium voor Natuur- en Weerkunde, Landbouwhogeschool, Wageningen

(Received 7 January 1952)

Summary—A synopsis is given of a recent theory of distillation of multicomponent mixtures in which the product of absorption factors is calculated from a summation equation. A constant ratio of volatilities is assumed. The calculation of a distillation at variable reflux can be reduced to one at constant molar reflux. The theory is applied to a distillation at constant reflux. The summation equation is solved either by successive calculation of the absorption factor product or algebraically or by graphical methods. The successive calculation is by far the quickest if only one reflux ratio is considered. The algebraic method involves the solution of two algebraic equations of higher order than two. It is shown that the multicomponent mixture may be approximated by two binary mixtures and if this is done quadratic or even linear equations have to be solved only. Even so, however, the algebraic solution takes up much time. The graphical method is also based upon the approximation by binary mixtures. It is preferred to the algebraic method on account of its quickness and it is easily surveyable. Graphs are given from which all possible columns and reflux ratio's which lead to the desired distillate and residue, can be found.

Zusammenfassung—Ein Abriß einer neuen Theorie der Destillation von Mehrkomponentensystemen wird gegeben. Das Produkt der Absorptionsfaktoren wird aus einer Summengleichung berechnet. Konstante relative Flüchtigkeit wird angenommen. Die Destillation mit veränderlichem Rücklauf wird auf die Destillation mit konstantem Rücklauf zurückgeführt. Eine Destillation mit konstantem Rücklauf wird als Beispiel behandelt. Die Summengleichung wird gelöst mittels sukzessiver Berechnung des Produktes der Absorptionsfaktoren. Eine algebraische Lösung und graphische Methoden kommen gleichfalls zur Verwendung. Von diesen führt die sukzessive Berechnungsweise weitaus am schnellsten zum Ziele falls nur ein Rücklaufverhältnis berücksichtigt wird. Die algebraische Methode beruht auf der Lösung zweier Gleichungen höheren Grades. Das Mehrkomponentensystem kann aber durch zwei Zweikomponentensysteme approximiert werden und das eröffnet die Möglichkeit, die algebraische Lösung auf die Lösung linearer Gleichungen zurückzuführen. Dennoch sind die Rechnungen verhältnismäßig zeitraubend. Die graphische Methode beruht gleichfalls auf der Näherung durch Zweikomponentensysteme. Es wird dieser Methode wegen ihrer Übersichtlichkeit und Kürze der Vorzug vor der algebraischen gegeben. Alle möglichen Kolonnen und Rücklaufverhältnisse mit welchen man das gewünschte Destillat und Bodenprodukt bereiten kann, sind mittels einiger graphischer Darstellungen zu finden.

INTRODUCTION

During the past five years several papers have appeared on the subject of distillation of mixtures consisting of many components. Alternative analytical calculation methods have been developed by HARBERT [1], UNDERWOOD [4], MURDOCK [2] and SMITHUYSEN [3]. They are applicable to a distillation in which the molar reflux is constant and the volatilities of the components have a constant ratio. In these methods an algebraic equation of the Nth degree is arrived at, when the system contains N components and the calculation of the distillation is in principle reduced to the solution of two such algebraic equations, one for the stripping section and one for the top-section.

An extremely elegant method for calculating minimum reflex ratio has been given by UNDERWOOD but the calculation by these methods of a distillation at a finite reflux ratio, which is higher than the minimum reflux, has still remained a laborious procedure, involving a large number of numerical calculations.

One of the present authors has developed a theory in which the absorption factors of an arbitrary reference component are calculated on the different trays in a distillation column. The equation of conservation of heat is used to calculate these absorption factors and therefore, a variable reflux can be taken into account [6]. The theory is applicable to the most general type of distillation in which the relative volatilities may vary, heat loss may occur or even chemical reactions may take place between the components. In practical calculations, however, one has always first to consider the case of a constant relative volatility and further refinements are taken into account by successive approximation. No trial and error is involved thereby.

In this paper, a short summary will first be given of the theory, which is then applied to the calculation of a practical distillation.

It is impossible to present even an abridged version of the theory in the space available here. Therefore only the course of the reasoning is indicated and all equations that are of fundamental importance, or are used in the practical application, are given without proof. The reader, who is interested in the derivations, is referred to the original publication.

General Equations

Let us consider the stripping section of a distillation column. The trays are numbered upwards, so tray number m lies below the $(m+1)$th tray. The reboiler is indicated by $m = 0$.

The liquid and vapour rates of any arbitrary component are related by the basic equations:

$$L_{i,m+1} = V_{i,m} + B_i \tag{1}$$

$$L_{i,m} = V_{i,m} A_m/\alpha_{i,m} \dagger. \tag{2}$$

From these equations one can calculate $L_{i,m+1}$ and doing this one obtains the well known expression:

$$L_{i,m+1} = B_i \sum_{k=0}^{k=m} 1/(A_m \alpha_{i,m}^{-1} A_{m-1} \alpha_{i,m-1}^{-1} \ldots A_{m-k} \alpha_{i,m-k}^{-1}) + \left. \begin{array}{r} \\ + V_{i,0}/(A_m \alpha_{i,m}^{-1} \ldots A_1 \alpha_{i,1}^{-1}) . \end{array} \right\} \tag{3}$$

The product of the absorption factors of the reference component on the successive trays $1, 2 \ldots k$ will be written as $Ap(k)$. So,

$$Ap(k) = A_1 . A_2 \ldots A_k$$

and by definition

$$Ap(0) = 1 \tag{4}$$

A similar notation is adopted for the product of the relative volatilities:

$$\alpha p(i,k) = \alpha_{i,1} . \alpha_{i,2} \ldots \alpha_{i,k} \quad \text{and} \quad \alpha p(i,0) = 1 . \tag{5}$$

Introducing the newly defined functions $Ap(k)$ and $\alpha p(i,k)$ in eq. (3) and abbreviating $\sum_{k=0}^{k=m}$ to Σ_k leads to:

$$L_{i,m+1} = \frac{1}{Ap(m)} \left\{ B_i \Sigma_k \frac{\alpha p(i,m)}{\alpha p(i,k)} Ap(k) + V_{i,0}\, \alpha p(i,m) \right\} . \tag{6}$$

For a constant relative volatility one has $\alpha p(i,k) = \alpha_i^k$ and then eq. (3) becomes:

$$L_{i,m+1} = \frac{1}{Ap(m)} \left\{ B_i \Sigma_k \alpha_i^{m-k} Ap(k) + V_{i,0} \alpha_i^m \right\} . \tag{7}$$

A constant relative volatility will be assumed in the following.

This equation expresses $L_{i,m+1}$ in terms of the absorption factor product for all components for which a residue rate B_i and a vapour reflux $V_{i,0}$ is specified. It is, however, not possible to specify beforehand both the distillate rate and the residue rate for all components in a multicomponent mixture. It can be proven that this can be done for 4 components at most, so that there are a number of components for which either the distillate rate or the residue rate remains unspecified. Components for which both D_i as well as B_i are specified are called key components. If the distillate rate is unspecified but diminishing as compared with the total distillate rate, the component is called unspecified in the top, and, if the residue rate is negligible, the component is unspecified in the bottom section. Components which have a residue- and distillate rate that cannot be specified *a priori* but which are both non-negligible are called intermediate components.

In the following, only two key components are assumed to be present and no intermediate components. There are, however, unspecified components. For those which have a negligible residue rate (they are volatile components) it is not practical to use eq. (6), especially since their residue rate varies with number of plates and reflux, though it remains extremely small. These components are present in finite quantities only in the top section and on a few trays below the feed tray. We shall, therefore, express their liquid rate in the absorption factor product and in their vapour rates at the feed tray. One obtains from eq. (1) and (2) if B_i becomes equal to zero:

$$L_{u,m+1} = \frac{\alpha_u^{m-(M+1)}}{Ap(m)} Ap(M+1) \frac{V_b}{V_t} V_{u,N+1} . \tag{8}$$

The index $M+1$ is used to denote the feed plate when it is considered as a tray in the bottom section and $N+1$ is used when it is considered as belonging to the top section. The magnitude $Ap(M+1)$ is the product of absorption factors in the stripping section on tray $M+1$, which is the feed tray.

It has been shown that a distillation in which the reflux is variable can be calculated in exactly the same way as a distillation at constant reflux, if instead of the liquid and vapour rates other quantities are introduced. They are called generalized liquid and vapour rates and have been defined in the previous papers [5], [6]. For simplicity, constant reflux only is discussed here.

Constant Molar Reflux

For a distillation in which the molar liquid rate may be considered as constant in the stripping section, addition of the liquid rates for all components leads to a constant value L_b. The resulting equation is used for the calculation of the absorption factor product. One obtains on addition of eq. 7 and 8 for all components:

$$Ap(m)\, L_b = \Sigma_i' \left\{ \Sigma_k B_i \alpha_i^{m-k} Ap(k) + V_{i,0} \alpha_i^m \right\} + \left. \begin{array}{r} \\ + Ap(M+1) \frac{V_b}{V_t} \Sigma_u'' \alpha_u^{m-(M+1)} V_{u\,N+1} . \end{array} \right\} \tag{9}$$

† A list of notations is given at the end of the paper.

VOL. 1 1952

The notation Σ_i' indicates that only the components with a specified residue rate are included in the summation and Σ'' means a summation over the unspecified components. It may be recalled that besides constant reflux, constant ratio of volatilities is assumed and two keys and no intermediate components present. One obtains for the solution of eq. (9) the following expression:

$$Ap(m) = Ap_1(m) + Ap(M+1)\,\Sigma_u'' C_u \alpha_u^{m-(M+1)}. \quad (10)$$

In this equation $Ap_1(m)$ has been written for the solution of eq. (9) if all unspecified components are omitted and C_u is:

$$C_u = \frac{V_b}{V_t}\,\frac{V_{u,N+1}}{L_b - \Sigma_k' \alpha_u^{k-m}\,u(m-k)}\,\dagger. \quad (11)$$

The function $u(m-k)$ is written as an abbreviation of

$$\Sigma_i' B_i \alpha_i^{m-k}.$$

At the feed tray the same temperature and, if the variation of the pressure along the column must be taken into account, the same pressure must be found, irrespective of the fact that its absorption factor is obtained by a calculation from the absorption factor product in the stripping section or from the top section. Therefore, the same equilibrium constant of the reference component must be obtained in both cases. This condition provides a relation between the numbers of ideal trays in both sections and the reflux ratio. The absorption factor in the stripping section at the mth tray is equal to $Ap(m)/Ap(m-1)$ and therefore, the reciprocal value of the equilibrium constant at the mth tray is equal to

$$K_{r,m}^{-1} = \frac{V_b}{V_t}\,\frac{Ap(m)}{Ap(m-1)}. \quad (12)$$

In the top section similar equations are obtained as for the stripping section if $V_{i,n+1}$, $L_{i,n}$, D_i and $S_{i,n}$ are substituted for $L_{i,m+1}$, $V_{i,m}$, B_i and $A_{i,m}$ respectively. The plates are numbered downwards and $n = 0$ for the condensor. Instead of the absorption factor product, here the stripping factor product $Sp(n)$ can be calculated from a linear summation equation, which is the analogon of eq. (9). One finds for a component which is specified in the top section:

$$V_{i,n+1} = \frac{1}{Sp(n)}\left\{D_i \Sigma_k' \alpha_i^{-n+k}\,Sp(k) + L_{i,0}\,\alpha_i^{-n}\right\} \quad (13)$$

and for an unspecified component:

$$V_{u,n+1} = \frac{\alpha_u^{-n+(N+1)}}{Sp(n)}\,Sp(N+1)\,\frac{L_b}{L_t}\,L_{u,M+1}. \quad (14)$$

The equation for the calculation of $Sp(n)$ becomes:

$$\left.\begin{aligned} Sp(n)\,V_t = \Sigma_i'\left\{\Sigma_k' D_i \alpha_i^{-(n-k)}\,Sp(k) + L_{i,0}\,\alpha_i^{-n}\right\} + \\ + Sp(N+1)\,\frac{L_b}{L_t}\,\Sigma_u'' \alpha_u^{-n+(N+1)}\,L_{u,M+1}. \end{aligned}\right\} \quad (15)$$

Of course the components which are unspecified in the top section are different from those in the bottom section and, therefore, a component with index u in eq. (15) is different from the components denoted by u in eq. (9). If it is necessary to point to this distinction, a second subscript b or t respectively, is added to indicate that the component is unspecified in the bottom or top section, respectively.

The solution of eq. (15) is:

$$Sp(n) = Sp_1(n) + Sp(N+1)\,\Sigma_u'' C_u \alpha_u^{-n+(N+1)} \quad (16)$$

for moderate and large values of N and

$$C_u = \frac{L_t}{L_b}\,\frac{L_{u,M+1}}{V_t - \Sigma_k' \alpha_u^{n-k}\,u(n-k)}. \quad (17)$$

Here $u(n-k)$ is written for $\Sigma_i' D_i \alpha_i^{-(n-k)}$. Since $Sp(n)/Sp(n-1)$ is the stripping factor in the top section, the equilibrium constant of the reference component is obtained as:

$$K_{r,n} = \frac{L_t}{V_t}\,\frac{Sp(n)}{Sp(n-1)}. \quad (18)$$

At the feed tray we must have:

$$K_{r,M+1}^{-1} = K_{r,N+1}^{-1} = \frac{V_b}{L_b}\,\frac{Ap(M+1)}{Ap(M)} = \frac{V_t}{L_t}\,\frac{Sp(N)}{Sp(N+1)}. \quad (19)$$

It is clear from eq. (10) and (16), that first the absorption factor product and the stripping factor product must be calculated, neglecting the unspecified components. This can be done either step by step, so that first $Ap(1)$ is calculated for $m = 1$, then this value is inserted in eq. (9) for $m = 2$ and $Ap(2)$ is calculated and so on, or by solving eq. (10) analytically. The analytical solutions are:

$$Ap_1(m) = \Sigma_i' c_{i,b}\,\varphi_{i,b}^m \quad (20)$$

$$Sp_1(n) = \Sigma_i' c_{i,t}\,\varphi_{i,t}^n. \quad (21)$$

The second subscripts are added here in order to make it clear that different constants are obtained in both formulae, but they will not be retained in cases where confusion is out of question. The symbols have the following meaning:

† In the first publication c_u was used instead of C_u. This might, however, cause confusion with constants c_i, defined in that article, which have a slightly different meaning. The approximative value D_u is used in that paper in the final equations, instead of $V_{u,N+1}$ which was used in the derivation itself [5].

The quantity $\varphi_{i,b}^{-1}$ is a root of the algebraic equation containing the purely mathematical magnitude t as unknown variable:

$$L_b = \Sigma_i' \frac{B_i}{1-\alpha_i t} \tag{22}$$

$$e_{j,b} = \lim_{t=\varphi_{j,b}^{-1}} (1-\varphi_{j,b}\, t)\, \frac{\Sigma_i' V_{i,0}/(1-\alpha_i t)}{L_b - \Sigma_i' B_i/(1-\alpha_i t)} \tag{23}$$

and $\varphi_{i,t}^{-1}$ is a root of the algebraic equation:

$$V_t = \Sigma_i' \frac{D_i}{1-\alpha_i^{-1}} \tag{24}$$

$$e_{j,t} = \lim_{t=\varphi_{j,t}^{-1}} (1-\varphi_{j,t}\, t)\, \frac{\Sigma_i' L_{i,0}/(1-\alpha_i^{-1} t)}{V_t - \Sigma_i' D_i/(1-\alpha_i^{-1} t)}. \tag{25}$$

Table 1. Separation scheme of 6 comp. system, pressure 20 atm. The product rates are in moles per unit of time

Comp.	*Dist.*	*Res.*	*Vapour feed*	*Liq. feed*	$\alpha_{i,F}$	$\alpha_{i,t}$	$\alpha_{i,b}$
1	0·259	—	0·250	0·010	20·6	34·4	—
2	0·090	—	0·078	0·012	5·07	7·23	—
3	0·247	0·004	0·180	0·070	2·06	2·63	1·96
4	0·003	0·167	0·095	0·075	1·00	1·00	1·00
5		0·110	0·038	0·072	0·429		0·497
6		0·120	0·025	0·095	0·206		0·272
	0·599	0·401	0·666	0·334			

The eq. (22) and (24) are, in principle, the same equations which have also been obtained by the authors referred to in the beginning of this paper. However, it follows from the structure of the eq. (10) and (16) that not the individual components but only the functions $u(m-k)$ and $u(n-k)$ appear under the sign of summation. This means that all distillations in which these functions are the same, lead to the same eq. (22) and (24). In the authors' opinion, this is a point of fundamental importance for the theory of distillation. It is also very important for practical application, since it opens the possibility of a well founded method for approximation of a multi-component mixture by a mixture containing less components. The degree of the eq. (22) and (24) may thereby appreciably be reduced [7].

After the functions $Ap_1(m)$ and $Sp_1(n)$ have been obtained a simple calculation shows that:

$$\left.\begin{aligned} \frac{V_b}{L_b}\,\frac{Ap(M+1)}{Ap(M)} = \frac{V_b}{L_b}\,\frac{Ap_1(M+1)}{Ap_1(M)} \times \\ \times \frac{1}{1-\Sigma_u'' C_u + Ap_1(M+1)\,(\Sigma_u'' C_u\, \alpha_u^{-1})/Ap_1(M)} \end{aligned}\right\} \tag{26}$$

and

$$\frac{V_t}{L_t}\,\frac{Sp(N)}{Sp(N+1)} = \frac{V_t}{L_t}\left\{(1-\Sigma_u'' C_u)\,\frac{Sp_1(N)}{Sp_1(N+1)} + \Sigma_u'' C_u\, \alpha_u\right\}.$$

Discussion of Example

The theory will now be applied to the actual calculation of a distillation. A separation will be considered that has been treated by another author (JENNY) who used a plate-to-plate calculation method of the liquid and vapour rates [2]. The separation scheme is as follows:

The temperature of the feed is 79·5° C. The relative volatilities $\alpha_{i,F}$ correspond to that temperature. There is some uncertainty about the best choice of the average relative volatilities in both sections owing to the variation of α_i with temperature. The arithmetic mean value of the top- and feed temperature has been taken as the relevant temperature for $\alpha_{i,t}$ and similarly the arithmetic mean value between bottom- and feed temperature has been used for $\alpha_{i,b}$. This applies in both cases to the specified components only. The relative volatility of an unspecified component will be taken equal to $\alpha_{i,F}$ since these components occur only on a few trays near the feed tray. There exist theoretical reasons for a choice of the average α of the specified components which is closer to the relative volatility at the feed tray, if large numbers of trays are involved.

In the following calculations the values from Table 1 have, however, been used in all cases since it is thought that before refinements are introduced, the straight forward calculation methods should be discussed first. The functions $u(m-k)$ for the bottom section and $u(n-k)$ for the top section are represented in Fig. 1 a and b. These functions have been obtained as the sum of the 4 straight lines which are the graphs of $B_i \alpha_i^{m-k}$ or $D_i \alpha_i^{-(n-k)}$ when plotted on semi-logarithmic paper. The dotted lines and the circles in the figures will be discussed later.

Stepwise Calculation of $Ap(m)$ and $Sp(n)$

The absorption factor product for any assumed reflux ratio can now be calculated from eq. (9) in which the unspecified components are neglected. For a reflux

VOL. 1 1952

ratio $R_D = 1{\cdot}50$ in the top section one has $L_t = 0{\cdot}899$, $V_t = 1{\cdot}498$, $L_b = 1{\cdot}233$, $V_b = 0{\cdot}832$ and thus one has if $V_{i,0}$ is set equal to $B_i V_b/B$ *i.e.* if the vapour reflux has the same composition as the residue $Ap_1(0) = 1$, $Ap_1(1) \times 0{\cdot}832 = 0{\cdot}264 + 2{\cdot}06 \times 0{\cdot}264$, $Ap_1(1) = 0{\cdot}972$.

$Ap_1(2) \times 0{\cdot}832 = 0{\cdot}972 \times 0{\cdot}264 + 0{\cdot}218 + 2{\cdot}06 \times 0{\cdot}218$,

$Ap_1(2) = 1{\cdot}115$.

$Ap_1(3) \times 0{\cdot}832 = 1{\cdot}115 \times 0{\cdot}264 + 0{\cdot}972 \times 0{\cdot}218 + 0{\cdot}213 + 2{\cdot}06 \times 0{\cdot}213$,

$Ap_1(3) = 1{\cdot}395$

and so on. For the calculation of $Sp_1(n)$ in the top section eq. (15) is used and we have $L_{i,0} = D_i \,.\, L_t/D$ in this case. The values of $Ap_1(m)$, $Sp_1(n)$ and $V_b Ap_1(M+1)/L_b Ap_1(M)$ and $V_t Sp_1(N)/L_t Sp_1(N+1)$ are given in Table 2. The latter two variables have been denoted by ξ_1 and η_1 respectively. They are equal to the reciprocal value of the equilibrium constant of the reference component. This is, however, no longer so with variable reflux.

This stepwise calculation is different from conventional plate-to-plate calculations. In the latter material balance equations and equilibrium conditions are used alternatively for each component to calculate its flow rate or concentration. Here the single eq. (9) or (15) is used to calculate the absorption or stripping factor product. The equilibrium conditions are automatically satisfied.

The unspecified components have been neglected in these calculations as is indicated by the subscript 1 added to $Ap(m)$, $Sp(n)$, ξ and η.

CORRECTION FOR UNSPECIFIED COMPONENTS

We shall now correct the above values for the presence of the unspecified components, assuming that the tray under consideration has been selected as the feed tray.

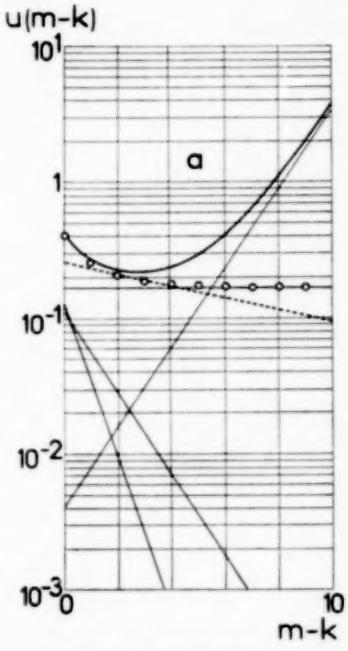

Fig. 1a. Characteristic function for stripping section.

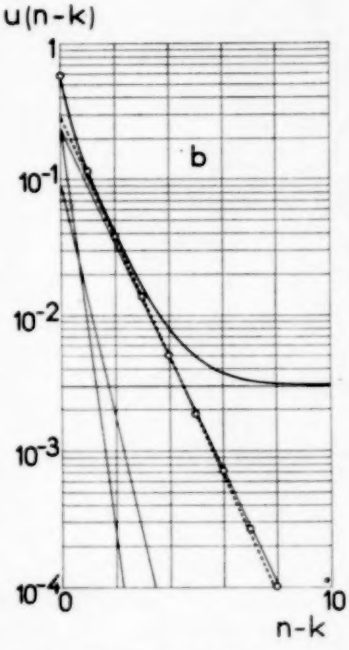

Fig. 1b. Characteristic function for top section.

In that case ξ and η are given by the expressions 26 and 27 respectively. The constants C_u are calculated by eq. (11) for the stripping section and by eq. (17) for the top section. Owing to the fact that the relative volatility of an unspecified component is high in the bottom section and that it is small in the top section, important simplifications can be introduced in these formulae.

Table 2. Absorption and stripping factors and ξ, η values for 6 component system at $R_D = 1{\cdot}50$

morn	$Ap_1(m)$	$Sp_1(n)$	$\xi_1(m)$	$\eta_1(n)$	$\xi_I(M+1)$	$\eta_I(N+1)$	$\xi_{II}(M+1)$	$\eta_{II}(N+1)$
1	0·972	0·328	0·656	5·080				
2	1·115	0·156	0·799	3·504				
3	1·395	0·0822	0·844	3·162				
4	1·840	0·0465	0·890	2·945	1·157	2·19	1·18	2·41
5	2·560	0·0293	0·939	2·641	1·220	1·96	1·24	2·16
6	3·770	0·0211	0·994	2·321	1·291	1·72	1·32	1·89
7	5·849	0·0171	1·047	2·056	1·360	1·53	1·39	1·67
8	9·687	0·0151	1·110	1·884	1·442	1·40	1·48	1·53
9	16·920	0·0142	1·179	1·774	1·532	1·32	1·57	1·44
10	30·880	0·0137	1·232	1·723	1·601	1·28	1·64	1·39

If all terms containing α_u^{-1} are neglected in eq. (26), one finds in the stripping section for the function ξ corrected to the first order:

$$\xi_I(M+1) = \xi_1(M+1) \Big/ \left(1 - \frac{\Sigma'' D_u}{V_t}\right). \qquad (28)$$

Here $\Sigma'' D_u = D_1 + D_2 = 0{\cdot}349$ and $V_t = 1{\cdot}498$; therefore $\xi_I(M+1) = 1{\cdot}30\,\xi_1(M+1)$.

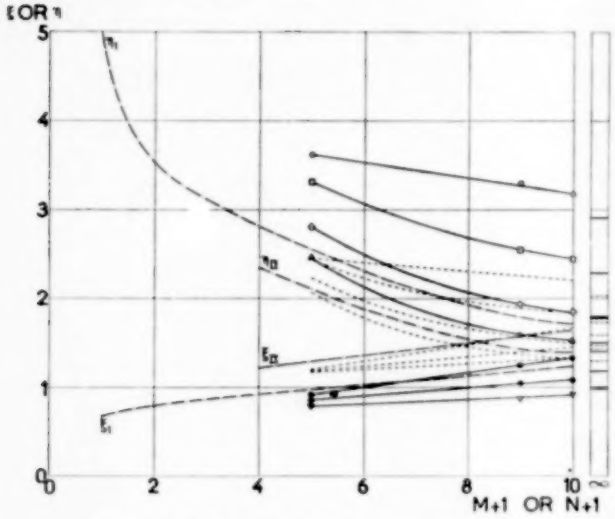

Fig. 2. Values of ξ and η for six component system as a function of $M+1$ and $N+1$. ·-·- Stepwise calculation for $R_D = 1{\cdot}50$. I. not corrected for unspec. comp. II. corrected to second order. —— Analytical calculation, not corrected for unspec. comp.

ξ: ◓ $R_D = 1{\cdot}78$; ◑ $R_D = 1{\cdot}12$; ▽ $R_D = 0{\cdot}765$

η: △ $R_D = 1{\cdot}94$; ◇ $R_D = 1{\cdot}27$; □ $R_D = 0{\cdot}764$; ○ $R_D = 0{\cdot}51$

----- Analytical calculation, corrected to second order.

In the top section, the first order correction of η_I is obtained by neglecting in eq. (27) all terms that contain a factor α_u. This gives:

$$\eta_I(N+1) = \left(1 - \frac{\Sigma'' B_u}{L_b}\right)\eta_1(N+1). \qquad (29)$$

Since $\Sigma'' B_u = B_5 + B_6 = 0{\cdot}230$ and $L_b = 0{\cdot}899$, one has $\eta_I(N+1) = 0{\cdot}744\,\eta_1(N+1)$.

The values of ξ and η corrected to the second order are obtained when terms containing a factor α_u^{-1} in eq. (11) and a factor α_u in eq. (16), respectively, are also retained but higher powers are still neglected. One has:

$$\left.\begin{aligned}\xi_{II}(M+1) &= \\ &\frac{\xi_1(M+1)}{1 - \dfrac{\Sigma'' D_u}{V_t} + \dfrac{\Sigma'' D_u \alpha_{u,F}^{-1}}{V_t}\left(\xi\dfrac{L_t}{V_t} + \dfrac{\Sigma' B_i \alpha_{i,b}}{V_b} - \dfrac{Ap_1(M+1)}{Ap_1(M)}\right)}\end{aligned}\right\} (30)$$

$$\left.\begin{aligned}\eta_{II}(N+1) &= \eta_1(N+1) \times \\ &\times\left\{1 - \frac{\Sigma'' B_u}{L_b} - \frac{\Sigma'' B_u \alpha_{u,F}}{L_b}\left(\frac{1}{\eta}\cdot\frac{V_b}{L_b} + \frac{\Sigma' D_i \alpha_{i,F}^{-1}}{L_t}\right)\right\} + \\ &+ \frac{\Sigma'' B_u \alpha_{u,F}}{L_b}\cdot\frac{V_t}{L_t}.\end{aligned}\right\} (31)$$

In the present example $\Sigma'' D_u \alpha_{u,F}^{-1} = 0{\cdot}030$, $\Sigma' B_i \alpha_{i,b} = 0{\cdot}247$ and $\Sigma'' B_u \alpha_{u,F} = 0{\cdot}0726$, $\Sigma'' D_i \alpha_{i,F}^{-1} = 0{\cdot}153$. If these values are inserted in eq. (30) and (31) one finds

$$\xi_{II}(M+1) = \xi_1(M+1) \Big/ \left\{0{\cdot}767 + 0{\cdot}020\left[0{\cdot}600\,\xi + 0{\cdot}296 - \frac{Ap_1(M+1)}{Ap_1(M)}\right]\right\}$$

and

$$\eta_{II}(N+1) = \eta_1(N+1)\left\{0{\cdot}744 - 0{\cdot}059\left[0{\cdot}675\,\frac{1}{\eta} + 0{\cdot}171\right] + 0{\cdot}099\right\}.$$

In these corrections it has been assumed that the product rates of the unspecified components are negligible compared with those of the specified components. This condition can only be fulfilled by a sufficient number of trays in each section. It is for that reason that only corrected values of ξ and η from m or $n = 4$ upwards have been included in Table 2. The amount of unspecified components in the terminal products can be estimated from eq. (8) or (14).

The values ξ and η have been plotted as a function of $M+1$ or $N+1$ respectively in the same graph (Fig. 2). The feed may be introduced at any tray for which $\xi = \eta$. This graph gives therefore all columns with which the separation can be performed for the selected value of L_b if the calculation of $Ap_1(m)$ and $Sp_1(n)$ is continued sufficiently far. Possible combinations are *e.g.* $M+1 = 10$ and $N+1 = 7$ or 9 trays below the feed tray and 6 trays above it, or $M+1 = N+1 = 8{\cdot}5$.

Analytical solution

The functions $Ap_1(m)$ and $Sp_1(n)$ may also be calculated from the analytical solutions eq. (20) and (21) respectively. The eq. (22) and (24) are both of the fourth degree in our case and solving these would be a laborious procedure. We shall therefore approximate the functions $u(m-k)$ and $u(n-k)$ by those for a binary mixture. For this purpose the sum $B_6\alpha_6^m + B_5\alpha_5^m + B_4$ is approximated by a single exponential function $B_b\alpha_b^m$ in the stripping section from $m = 1$ on upwards [3]. The latter function is represented by the dotted straight line in Fig. 1 a; one has $\alpha_b = 0{\cdot}88$ and $B_b = 0{\cdot}253$. The function $u^*(m) = B_b\alpha_b^m + B_3\alpha_3^m$ is now an approximation for $u(m)$ from $m = 1$ upwards. Introducing $L_b^* = L_b + u^*(0) - u(0)$ and

VOL. 1 1952

Table 3. Data for analytical solution of eq. (9)

L_b^*	L_b	V_b	L_t	R_D	$\varphi_{3,b}$	φ_b	$c_{3,b}$	c_b
1·258	1·402	1·001	1·078	1·78	1·97	1·10	0·0219	0·69
0·856	1·000	0·599	0·666	1·12	1·98	1·25	0·0375	0·71
0·646	0·790	0·389	0·456	0·765	2·00	1·43	0·0775	0·71

inserting $u^*(m-k)$ instead of $u(m-k)$ for $m-k = 1, 2, 3$ etc. in eq. (9) leads to the equation:

$$Ap_1(m)\, L_b^* = \Sigma_k\, u^*(m-k)\, Ap_1(k) + R_B\, u^*(m). \quad (32)$$

The unspecified components are again neglected here. Its solution is $Ap_1(m) = c_b\, \varphi_b^m + c_3\, \varphi_3^m$ from $m = 1$ on upwards, whereas $Ap_1(0) = 1$ and φ_b^{-1} and φ_3^{-1} are the roots of the quadratic equation

$$L_b^* = \frac{B_b}{1-\alpha_b t} + \frac{B_3}{1-\alpha_3 t}.$$

The constants c are according to eq. (23) equal to

$$c_b = \frac{L_b^*}{u(0)} \cdot \frac{(1-\alpha_b\varphi_b^{-1})(1-\alpha_3\varphi_b^{-1})}{1-\varphi_3\varphi_b^{-1}}$$

and

$$c_3 = \frac{L_b^*}{u(0)} \cdot \frac{(1-\alpha_b\varphi_3^{-1})(1-\alpha_3\varphi_3^{-1})}{1-\varphi_b\varphi_3^{-1}}.$$

Instead of assuming a value for L_b^* and solving the quadratic equation it is more convenient to assume a value for one of the roots say φ_3^{-1} and calculate L_b^* and φ_b^{-1} which can be done by solving a linear equation in either case. One has $\varphi_3^{-1}\varphi_b^{-1} = (L_b^* - B_b - B_3)/\alpha_3\alpha_b$. The data for these calculations for some L_b^* values are given in Table 3.

The following values of $Ap_1^*(m)$ have been calculated from this Table.

Table 4. Values of $Ap_1^*(m)$

L_b^*	$Ap_1^*(4)$	$Ap_1^*(5)$	$Ap_1^*(8)$	$Ap_1^*(9)$	$Ap_1^*(10)$
1·258	1·343	1·76	6·47	11·23	21·08
0·856	2·331	3·34	13·03	22·80	41·30
0·646	4·200	6·72	32·20	57·40	100·00

The corresponding values of ξ_1 are plotted in Fig. 2 and also the values of ξ_{II} corrected to the second order. It follows from eq. (20) that $\xi_1(m=\infty) = \frac{V_b}{L_b}\varphi_{3,b}$.

In the top section $u(n)$ is approximated by $u^*(n) = D_t\alpha_t^{-n} + D_4$ from $n = 1$ on upwards. Here $\alpha_t = 2{\cdot}76$ and $D_t = 0{\cdot}287$. Introducing $V_t^* = V_t - u(0) + u^*(0)$ one obtains the following equation for $Sp_1(n)$

$$Sp_1(n)\, V_t^* = \Sigma_k\, u^*(n-k)\, Sp_1(k) + R_D\, u^*(n) \quad n = 1, 2, 3 \ldots$$

Its solution is $Sp_1(n) = c_t\, \varphi_t^n + c_4\, \varphi_4^n$ and $Sp_1(0) = 1$. The equation

$$V_t^* = \frac{D_t}{1-\alpha_t^{-1}t} + \frac{D_4}{1-t}$$

has the roots φ_t^{-1} and φ_4^{-1} and the constants c_t and c_4 are equal to

$$c_t = \frac{V_t^*}{u(0)} \cdot \frac{(1-\alpha_t^{-1}\varphi_t^{-1})(1-\varphi_t^{-1})}{1-\varphi_4\varphi_t^{-1}}$$

and

$$c_4 = \frac{V_t^*}{u(0)} \cdot \frac{(1-\alpha_t^{-1}\varphi_4^{-1})(1-\varphi_4^{-1})}{1-\varphi_t\varphi_4^{-1}}.$$

The roots φ_4 and φ_t are related by the expression $\varphi_4^{-1}\varphi_t^{-1} = (V_t^x - D_t - D_4)\,\alpha_4\,\alpha_t$. The calculated values of φ_4 etc. are collected in Table 5 and the η's are shown in Fig. 2.

In graph 3 the top reflux R_D has been chosen as the independent variable. The curves are ξ and η values for a constant number of trays in each section. The corrected curves for an infinite number of trays intersect at $R_D = 1{\cdot}0$. This is the minimum reflux for which JENNY has found 0·96 by plate to plate calculations. Differences of a few percent may be expected owing to the special choice of the relative

Table 5. Analytical solution for $Sp_1^*(n)$

V_t^*	V_t	L_t	L_b	R_D	$\varphi_{4,t}$	φ_t	$c_{4,t}$	c_t
1·45	1·759	1·160	1·494	1·94	1·003	0·450	0·01023	0·575
1·05	1·359	0·760	1·094	1·27	1·005	0·497	0·0144	0·615
0·747	1·056	0·457	0·791	0·764	1·010	0·585	0·027	0·660
0·595	0·904	0·305	0·639	0·510	1·020	0·690	0·060	0·670

volatilities. The curve $M+1=9$ intersects the curve $N+1=9$ at $R_D=1{\cdot}5$ so that $8+1+8$ trays are necessary to perform the separation at this reflux ratio, whereas we have found $7{\cdot}5+1+7{\cdot}5$ by the stepwise solution method. Graph 3 gives a complete survey of all possible columns and all the reflux ratios with which the desired distillate and residue can be obtained.

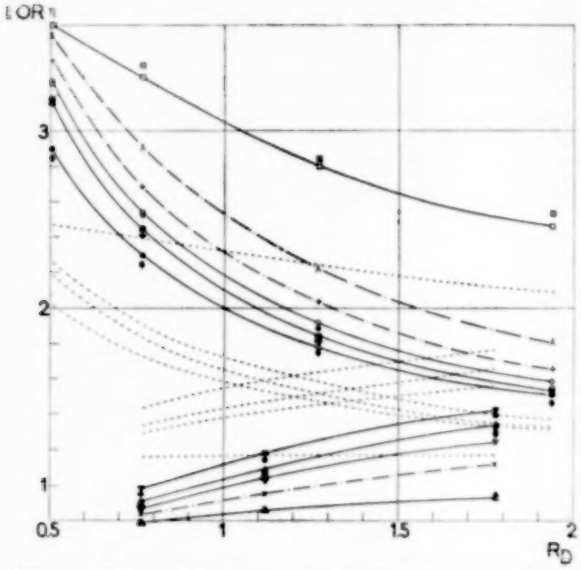

Fig. 3. Values of ξ and η for six component as a function of R_D. —— ξ and η not corrected for unspec. comp. from analytical calculation.

△ $M+1=5$ □ $N+1=5$
▽ $M+1=9$ ○ $N+1=9$
▲ $M+1=10$ ⊖ $N+1=10$
▼ $M+1=\infty$ ⌀ $N+1=\infty$

····· idem, but corrected for unspec. comp. to second order. —·— ξ and η not corrected for unspec. comp. from McCABE-THIELE diagrams.

ξ: ▲ $M+1=5$; ▽ $M+1=9$; ◐ $M+1=10$; ◒ $M+1=\infty$
η: ⊡ $N+1=5$; ⊙ $N+1=9$; ⊖ $N+1=10$; ⌀ $N+1=\infty$

and $\times\,\xi$ for $M+1=7$; $+\,\eta$ for $N+1=8$; $\lambda\,\eta$ for $N+1=7$.

Another useful representation is given in Fig. 4 in which the curves represent ξ and η values for a constant value of L_b and V_t respectively, and the number of trays in each section is plotted as absissa. This representation is still more general than the former one since it can also be used if the degree of vaporization of the feed is varied. This simply means that another L_b corresponds to a given V_t and so one has to combine different pairs of curves for different degrees of vaporization. So for example a minimum reflux of $R_D=0{\cdot}67$ would have been found in case of no vaporization of the feed $V_b=V_t$. The representation in Fig. 3 could also have been given a more general character if instead of R_D the corresponding L_b and V_t had been plotted.

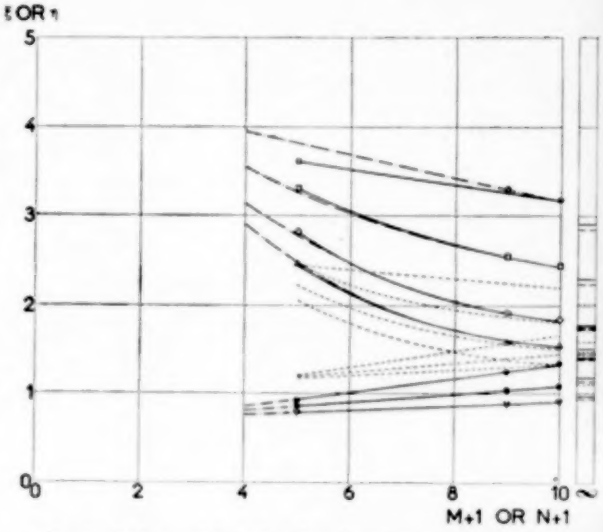

Fig. 4. Values of ξ and η for six component system as a function of $M+1$ and $N+1$. —— Not corrected for unspec. comp. from analytical calculation.

ξ: ◓ $L_b=1{\cdot}402$; ◑ $L_b=1{\cdot}000$; ▽ $L_b=0{\cdot}790$
η: ○ $V_t=1{\cdot}759$; □ $V_t=1{\cdot}359$; ◇ $V_t=1{\cdot}056$; △ $V_t=0{\cdot}904$

····· ξ and η corrected to second order for unspec. comp. —·— ξ and η not corrected from McCABE-THIELE diagrams.

GRAPHICAL SOLUTION

The simplified eq. (32) is very similar to the equation for the binary mixture of the components 3 and b. The only difference is that R_B appears in eq. (32) instead of

$$R_B^* = \{L_b^* - u^*(0)\}/u^*(0).$$

It can be shown that the absorption factor products calculated from eq. (32) are $(R_B+1)/(R_B^*+1)$ times the absorption factor products of the binary mixture [8]. Therefore, the absorption factors of the latter are equal to $Ap_1^*(m+1)/Ap_1^*(m)$ if m exceeds zero and the absorption factor at the first tray in the binary mixture is equal to

$$\{(R_B^*+1)/(R_B+1)\}Ap_1^*(1)$$

since $Ap(0)=1$ in each case. The absorption factors of the binary mixture can be found easily by one of

VOL. 1 1952

the current graphical methods, from McCABE and THIELE's diagram, for instance. This diagram is given in Fig. 5a for the bottom section and in Fig. 5b for the top section. The equilibrium line in Fig. 5a has been drawn for the components 3 and b which have a relative volatility of $1{\cdot}96/0{\cdot}88 = 2{\cdot}23$. The concentration of the volatile component in the residue is $x_3 = 0{\cdot}004/\{0{\cdot}253 + 0{\cdot}004\} = 0{\cdot}0156$. So the operating lines are drawn across the point $y = 0{\cdot}0156$ and $x = 0{\cdot}0156$ and their slopes are L_b^*/V_b^*. The ordinary construction is then carried out to arrive at the concentrations at any arbitrary tray. If x_m and y_m are the concentrations of component 3 in liquid and vapour respectively leaving the mth tray, one has $K_{3,m}^{-1} = x_m/y_m$ at that tray and the absorption factor for component 3 is $L_b^*/V_b^* K_{3,m}$. This absorption factor is equal to that of the same component in the simplified multicomponent system. Therefore, one obtains $\xi_1(m)$ for this latter system, by multiplication of this absorption factor by $V_b/L_b \alpha_3^{-1}$. So we have:

$$\xi_1(m) = (V_b L_b^*/L_b V_b^*) \cdot \alpha_3 \cdot (x_m/y_m) \qquad m = 2, 3, \ldots \quad (33)$$

The value of $K_{3,m}^{-1}$ is read at the upper horizontal line in the figure as the intersection with a straight line through the origin and the point representing the concentrations at the mth tray. So, for instance one reads for $L_b^* = 1{\cdot}258$ $K_{3,9}^{-1} = 0{\cdot}704$ and therefore $Ap_1^*(9)/Ap_1^*(8) = 1{\cdot}73$ and $\xi_1(9) = 1{\cdot}235$. This tallies with the value 1·74 calculated from Table 5. As can be seen from Figures 3 and 4, all ξ and η values calculated from the McCABE-THIELE diagrams agree excellently with the other values.

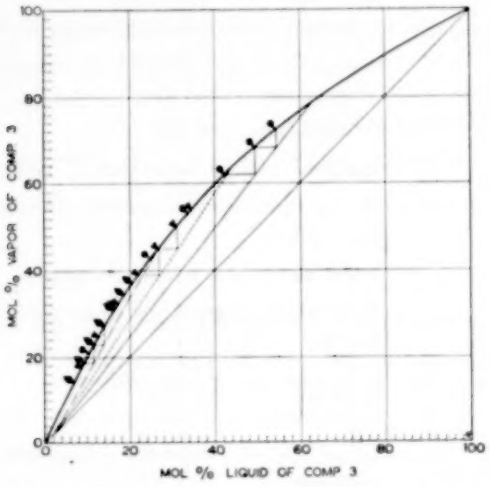

Fig. 5a. Separation of components b and 3 in stripping section, relative volatility = 2·23.

—— for $R_D = 1{\cdot}78$
- - - - - for $R_D = 1{\cdot}12$
— · — for $R_D = 0{\cdot}765$

Indication of the trays

● belonging to $R_D = 1{\cdot}78$
▼ belonging to $R_D = 1{\cdot}12$
♦ belonging to $R_D = 0{\cdot}765$

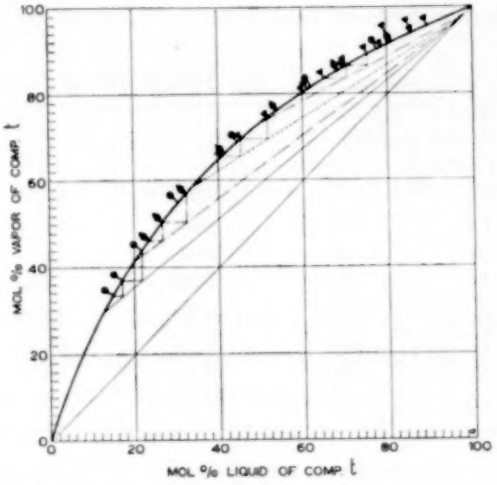

Fig. 5b. Separation of component t and 4 in top section, relative volatility = 2·76.

—— for $R_D = 1{\cdot}94$
— · — for $R_D = 1{\cdot}27$
- - - - - for $R_D = 0{\cdot}764$
— · · · — for $R_D = 0{\cdot}510$

Indication of the trays

● belonging to $R_D = 1{\cdot}94$
♦ belonging to $R_D = 1{\cdot}27$
▼ belonging to $R_D = 0{\cdot}764$
▼ belonging to $R_D = 0{\cdot}510$

In the top section one has $R_D^* = \{V_t^* - u^*(0)\}/u^*(0)$ and the stripping factor product of the binary mixture is $(R_D^* + 1)/(R_D + 1)$ times the stripping factor of the multicomponent mixture. The stripping factors $Sp(n+1)/Sp(n)$ are therefore equal in both cases except for $n = 0$.

A McCABE and THIELE diagram has been constructed for the components t and 4 (Fig. 5b). Their relative volatility is $\alpha_t/\alpha_4 = 2{\cdot}76$ and $y_t = 0{\cdot}287/(0{\cdot}287 + 0{\cdot}003) = 0{\cdot}990$. Operating lines have been drawn for the vapor rates in Table 4. Their slopes are L_t^*/V_t^*. The absorption factor of component t at the nth tray is $L_t^*/V_t^* K_{t,m}$ and $K_{t,m}^{-1} = x_n/y_n$. The absorption factor of the reference component 4 is, therefore,

$$(L_t^*/V_t^*)(x_n/y_n)\alpha_t$$

This gives for $\eta_{l1}(n)$:

$$\eta_{l1}(n) = (V_l L_l^*/L_l V_l^*)\,\alpha_l\,(x_n/y_n) \qquad n > 1. \qquad (34)$$

From Fig. 5b one reads *e.g.* for $V_l^* = 0{\cdot}747$ at the 9th tray $x_n/y_n = 0{\cdot}647$. This gives $\eta_{l1}(9) = 2{\cdot}51$, which again tallies excellently with the analytical calculation.

A list of ξ and η values calculated by this graphical method is given in Table 6.

Table 6. ξ_1 and η_{l1} values from McCABE-THIELE *diagrams*

ξ_1	$R_D = 1{\cdot}78$	$R_D = 1{\cdot}12$	$R_D = 0{\cdot}765$
(∞)	1·39	1·15	0·951
(10)	1·31	1·06	0·898
(9)	1·28	1·03	0·872
(8)	1·20	0·994	0·856
(7)	1·12	0·951	0·834
(6)	1·02	0·900	0·813
(5)	0·942	0·855	0·787
(4)	0·880	0·814	0·761

η_{l1}	$R_D = 1{\cdot}94$	$R_D = 1{\cdot}27$	$R_D = 0{\cdot}764$	$R_D = 0{\cdot}510$
(∞)	1·46	1·75	2·24	2·84
(10)	1·51	1·81	2·40	3·15
(9)	1·54	1·88	2·52	3·26
(8)	1·65	2·03	2·68	3·39
(7)	1·81	2·22	2·90	3·54
(6)	2·15	2·50	3·14	3·68
(5)	2·53	2·84	3·37	3·82
(4)	2·87	3·13	3·56	3·94

Acknowledgement—The authors are indebted to the Netherlands organisation for the stimulation of scientific research "Z.W.O." for a grant, which has permitted one of them (H. A. C. THIJSSEN) to carry out this investigation.

NOTATION

The standard system of nomenclature for chemical engineering operations (Trans. Amer. Inst. Chem. Engrs 1944 **40** 251) has been followed as far as possible. A* indicates that the quantity refers to the binary mixture approximating a multicomponent mixture.

α_i (alpha) = Relative volatility of component i towards a reference component.

$\mathbf{A} = \sum_{k=0}^{k=\infty} Ap(k)\,t^k$ Generating function of $Ap(m)$.

$A_{i\,m}$ = Absorption factor for component i on tray m.

A_m = Absorption factor for reference component on tray m.

$Ap(m) = A_1 A_2 \ldots A_m$. Absorption factor product of reference component on tray m.

B = Residue rate, moles/sec.

B_i = Residue rate of component i, moles/sec.

b = Subscript referring to bottom section.

c = Constants in analytical expression of **A**.

C = Constant used in correction for unspecified components.

D = Distillate rate, moles/sec.

D_i = Distillate rate of component i, moles/sec.

φ (phi) = Root of equation to be solved to obtain poles of **A** or **S**.

i = Index denoting a certain component.

$K_{i\,m}$ = Equilibrium constant for component i at tray m.

L_m, L_b = Liquid rate below feed, moles/sec.

L_n, L_t = Liquid rate above feed, moles/sec.

$L_{i\,m}$ = Liquid rate of component i from tray m, moles/sec.

m = Index for tray below feed, $m = 0$ means reboiler.

$M+1$ = Index for feed tray.

n = Index for tray above feed, $n = 0$ means condensor. If in the symbols m is replaced by n they refer to the top section.

N = Number of components.

$N+1$ = Index for feed tray.

R_D, R_B = Reflux ratio in top and bottom resp.

$\mathbf{S} = \sum_{k=0}^{k=\infty} Sp(k)\,t^k$ Generating function of $Sp(n)$.

$S_{i\,n}$ = Stripping factor of comp. i at tray n.

S_n = Stripping factor for reference component on tray n.

$Sp(n) = S_1 S_2 \ldots S_n$ Stripping factor product of reference component on tray n.

t = Variable in generating functions or subscript referring to top section.

$$u(m-k) = \sum_{i=1}^{i=N} B_i\,\alpha_i^{(m-k)}$$

$$u^*(m-k) = B_{l\,k}\,\alpha_{l\,k}^{(m-k)} + B_b\,\alpha_b^{(m-k)}.$$

$$u(n-k) = \sum_{i=1}^{i=N} D_i\,\alpha_i^{-(n-k)}$$

$$u^*(n-k) = D_{h\,k}\,\alpha_{h\,k}^{-(n-k)} + D_t\,\alpha_t^{-(n-k)}.$$

VOL. 1 1952

$\mathbf{U} = \sum_{k=0}^{k=\infty} u(k)\,t^k$. Generating function of $u(m-k)$ or $u(n-k)$ respectively.

V_m, V_b = Vapor rate below feed, moles/sec.

V_n, V_t = Vapor rate above feed, moles/sec.

$V_{i\,m}$ = Vapor rate of component i from tray m, cal/sec.

$x_{i\,m}$, $x_{i\,B}$ = Molal liquid concentration of component i at tray m or in residue, respectively.

ξ (xi) $= Ap(M+1)\,V_{(b)}/Ap(M)\,L_{(b)}$, parameter for feed tray.

$y_{i\,m}$, $y_{i\,D}$ = Molal vapor concentration of component i at tray m or in distillate, respectively.

η (eta) $= Sp(N)\,V_{(t)}/Sp(N+1)\,L_{(t)}$, parameter for feed tray.

$\mathbf{Z} = \sum_{k=0}^{k=\infty} z(k)\,t^k$.

$z(m) = \sum_{i=1}^{i=\mathbf{N}} V_{i\,o}\,z_i^m$ in bottom section.

$z(n) = \sum_{i=1}^{i=\mathbf{N}} L_{i\,o}\,\alpha_i^{-n}$ in top section.

REFERENCES

[1] HARBERT, W. D.; Ind. Eng. Chem. 1946 **37** 1162. [2] JENNY,; Amer. Inst. Chem. Engrs. 1939 **35** 635. [3] MURDOCH, P. G.; Chem. Eng. Progress 1948 **44** 855. [4] SMITHUYSEN, H. B.; Amsterdam, private communication. [5] UNDERWOOD, A. J. V.; Chem. Eng. Progress, 1948 **44** 603. [6] VAN WIJK, W. R.; Physica ('s-Gravenhage) 1949 **15** 634. VAN WIJK, W. R.; Physica ('s-Gravenhage) 1949 **15** 933. VAN WIJK, W. R.; Physica ('s-Gravenhage) 1951 **17** 485.

Note on the free energies of formation of the fluorides, chlorides and oxides of the alkali alkaline earth and rare earth metals, and on the occurrence in fused salt mixtures of double decomposition reactions involving these substances*

E. F. EMLEY, Ph.D., A.I.M., F.R.I.C.

(Received 4 February 1952)

Summary—The free energies of formation (ΔG) of the fluorides, chlorides and oxides of the alkali, alkaline earth and rare earth metals are inferred tentatively from available data, and the results are given in the form of "Ellingham" diagrams** in which ΔG is plotted against T.

From the ΔG values the relative tendencies of the various chlorides to convert a fluoride or oxide to the corresponding chloride are deduced and the results found to accord with experiment in cases for which information is available.

Indications have been given elsewhere [2], [3] of the interest to the magnesium industry of a knowledge of the positions of magnesium in the chloride and fluoride electropotential series, since these positions will largely govern the choice of possible constituents of salt mixtures for alloying and purifying the metal. The order of metals in the two series is different, the differences arising from variations in the magnitude and sign of the heat of solution of the salts concerned. In the present paper an attempt is made to infer the free energy - temperature relationships for the chlorides, fluorides and oxides of the alkali, alkaline earth, rare earth and certain other metals from published data on decomposition potentials and exchange reactions, supplemented by approximate thermochemical calculation. Consideration is also given to the occurrence of double decomposition reactions involving these substances.

Since drafting this paper, Ellingham diagrams based on calculations of the extended type have been published for chlorides by OSBORN [43], KELLOGG [44] and VILLA [54], and for fluorides by KELLOGG [55]. Data for chlorides and fluorides have also been published by BREWER, BROMLEY, GILLES and LOFGREN [45].

OSBORN shows curves for four of the chlorides of present interest, namely, NaCl, $MgCl_2$, $CaCl_2$, and $BaCl_2$. The relative positions given for the first three do not accord in any way with the conclusions of the present paper†. On the other hand the results of

* This paper is based on work forming an appendix to a thesis approved by the *University of London* for the degree of Ph. D. (Thesis submitted 1st May 1950.)

** This convenient term has been used by PARSONS [1].

† Note added in proof: It has since been explained by OSBORN [78] that 50 kcal should be added to the curves for NaCl and $CaCl_2$, and this evidently applies also to that for $BaCl_2$. OSBORN's results have been added to Table 10.

KELLOGG and VILLA for these chlorides, and for the other halides of present interest with which they deal, are in reasonably good agreement with the results here deduced (Table 10).

BREWER, BROMLEY, GILLES and LOFGREN alone give data for all the chlorides and fluorides of Tables 2 and 4. Their figures have been selected critically, but apparently without consideration having been given to the available experimental data on decomposition potentials. These figures are not therefore thought likely to give a truer picture of the *relative* stabilities of the chlorides and fluorides involved than the data deduced in the present paper, particularly since in the case of the fluorides, where decomposition potential measurements were not available for guidance, the more exact calculations of KELLOGG are in rather better agreement with the rough calculations of Table 2 than with BREWERs figures. A number of entropy determinations havem oreover become available since the latter were deduced. In one or two cases the BREWER entropy estimates appear to be somewhat in error*.

I. THE FLUORIDE ELECTROPOTENTIAL SERIES

Published information

No satisfactory measurements of the decomposition potentials of fluorides appear to be available. CAMBI and DEVOTO [4] were unable to achieve electrode reversibility; and the earlier measures of NEUMANN and RICHTER [5] were made by an unsatisfactory method [6]–[8]. The results obtained by NEUMANN and RICHTER are numerically below the corresponding figures found for the chlorides and evidently much too low, despite agreement between the calculated values of the heat of formation per mol ($Q_f = -\Delta H$) and

* TODDs [62] recent experimental determination of 13·68 for MgF_2 is considerably below BREWERs estimate of 18, though it agrees with a published estimate [50] of 13·6 based on semi-empirical methods [56], [57].

Table 1. Calculated approximate free energy of formation of various fluorides

Substance	ΔH^{298}* $(-Q_f)$ *(kcals)*	$S^{298}_{MF_n}$† *(E.U.)*	S^{298}_M *(E.U.)*	$\frac{n}{2} S^{298}_{F_2}$ *(E.U.)*	$\Delta S^{298} = S^{298}_{MF_n} - S^{298}_M - \frac{n}{2} S^{298}_{F_2}$ *(E.U.)*	$\frac{1}{n}\Delta G^{298}$ *(Free energy per gm. equiv)* $= \frac{1}{n}(\Delta H^{298} - T\Delta S^{298})$ *(kcals)*
LiF	−145·57	8·5[j]	6·7	24·3	−22·5	−138·9
NaF	−135·95	12·5[a]	12·2	24·3	−24·0	−128·8
KF	−134·51	15·8[a]	15·2	24·3	−23·7	−127·5
MgF_2	−263·8	13·6[g]	7·76	48·6	−42·76	−125·5
CaF_2	−290·2	16·4	9·9	48·6	−42·1	−138·8
SrF_2	−289·0	20·6[g]	13·3	48·6	−41·3	−138·4
BaF_2	−287·9	23·03	15·1	48·6	−40·67	−137·9
BeF_2	< −240·8[aq]	10[b]	2·28	48·6	−40·88	< −114·3
AlF_3	−329·0[d]	12·5[c]	6·73	72·9	−67·1	−103·0
CeF_3	< −399·6[e]	35·4[b]	13·8	72·9	−51·3	< −128·1
ThF_4	< −551·3[e]	54[f]	13·6[h]	97·2	−56·8	< −133·6

* Unless otherwise stated these figures have been taken from BICHOWSKI and ROSSINI [17].

† Unless otherwise stated these figures have been taken from WENNER [56].

[a] Calculated from data of TREADWELL and MAUDERLI [57] and in close agreement with the values given by DROSSBACH (*op. cit.* p. 24) and GLASSTONE [58]. (A subsequent determination of 15·91 E.U. has been made for KF by WESTRUM and PITZER [59]).

[b] Estimated from plot of S against log. mol. wt. for all metal halides of the same valency, based on data given by WENNER [56] and subsequent literature.

[c] Estimated by GROSS [60].

[d] Given as −332·0 to −500·0 by RENAULT [61].

[e] The figure given is the sum of the heats of formation of the aqueous ions.

[f] Estimated from LATIMERs Formula [63].

[g] Estimated by method [b] and also by application of the method of TREADWELL and MAUDERLI [57] using the known values for CaF_2 and BaF_2. (A subsequent determination of 13·68 E.U. for MgF_2 has been made by TODD [62]).

[h] Metals Reference Book [64].

[j] CLUSIUS, GOLDMANN and PERLICK [65].

Note: The sign < means here "numerically less than."

VOL. 1 1952

calorimetric determinations. This agreement may be attributed to the very high numerical values found for the temperature coefficient* of the decomposition potential, dE/dT, the effect of which has been to offset the low figures obtained for the decomposition potential** itself. AGAR and BOWDEN [9] showed that there are three main causes of irreversibility in electrode reactions: "concentration potential," "activation overpotential" and "resistance overpotential." Since these quantities decrease with increasing temperature and dE/dT is negative, all three sources of irreversibility would tend to increase the numerical value of dE/dT, and the high values found by NEUMANN and RICHTER are probably attributable to irreversibility.

Exchange experiments between magnesium and mixtures of alkali and alkaline earth metal fluorides have been made by RUFF and BUSCH [11], and from these they infer that the electropotentials of the metals in their fluorides decrease in the following order: Ca—Li—Ba—Mg—Na—K, thus representing a reversal of the usual order so far as Mg, Na and K are concerned. This inference, however, involves the assumption that the alkali metals are associated in molten magnesium, as was found to be the case in molten tin, antimony and bismuth [12]: otherwise the order would begin Li—Ca—Ba—. Other difficulties in interpreting such experimental results are the lack of information on activity coefficients or on the free energy of mixing or of compound formation in the metal phase.

Although DROSSBACH [13] considered the decomposition potential of NaF to be about 0·7 v above that of MgF_2, there is no doubt that NaF and KF are readily reduced by molten magnesium; if these fluorides are also molten the reduction is violent with NaF and mildly explosive with KF. The necessity of removing NaF from all-fluoride welding fluxes for magnesium so as to avoid sodium introduction into the metal [14] and of the need for special steps to avoid explosive reaction between K_2ZrF_6 and magnesium [15] are practical reflections of the reducibility of these fluorides. The reduction of KF by magnesium has moreover been suggested as a method for the production of potassium †.

The position of aluminium in the fluoride series appears to require clarification [2].

Thermochemical calculations

Before attempting to infer the position of magnesium in the fluoride electropotential series, it may be of interest to consider the matter briefly from the thermodynamic point of view. Values of the free energy of formation per gram equivalent calculated from experimental or estimated data are given in Table 1.

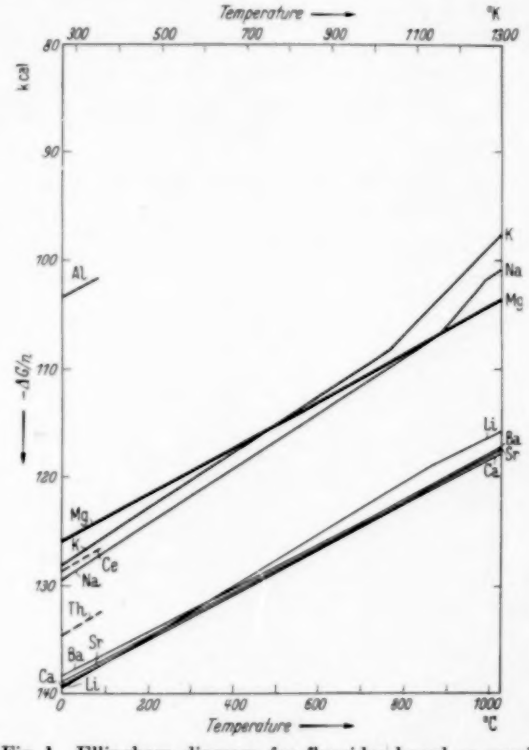

Fig. 1. Ellingham diagram for fluorides based on rough thermochemical calculations.

Note. The Ellingham diagrams in Figs. 1–5 show the temperature variation of the free energy of formation of the halide or oxide from one gram equivalent of metal.

The $\Delta G/T$ curves for reactions such as the formation of the metal halides from their elements are approximately linear above room temperature, and a linear equation will frequently represent the

* Since $dE/dT = \Delta S/nF$, where ΔS is the entropy increase accompanying formation of 1 mol of halide of valency n and F is the Faraday, and since the ΔS values for the formation of the fluorides and chlorides are similar (see below), the values of dE/dT found for chlorides and fluorides should not differ widely; and yet NEUMANN's values for fluorides are many times those obtained for the chlorides, his figures for MgF_2 for example, being seven times that found by COHEN [10] for $MgCl_2$. The latter's figures are in good accord with calculation.

** $Q_f = E + T\,|dE/dT|$.

† The low boiling point of potassium apparently enables the metal to be produced by reduction of KF even with aluminium [16].

observed data with the accuracy of the more complicated form of expression obtained by integrating the equation showing the temperature dependence of ΔC_p. The justifiability of straight $\Delta G/T$ curves in the higher temperature ranges is illustrated by the linear dependence on temperature found by all workers for the decomposition potentials of various chlorides. If the necessary high temperature data were available in all cases, the $\Delta G/T$ relationship could be computed in the usual way and the results then represented by a linear equation for convenience. But such data are available only for some of the fluorides in the table and the values of ΔG°_{298} for even these are in some cases so uncertain* as to render attempts to apply the high temperature data of doubtful value. This is particularly true of the present investigation where the differences in the free energies of formation of the various fluorides are of more concern than the absolute values involved. A uniform procedure applicable to all cases seems therefore desirable, and for the present purpose it will suffice to indicate the temperature dependence of ΔG by straight lines of slope ΔS°_{298} with inflections corresponding to the entropy changes accompanying changes of phase of the fluoride or its constituent elements. The results of such calculations are indicated in Table 2 and Fig. 1.

* The calculations have been revised to incorporate recent entropy determinations where available.

Probable electropotential order of the fluorides

It will be seen that, except for lithium, the calculated order of electropositiveness of the metals in their

Table 2. Calculated approximate temperature variation of free energy of formation of various fluorides

Substance	ΔH^{298} Table A (kcals)	ΔS^{298} Table A (E.U.)	Phase transformations			$\Delta G/T$ equation . $\Delta G = A + B(T-C)$				
			Temp. (°K)	Nature of transform.	ΔS^*_{trans} ($= L/T$)	Range of T. (°K)	A	1000 B	C	$\frac{1}{n}\Delta G^{1300}$
LiF	−145·57	−22·5				298– 459	−145·57	22·5	0	
			459	Li melts	1·66	459–1133	−135·24	24·16	459	
			1133	LiF melts	5·25	1133–1300	−118·95	18·91	1133	−115·8
NaF	−135·95	−24·0				298– 371	−135·95	24·0	0	
			371	Na melts	1·70	371–1151	−127·05	25·7	371	
			1151	Na boils	20·2[a]	1151–1263	−107·0	45·9	1151	
			1263	NaF melts	6·18	1263–1300	−101·8	39·72	1263	−100·4
KF	−134·51	−23·7				298– 337	−134·5	23·7	0	
			337	K melts	1·92	337–1031	−126·53	25·62	337	
			1031	K boils	20[b]	1031–1119	−108·75	45·62	1031	
			1119	KF melts	5·56	1119–1300	−104·73	40·06	1119	− 97·5
MgF_2	−263·8	−42·76				298– 924	−263·8	42·8	0	
			924	Mg melts	1·95	924–1300	−224·25	44·75	924	−103·7
CaF_2	−290·2	−42·1				298–1124	−290·2	42·1	0	
			1124	Ca melts	1·84[c]	1124–1300	−242·88	43·94	1124	−117·8
SrF_2	−289·0	−41·3				298–1044	−289·0	41·3	0	
			1044	Sr melts	1·37	1044–1300	−245·9	42·6	1044	−117·5
BaF_2	−287·9	−40·67				298– 977	−287·9	40·67	0	
			977	Ba melts	1·51	977–1300	−248·17	42·18	977	−117·3
AlF_3	−329·0	−67·1				298– 933	−329·0	67·1	0	
			933	Al melts	2·47	933–1300	−266·4	69·57	933	− 80·3

* While the ΔS transf. values have been calculated using heats of transformation and temperatures given by BICHOWSKI and ROSSINI [17], the transformation temperatures given have mostly been taken from WEST [66] and KAYE and LABY [67].

(a) S. GLASSTONE, *op. cit.*, p. 449.

(b) The figure is assumed to be the same as for sodium.

(c) Metals Reference Book [64]. The figure of 8·95 E.U. corresponding to the latent heat of fusion given in references [68] and [17] is almost certainly incorrect, being not only widely different from the entropies of fusion of magnesium, strontium and barium, but lying outside the normal range of values found for elements.

VOL. 1 1952

fluorides agrees above 850° C with that inferred for 800° C from the exchange experiments of RUFF and BUSCH. Such a difference in the position of lithium in the two series is easely explained, since the curves for lithium, calcium, strontium and barium evidently lie ciose together, and lithium differs from the other three metals in forming solid solutions with magnesium and not compounds. When molten magnesium and NaF at temperatures above about 750°C are mixed in open crucibles, heat is evolved resulting in extensive local boiling of sodium. The percentage reduction reached under such conditions must therefore considerably exceed the true equilibrium percentage at 750° C, both because of the loss of sodium by volatilisation and also because the heat of reaction will have raised the temperature to a higher value at which a greater percentage reduction would be obtained at equilibrium. For practical purposes then, the result of the heat of reaction will be equivalent to lowering the temperature at which the kink in the free energy/temperature curve occurs by some 100° C or more, according to the scale of the experiment; and such an effect may even be present to some extent in closed bomb experiments such as those of RUFF and BUSCH. Similar remarks apply to the KF curve. The rough calculations indicate therefore that the fluoride electropotential series inferred from RUFF and BUSCHs results is in general accord with expectation, and it is not necessary to assume that it results primarily from complex formation as they suggest.

Table 1 shows that the cerium rare earth metals evidently lie very close to magnesium in the fluoride electropotential series, and experiments have in fact confirmed that the rare earth metals are slightly more electropositive at normal alloying temperature*. The same applies to thorium. No information appears to be available concerning the position of uranium in the fluoride series**. Common membership of the actinide series might suggest a similar position to thorium, and heat data [17], [76] indicate that this is the case in the chloride electropotential series.

$$ThCl_4 : \tfrac{1}{4}\Delta H^\circ_{298} = -71{\cdot}1 \text{ kcal}$$
$$UCl_3 : \tfrac{1}{3}\Delta H^\circ_{298} = -71 \text{ kcal}.$$

Insufficient data appear to be available to estimate the free energy of formation of ZrF_4, but it is evident that the curve for ZrF_4 would lie well above that for MgF_2 on Fig. 1 since ZrF_4 can be reduced by sodium [19]. Moreover no unreacted ZrF_4 has been detected in magnesium-zirconium alloys made by the "inert fluoride" process [20].

II. THE CHLORIDE ELECTROPOTENTIAL SERIES

Published information

For the present purposes, a knowledge of the relative decomposition potentials of the various chlorides is of more importance than the establishment of the true reversible values for a few of them; consequently in considering the available information, attention will be directed mainly to the work of those who have determined decomposition potentials for a number of the chlorides which are of interest, even where it is probable that systematic errors are present and more accurate determinations on particular single salts have been made by others.

The $\Delta G/T$ curves for the various chlorides calculated from the decomposition potential data of NEUMANN and RICHTER [21], and CAMBI and DEVOTO [22] are shown in Figs. 2 and 3†. NEUMANN and RICHTERs figures are markedly lower than those of CAMBI and DEVOTO; this is to be expected for the reasons already indicated in discussing the information on the fluoride electropotential series. On the other hand their values for dE/dT do not appear to be improbably high as was the case with the fluoride determinations, and it seems likely that the low decomposition potentials are here attributable mainly to the inherent defects of their method rather than to highly irreversible electrode behaviour. In these circumstances it is probably fair to include NEUMANN and RICHTERs measurements when considering the relative electropotentials of the chlorides but to exclude them when questions of absolute magnitude arise. Some equilibria in metal/metallic chloride exchange reactions involving alkali and alkaline earth metals have been measured [23]–[27], but in the absence of information on activity coefficients and on compound formation, particularly in the metal phase, there is no basis on which such results can be satisfactorily treated, and measurements of decomposition potential appear preferable for inferring the chloride electropotential series.

Thermochemical calculations

The results of thermochemical calculations of the free energy of formation of chlorides are given in Tables 3

* This conclusion is based on exchange experiments assuming ideal behaviour.

** Recent work by SAUERWALD [18] indicates that uranium resembles chromium, molybdenum, and tungsten in being insoluble in magnesium.

† In converting the potential measurements to calories the Faraday has been taken as 23066 cals. per volt.

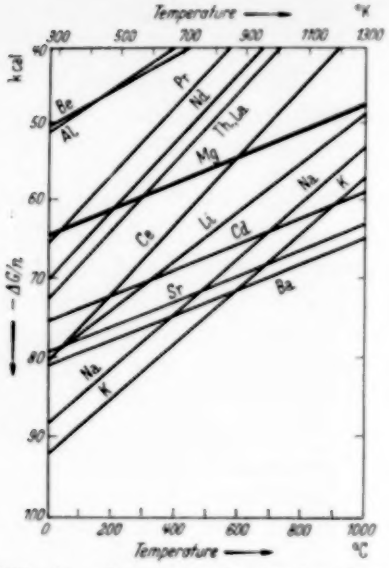

Fig. 2. Ellingham diagram for chlorides based on current potential measurements of NEUMANN and RICHTER.

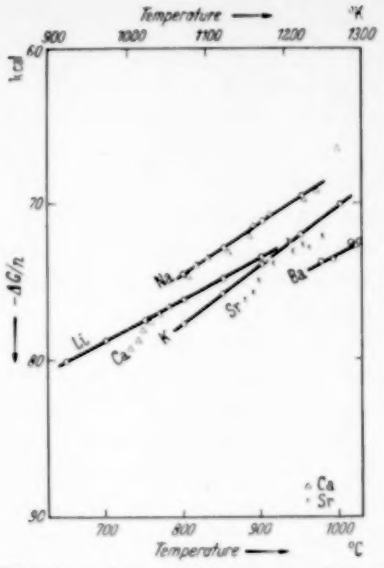

Fig. 3. Ellingham diagram for chlorides based on the decomposition potential measurements of CAMBI and DEVOTO.

Table 3. Calculated approximate free energy of formation of various chlorides

Substance	ΔH^{298} * $(-Q_f)$ *(kcals)*	$S^{298}_{MCl_n}$ † *(E.U.)*	S^{298}_{M} *(E.U.)*	$\frac{n}{2} S^{298}_{Cl_2}$ *(E.U.)*	ΔS^{298} $\left(= S^{298}_{MCl_n} - S^{298}_{M} - \frac{n}{2} S^{298}_{Cl_2}\right)$ *(kcals)*	$\frac{1}{n}\Delta G^{298} = \frac{1}{n}(\Delta H^{298} - T\Delta S^{298})$ *(kcals)*
LiCl	— 97·65	13·9[k]	6·7	26·66	—19·46	—91·9
NaCl	— 98·33	17·0[b]	12·2	26·66	—21·86	—91·8
KCl	—104·36	19·35[b]	15·2	26·66	—22·51	—97·7
$MgCl_2$	—153·3	21·4[d]	7·76	53·32	—39·68	—70·7
$CaCl_2$	—190·6	27·2[d]	9·9	53·32	—36·02	—89·9
$SrCl_2$	—197·87	27·5[e]	13·3	53·32	—39·12	—93·1
$BaCl_2$	—205·28	28·6	15·1	53·32	—39·82	—96·7
$BeCl_2$	—112·6	19[e]	2·28	53·32	—36·6	—50·8
$CeCl_3$	—259·8[a]	42[e]	13·8	79·98	—51·78	—81·4
$LaCl_3$	—263·7[a]	42[e]	13·7	79·98	—51·68	—82·8
$ThCl_4$	—284·5[n]	54[j]	13·6[h]	106·64	—66·24	—66·2
$AlCl_{3\,(s)}$	—167·9[f]	22·4[c]	6·73	79·98	—64·31	—49·6
$ZrCl_4$	—268·9	44·5[m]	9·3[m]	106·64	—71·44	—61·9

* Unless otherwise stated the figures have been taken from BICHOWSKI and ROSSINI (*op. cit.*).

† Unless otherwise stated the figures have been taken from WENNER (*op. cit.*).

[a] BOMMER and HOHMANN [69].

[b] B. H. ZIMM and J. E. MAYER [70].

[c] KELLEY [71].

[d] K. K. KELLEY and G. E. MOORE [72].

[e] Estimated from a plot of entropy against log mol. wt. for equi-valent halides based on data given by WENNER, *op. cit.* and subsequent literature.

[f] ROTH and BÜCHNER [73].

[h] Metals Reference Book [64].

[j] Estimated from LATIMER's formula [63].

[k] K. K. KELLEY [74].

[m] S. S. TODD [62].

[n] L. EYRING and E. F. WESTRUM [76].

VOL. 1 1952

Table 4. Calculated approximate temperature variation of free energy of formation of various chlorides

Substance	ΔH^{298} Table 3 (kcals)	ΔS^{298} Table 3 (E.U.)	Phase transformations			$\Delta G/T$ equation : $\Delta G = A + B(T-C)$				
			Temp. (°K)	Nature of transform.	$\Delta S^{\bullet}_{trans}$ $(=L/T)$ (E.U.)	Range of T. (°K)	A	1000 B	C	$\frac{1}{n}\Delta G^{1300}$ (kcals)
LiCl	— 97·65	—19·46				298– 459	97·65	19·46	0	
			459	Li melts	1·66	459– 887	88·72	21·12	459	
			887	LiCl melts	5·63	887–1300	79·68	15·49	887	—73·3
NaCl	— 98·33	—21·86				298– 371	98·33	21·86	0	
			371	Na melts	1·70	371–1074	90·22	23·56	371	
			1074	NaCl melts	6·73	1074–1151	73·66	16·83	1074	
			1151	Na boils	20·2[e]	1151–1300	72·36	37·03	1151	—66·8
KCl	—104·36	—22·51				298– 337	104·36	22·51	0	
			337	K melts	1·92	337–1031	96·78	24·43	337	
			1031	K boils	20[d]	1031–1063	79·82	44·43	1031	
			1063	KCl melts	6·02	1063–1300	78·4	38·41	1063	—69·3
$MgCl_2$	—153·3	—39·68				298– 924	153·3	39·68	0	
			924	Mg melts	1·95	924– 986	116·64	41·63	924	
			986	$MgCl_2$ melts	10·44[b]	986–1300	114·06	31·19	986	—52·1
$CaCl_2$	—190·6	—36·02				298–1047	190·6	36·02	0	
			1047	$CaCl_2$ melts	6·42[b]	1047–1124	152·86	29·60	1047	
			1124	Ca melts	1·84[c]	1124–1300	150·61	31·44	1124	—72·5
$SrCl_2$	—197·87	—39·12				298–1044	197·87	39·12	0	
			1044	Sr melts	1·37	1044–1145	157·03	40·49	1044	
			1145	$SrCl_2$ melts	6·5[d]	1145–1300	152·94	33·99	1145	—73·8
$BaCl_2$	—205·28	—39·82				298– 977	205·28	39·82	0	
			977	Ba melts	1·51	977–1233	166·38	41·33	977	
			1233	$BaCl_2$ melts	6·5[d]	1233–1300	155·8	54·83	1233	—76·7
$CeCl_3$	—259·8	—51·78				298–1088	259·8	51·78	0	
			1088	Ce melts	2·5[d]	1088–1121	203·46	54·28	1088	
			1121	$CeCl_3$ melts	6·5	1121–1300	201·67	47·78	1121	—64·4

* See note * to Table 2.
(b) G. E. MOORE [75].
(c) Metals Reference Book [64].
(d) Estimated from known values for similar elements and compounds.
(e) S. GLASSTONE, *op. cit.*, p. 449.

and 4, the calculations being carried out in the approximate manner already used for fluorides.

Probable electropotential order for the chlorides

(a) *Alkali and alkaline earth metals*

In view of the various phase changes of the salts and their constituent elements which occur within the temperature range of practical interest and the instances of crossing of the decomposition potential/temperature curves found by various workers, the chloride electropotential order may be expected to show considerable changes with temperature.

In comparing the figures of NEUMANN and RICHTER, CAMBI and DEVOTO, and the present rough calculations, several features are seen to be common to at least two of the three sets of results.

1. The most electropositive metal is barium.

2. Potassium follows next at the lower temperatures but becomes relatively less electropositive as the temperature increases.

3. The KCl and LiCl curves cross between 1100 and 1250° K.

Table 5. Calculated approximate temperature variation of free energy of formation of some oxides

Substance	ΔH^{298} (kcals)	S^{298}_{MO}	S^{298}_{M}	S^{298}_{O}	ΔS^{298} $(=S_{MO}-S_M-S_O)$	$\frac{1}{n}\Delta G^{298}$ (kcals)	Phase transformations			$\Delta G/T$ equation: $\Delta G = A + B(T-C)$				
		For No. of gm. atoms in formula weight (E.U.)					Temp. (°K)	Nature of transform.	ΔS_{trans} (E.U.)	Range of T.	A	1000 B	C	$\frac{1}{n}\Delta G^{1300}$ (kcals)
										298– 459	—142·3	28·86	0	
Li_2O	—142·3	9·06†	13·4	24·52	—28·86	—66·9	459	Li melts	1·66	459–1300	—129·1	30·52	459	51·7
K_2O							337	K melts	1·92	298– 337	— 86·2	34·32	0	
	— 86·2	20·6*	30·4	24·52	—34·32	—38·0	1031	K boils	20	337–1031	— 74·64	36·24	337	
										1031–1300	— 49·49	56·24	1031	—17·2
BeO	—135·0	3·37	2·28	24·52	—23·43	—64·0				298–1300	—135·0	28·43	0	—52·3
BaO	—133·0	16·8	15·1	24·52	—22·82	—63·1	977	Ba melts	1·51	298– 977	—133·0	22·82	0	
										977–1300	—110·705	24·33	977	—51·4
La_2O_3	—457·0	30*	27·4	73·55	—70·95	—72·6	1158	La melts	2·5**	298–1158	—457·0	70·95	0	
										1158–1300	—374·84	73·45	1158	—60·7
CeO_2	—233·4	17·7	13·8	49·03	—45·13	—55·0	1088	Ce melts	2·5	298–1088	—233·4	45·13	0	
										1088–1300	—184·3	47·63	1088	—43·6
ThO_2	—293·0	19·6	13·6††	49·03	—43·03	—70·0				298–1300	—293·0	43·03	0	—59·3
SrO	—140·8	13·0	13·3	24·52	—24·82	—66·7				298–1300	—140·8	24·82	0	—54·2

Notes. Except where otherwise stated values of ΔH have been taken from BICHOWSKI and ROSSINI (*op. cit.*), entropies from WENNER (*op. cit.*) and other data from the previous tables.

* Estimated from plot of entropy against log mol. wt. for oxides of metals of similar valency.

** Estimated from known values for similar elements.

† JOHNSTONE and BAUER [77].

†† Metals Reference Book [64].

4. The NaCl and $CaCl_2$ curves lie close together and possibly intersect*.

5. Sodium and calcium are the least electropositive of the metals considered.

If the slopes of the free-energy/temperature curves are considered, it will be noticed that NEUMANN and RICHTER found the chlorides to fall into well defined groups, the members of which had sensibly the same slope: the alkaline earth metal chloride curves had a comparatively gentle slope, LiCl was steeper, and the alkali metal chlorides had a uniformly steep slope**. Such a grouping of the slopes was not however found by CAMBI and DEVOTO, nor does it appear probable from the present rough calculations.

None of the experimental determinations of dE/dT indicate the changes of slope which would be expected to occur at the temperatures corresponding to phase changes of the chlorides or their constitutent elements and which in the case of KCl appear to be of appreciable magnitude.

With regard to the actual values of the slopes of the free-energy/temperature curves, the calculated slopes, which should presumably be at least of the right order, agree quite closely with the lowest experimental slopes (CAMBI and DEVOTO) in both the cases which have been fairly thoroughly investigated, namely, NaCl and KCl, and where the data available for the rough calculations are probably the most reliable†. In addition the calculated free energies of formation agree quite closely with the measurements of CAMBI and DEVOTO (Table 6). A close approximation to the $\Delta G/T$ curves for NaCl and KCl can probably therefore be obtained by plotting the mean values of ΔG and $\frac{\partial(\Delta G)}{\partial T}$ given in the table (Fig. 4).

The general form of the curves for the other chlorides considered can then be roughly indicated by

* An intersection of these curves between 600 and 800° C would accord with the observations of DANNEEL, STOCKEM and v. KUEGELGEN [28] in electrolysing NaCl-$CaCl_2$ mixtures.

** NEUMANN and RICHTER include figures for RbCl and CsCl.

† In these two cases, moreover, complications due to incomplete dehydration and sub-chloride formation do not arise. (KROLL [29] states that in the electrolysis of $BaCl_2$ sub-chloride only is produced.)

VOL. 1 1952

Table 6. Comparative values of ΔG and $\partial \frac{(\Delta G)}{\partial T}$ for NaCl and KCl (kcal)

Substance	$-\Delta G$				$-\partial \frac{(\Delta G)}{\partial T} \times 1000$			
	Temp. (°K)	C—D	E	Mean	Temp. (°K)	C—D	E	Mean
NaCl	1100	73·5	73·2	73·4	>1150	34	37·0	35·5
	1200	70·2	70·5	70·4				
KCl	1100	76·5	77·7	77·1	>1050	38	38·4	38

C—D = CAMBI and DEVOTO [22]; E = Calculated figure from Table 4.

relating them with those of NaCl and KCl in accordance with the broad conclusions already reached and giving them as far as possible the calculated gradients,

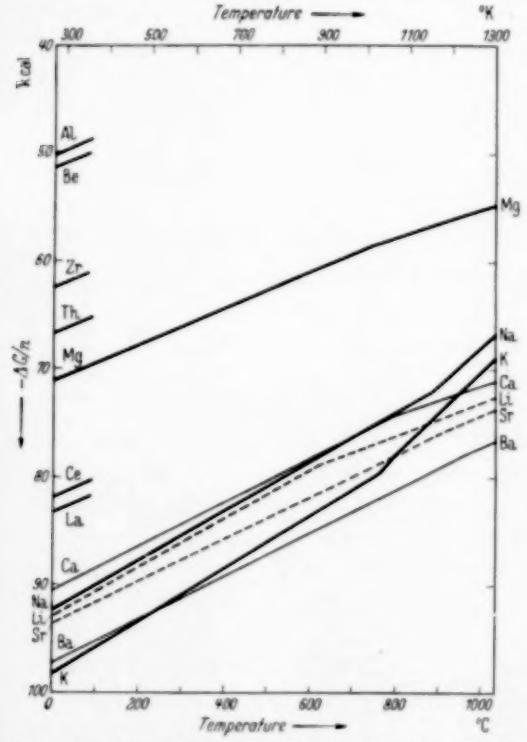

Fig. 4. Ellingham diagram for chlorides based on all data discussed.

consistent with their passing through the calculated values at 298° K [30].

(b) *Magnesium and the rare earth metals*

Various determinations have been made of the decomposition potential of magnesium chloride [4], [10], [31]–[34]. Without attempting a critical discussion of these figures, which range from 2·50 to 2·59 v at the melting point with temperature coefficients varying from 0·00057 to 0·00090 v/deg., the most satisfactory measurement appears to be that of COHEN, not only because of the care taken in the determination but also because his value of 13 cals/deg. C for dE/dT, which is the lowest, agrees fairly well with calculation (15·5 cals/deg.). LORENZ and VELDES value of dE/dT is almost identical with the calculated figure, but their value of E is much the lowest and likely to be low from consideration of the experimental procedure*. COHENS values for both E and dE/dT are therefore used for plotting on Fig. 4, the value for $\Delta G^{\circ\,298}$ being taken from Table 3.

No reliable determinations of the decomposition potential of the rare earth metal chlorides appear to be available. NEUMANN and RICHTERS figures are certainly low in absolute value, ranging at 800° C from 1·3 v for $PrCl_3$ to 1·9 v for $CeCl_3$. They are also very probably low relatively to $MgCl_2$ which is given as 2·2 v instead of 2·5 v; for it is well known in the industry that cerium will reduce $MgCl_2$ to a considerable extent, $MgCl_2$ being in fact usually excluded from fluxes for alloys containing rare earth metals [35]–[37]. The value of dE/dT found by NEUMANN and RICHTER (0·002 v/°) moreover, corresponds to an entropy of formation for $CeCl_3$ of 138 *E.U.* compared with the calculated figure of 52. DROSSBACH has studied the electrolysis of the double chlorides of cerium and neodymium with potassium, and the deposition potentials observed (Table 7), although probably not simply related to the reversible potentials, appear to indicate (a) that the reversible potentials are similar to but higher than that of $MgCl_2$ thus according qualitatively with calculation**, and (b) that (in the chloride

* The chlorine stream was interrupted during the measurement and the voltage observed remained constant for only a very short interval.

** The calculated free energy difference corresponds to nearly half a volt.

Table 7. Deposition potentials observed by DROSSBACH

Salt	*Temp.* (°C)	*Deposition potential* (v)	*Reversible decomposition potential* (v) *of single chloride where known*
$2KCl\ MgCl_2$	740	2·71–2·85	2·54 (740° C) 2·47 (860° C)
$2KCl\ CeCl_3$	860	2·96–3·10	
$2KCl\ NdCl_3$	860	2·75–3·00	

series) cerium is a little more electropositive than neodymium, as was found by NEUMANN and RICHTER. Experiments on the reduction of $NdCl_3$ and $GdCl_3$ by magnesium have been made by TROMBE and MAHN [38] who reproduce NEUMANN and RICHTERS measurements without comment as to the probable accuracy of the decomposition potentials and their temperature coefficients. TROMBE and MAHN obtained percentage reductions of the order of 50%, indicating either that magnesium and the rare earth metals do in fact differ little in electropotential in their chlorides, or, more probably, that the activity of cerium in magnesium is low. This would be expected in view of compound formation. The small difference in maximum percentage reduction obtained with $NdCl_3$ and $GdCl_3$ (42 and 52% respectively) is such as to cast doubt on the large difference in decomposition potential of 0·65 v between $CeCl_3$ and $NdCl_3$ found by NEUMANN and RICHTER. A difference of this magnitude should render fractionation of the rare earth metals by electrolysis or chemical exchange a simple process. But in fact no appreciable enrichment in any constituent can be obtained by (a) reducing mischmetal* chloride or fluoride with magnesium (b) "fluorinating" mischmetal chloride with KF or (c) fluxing magnesium-mischmetal alloys with fluxes containing $MgCl_2$.

The $\Delta G/T$ curves for the various rare earth metal chlorides and for $MgCl_2$ should lie very close together and slightly below** (*i.e.* representing higher numerical free energy) that of $MgCl_2$ (Fig. 4). In accordance with NEUMANN and RICHTERS measurements, and TROMBE and MAHNS observations that the percentage reduction increases with temperature, the slopes of the $\Delta G/T$ curves for the RE metals are probably somewhat steeper than that of the $MgCl_2$ curve, the contrary indication of the calculation being here of little value in the absence of measured values for the entropy of $CeCl_3$ and the latent heats of fusion of cerium and $CeCl_3$.

Magnesium reduction experiments have been carried out on $ThCl_4$ by FOX [39], but the low alloying efficiencies obtained do not necessarily indicate that the salt is only slightly reducible since the sample used may not have been completely anhydrous. The rough calculations indicate that reduction of $ThCl_4$ by magnesium should be substantially complete and this has been confirmed experimentally. It is therefore evident that in the chloride electropotential series thorium lies somewhat below magnesium†. Zirconium must lie well below magnesium since reduction of $ZrCl_4$ by magnesium is complete and the decomposition potential of the salt appears to be very low [40].

VOL. 1 1952

III. THE OXIDE ELECTROPOTENTIAL SERIES

A recent critical compilation of free energy data of oxides has been made by RICHARDSON and JEFFES [42]. The results of rough thermodynamical calculations are given in Table 5 for such of the oxides not considered by RICHARDSON and JEFFES as are of present interest. These data are combined in Fig. 5. Since preparing this paper, calculated data have been published for BaO and ZrO_2 by OSBORN [43]. His results for BaO agree very closely with Table 7. Those for ZrO_2 have been added to Fig. 5, but it must be remembered that they are not of much significance where reduction is concerned in view of the readiness with which oxygen dissolves in zirconium.

IV. NOTE ON APPLICATION OF THE FREE ENERGY DATA TO MAGNESIUM TECHNOLOGY

The free energy data collected in Figs. 1, 4 and 5 should enable very useful indications to be obtained immediately of the practicability of proposed reactions††.

Strict application of the data to a particular case, would however require additional knowledge, such as the free energies of formation of compounds

* "Mischmetal" refers to a mixture of the cerium group of rare earth metals roughly in the proportions Ce 50%, La 25%, Nd 18%, Pr 7%.

** Even if RAOULT'S law is assumed, TROMBE and MAHNS percentage reduction figures of about 50% with equal weights of magnesium and "$RECl_3$" (*i.e.* a 10:1 molecular ratio) would correspond to values of K (the equilibrium constant) less than unity for the reaction $3Mg + 2RECl_3 = 3MgCl_2 + 2RE$.

† This accords with HAISSINSKY'S claim [41] that thorium is a true analogue of zirconium and resembles it in electrochemical properties; but in the fluoride series thorium certainly resembles the rare earth metals, ThF_4 being very incompletely reduced by magnesium.

†† For examples of the application of such data see references [42], [44], [45].

formed in the metal or flux phases and the relevant activity coefficients*. While the experimental determination of such data might yield results of great interest from a fundamental point of view, the practical value of the work would be small in proportion to the

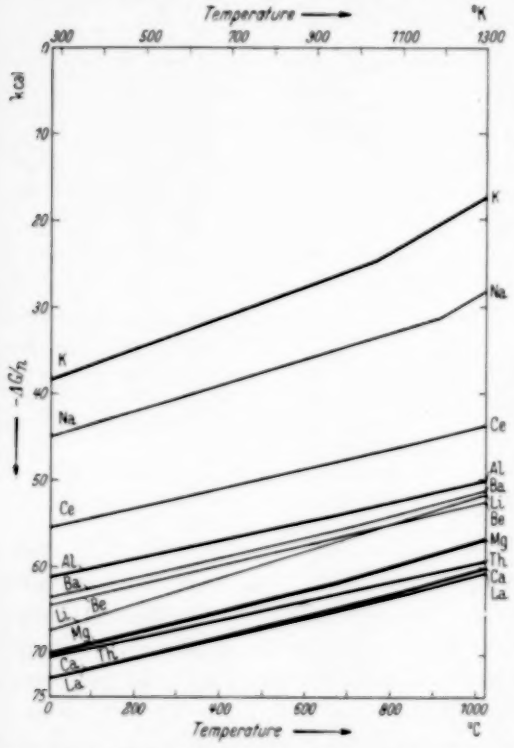

Fig. 5. Ellingham diagram for oxides. (The curves for Na, Al, Mg and Ca are due to Richardson and Jeffes and that for Zr to Osborn. Others are based on rough thermochemical calculations.)

labour involved. Of greater practical value, however, would be a knowledge of the concentrations of sodium, potassium, etc. in magnesium which are in equilibrium with constant molecular proportions of their chlorides. Such information would enable one to draw up a "Chloride Chemical Displacement Series" with respect to magnesium which would be of immediate practical application. The order of elements in this chemical displacement series might differ considerably from that in the electropotential series in the case of elements with chlorides of similar stability. Thus the free energy curves for NaCl and LiCl are seen from Fig. 4 to lie close together and, in the absence of activity data, it would be thought that NaCl would tend to flux lithium from magnesium**. Actually the reverse tendency is found to occur, LiCl being quite effective in removing sodium [46]. This could be foreseen at once from a chemical displacement series. The exchange experiments needed to establish the latter series would require precautions to ensure the achievement of equilibrium; and in determining a similar series for fluorides it might be difficult to avoid complicating the issue by using a suitable solvent for the fluoride†. Such solvents would however have to be used in industry, so that the thermal effects of possible double halide formation would not invalidate the results from a practical point of view††. From the experimental results obtained, rough estimates of the amounts of impurities in metal treated with any particular flux composition could be made.

V. Double Decomposition Reactions in Molten Salt Mixtures

Since in fused salt mixtures the constituents appear to be completely ionised [47], the contrary evidence of Sackur [48] from freezing point determinations resting on an erroneous basis [49], it may be assumed that the compounds present at equilibrium will depend on the activity solubility products of the various possible compounds. The insolubility of MgF_2 in chloride mixtures other than those very rich in $MgCl_2$ has been mentioned elsewhere [50], and in many experiments with fluxes and alloying salts it has been observed that, wherever MgF_2 could form from the

* It is often possible to infer qualitatively the effect of the deviations from Raoult's law to be expected in particular cases. For example sodium shows limited miscibility with magnesium and $MgCl_2$ forms a compounds with NaCl. These deviations are likely to offset each other, so that the sodium content of magnesium made electrolytically from a bath containing NaCl is likely to be of the order indicated by Raoult's law. On the other hand calcium forms a compound with magnesium and the two chlorides from a eutectic system, so that the calcium content of electrolytic magnesium is likely to be considerably greater than Raoult's law indicates. These conclusions are borne out by published data on the sodium and calcium contents of electrolytic magnesium [3] and the composition of cell electrolyte [50].

** Recent determinations of the decomposition potential of LiCl by Grothe and Savelsberg [34] actually give lower values than that here accepted for NaCl. The temperature coefficient found is however twice the probable value, and, since the decomposition potential found for KCl is also considerable lower and its temperature coefficient higher than the probable values, these measurements evidently do not represent true reversible values.

† The alkaline earth metal fluorides are solid at normal alloying temperatures (700–850° C) and would not form with the MgF_2 produced on reaction mixtures melting within this temperature range.

†† Some work has in fact been carried out by the author along these lines, but the results are not yet complete.

constituents present, it did so and was precipitated out. Rare earth metal fluorides are also insoluble in most chloride mixtures, and, in the absence of $MgCl_2$, any soluble fluoride will generally precipitate as "REF_3" if rare earth metal chlorides are present. The solubility of other fluorides in chloride mixtures depends very much on the composition of the latter. In $CaCl_2$—NaCl—KCl mixtures, for example, BaF_2 and KF are relatively insoluble and NaF and CaF_2 relatively soluble. The stability at lower temperatures of KF in certain salt mixtures containing $CaCl_2$ and NaCl [51] is an example of the effect of solubility governing the constituents present in molten salts, since on thermochemical grounds CaF_2 would be expected, and even NaF should be formed in preference to KF. The preferential precipitation of fluorine as MgF_2 and "REF_3" is however to be expected on thermochemical as well as solubility considerations, and it is therefore of interest to consider what metathetic reactions would be expected to occur from thermochemical calculations alone, assuming complete solution of all constituents, and then to see how these results compare with observation in a few test cases.

Conversion of Fluoride to Chloride

Consider the conversion of fluoride to chloride represented by the equation: $MCl + ZF = ZCl + MF$. The change in free energy per mol (ΔG) may be regarded as being composed of two terms:

$$(\Delta G_{ZCl} - \Delta G_{ZF}) \quad \text{and} \quad (\Delta G_{MF} - \Delta G_{MCl}).$$

Since for any given fluoride, ZF, the first term is constant, the ability of chlorides to convert fluorides to chlorides will depend on the value of the second term. The second term will however always be of the same sign whether the reaction tends to go from left to right or vice versa. To obtain a rough measure of the relative "chlorinating powers" of the various chlorides, a standard fluoride could be chosen, preferably one whose chloride did not possess a high heat of solution so that the relative positions of the metal in the chloride and fluoride electropotential series would be similar. But it is probably more satisfactory to express the chlorinating powers relative to an "ideal"* fluoride by evaluating the term $(\Delta G_{Cl'_{aq}} - \Delta G_{F'_{aq}})$ and adding this to the second term $(\Delta G_{MF} - \Delta G_{MCl})$. Table 8 gives the chlorinating powers of various chlorides calculated in this way from the ΔG values at room temperature** given in Tables 1–4.

Table 8. Conversion of fluoride to chloride—approximate chlorinating powers of various chlorides

Chloride	$\frac{1}{n}(\Delta G^{298}_{MF} - \Delta G^{298}_{MCl})$	$\Delta G_{Cl'_{aq}} - \Delta G_{F'_{aq}}$	Chlorinating power† Col. 1 + Col. 2
$BeCl_2$	−63·5*	+33·8	−29·7*
$MgCl_2$	−54·8	+33·8	−21·0
$AlCl_3$	−53·4	+33·8	−19·6
$CeCl_3$	−49·1*	+33·8	−15·3*
$CaCl_2$	−48·9	+33·8	−15·1
LiCl	−47·0	+33·8	−13·2
$BaCl_2$	−41·2	+33·8	− 7·4
NaCl	−37·0	+33·8	− 3·2
KCl	−29·8	+33·8	+ 4·0

† *i.e.* Free energy increase (kcal) per gram equivalent accompanying conversion of an "ideal" fluoride to an "ideal" chloride. (n = valency of cation.)

* The correct figure will be numerically less, the value of $\Delta H^{298}_{BeF_2}$ having been here taken as $\Delta H^{298}_{Be^{++}_{aq}} + 2\Delta H^{298}_{F'_{aq}}$ in the absence of information on the value of the heat of solution. The same applies to $\Delta H^{298}_{CeF_3}$.

The arrangement of the common Group II chlorides in the table, namely, Mg—Ca—Ba in order of decreasing chlorinating power, agrees with that observed in the chlorination of ZrF_4 [15]. The table also shows clearly why KCl will not chlorinate ZrF_4; and why in the reciprocal systems Na^+Ca^{++}/Cl^-F^- and K^+Ca^{++}/Cl^-F^-, the stable fluoride is in each case CaF_2 [52]. The correctness of the relative positions of $BaCl_2$ and LiCl indicated in the table has been checked experimentally, using a previously described method [50] to avoid possible interchange of radicals during analysis of the fused salt mixture obtained.

Conversion of oxide to chloride

Approximate date for conversion of oxides to chlorides are given in Table 9, the chlorinating power being here expressed as the free energy increase per gram equivalent accompanying conversion of BaO to $BaCl_2$ by the chloride in question. The barium compounds are taken as reference standard, since $BaCl_2$ has the smallest heat of solution of any of the chlorides in the table, with the exception of NaCl, in which case the chloride is obviously relatively much more stable than

* This would possess zero heat of solution as would the corresponding chloride.

** The calculated order of chlorinating power at 1000°K is unaltered so far as concerns the chlorides for which high temperature data have been estimated.

VOL. 1 1952

Table 9. Conversion of oxide to chloride—approximate relative chlorinating powers of various chlorides

Chloride	$\frac{1}{n}(\Delta G^{298}_{MO} - \Delta G^{298}_{MCl})$	$\frac{1}{n}(\Delta G^{298}_{BaCl_2} - \Delta G^{298}_{BaO})$	Approximate relative chlorinating power * Col. 2 + Col. 3
$BeCl_2$	−13·2	−33·6	−46·8
$AlCl_3$	−11·3	−33·6	−44·9
$MgCl_2$	+ 1·5	−33·6	−32·1
$LaCl_3$	+ 6·6	−33·6	−27·0
$CaCl_2$	+17·8	−33·6	−15·8
$CeCl_3$	+24·0	−33·6	− 9·6
LiCl	+24·7	−33·6	− 8·9
$BaCl_2$	+33·6	−33·6	0
NaCl	+47·3	−33·6	+13·7
KCl	+59·7	−33·6	+26·1

* *i.e.* Free energy increase (kcal) per gram equivalent accompanying conversion of BaO to $BaCl_2$. (n = valency of cation.)

the oxide. The order of ability to chlorinate oxides found by calculation for the alkali and alkaline earth metal chlorides is probably correct, since experiments on the addition of BaO to melts of $MgCl_2$—$CaCl_2$—NaCl—KCl

Table 10. Comparative values of free energy of formation per gram equivalent at 1000° K $-\left(\frac{\Delta G^{1000}}{n}\right)$ *estimated by various workers*

Metal	Fluoride			Chloride				
	E	Differences		E	Differences			
		B—E	K—E*		B—E	K—E*	V—E	O—E*
Li	122·2	+2·4	0	77·9	+2·1	N	N	N
Na	110·9	+1·2	+0·5	75·6	+0·7	−1·5	−0·2	+1
K	109·4	−0·5	+0·5	80·5	+1·1	N	+0·4	N
Mg	110·3	+2·5	+0·5	58·7	−1·1	−2·5	−0·8	−1
Ca	124·0	+0·9	+1·0	75·6	+2·6	+0·5	+2·3	+2·5
Sr	124·0	−0·7	N	79·4	+0·8	N	+3·1	N
Ba	123·6	+0·1	+0·5	82·8	+0·1	N	+2·5	+2·5

* Differences are here given only to the nearest half kilocal. in view of the difficulty of reading the diagram given by KELLOGG to a greater accuracy. (E = Estimate from Table 2 or Fig. 4; B = Estimate of BREWER, BROMLEY, GRILLES and LOFGREN; K = KELLOGG's estimate; V = VILLAS estimate; O = OSBORN's estimate; N = No estimate made.)

electrolyte showed that magnesium was first precipitated and only when the $MgCl_2$ had been reduced to below 1% was calcium precipitated. No Na_2O or K_2O were precipitated. These results would also be expected to occur on grounds of solubility since MgO is apparently insoluble in all mixtures of alkali and alkaline earth metal chlorides [53], CaO is soluble in $CaCl_2$, while SrO and BaO appear to show wider solubility [48].

Acknowledgements—The author is indebted to Dr. O. KUBASCHEWSKI for helpful advice, to Capt. A. C. JESSUP, Chief Metallurgist of *Magnesium Elektron Limited*, for help in locating and interpreting the earlier published work, and to the Directors of the Company for permission to publish the paper.

REFERENCES

[1] PARSONS, R.; J. Roy. Coll. Sci. 1949 **19** 28. [2] EMLEY, E. F.; Discuss. Faraday Soc. 1948 (4) 219. [3] EMLEY, E. F.; Symposium on Refining of Non-ferrous Metals, London: 1950, 407 (Inst. of Min. and Met.). [4] CAMBI, L. and DEVOTO, G.; Giorn. Chim. ital. 1927 **57** 836. [5] NEUMANN, B. and RICHTER, H.; Z. Elektrochem. 1925 **31** 481. [6] RUFF, O. and BUSCH, W.; Z. Elektrochem. 1925 **31** 614. [7] LORENZ, R.; Z. Elektrochem. 1926 **32** 172. [8] DROSSBACH, P.; Elektrochemie geschmolzener Salze, pp. 89, 127. Berlin 1938. [9] AGAR J. N. and BOWDEN, F. P.; Proc. Roy. Soc. (A) 1939 **169** 206 [10] COHEN, A.; *Thesis*, Technical Highschool, Zurich, 1938. [11] RUFF, O. and BUSCH, W.; Z. anorg. chem. 1925 **146** 87. [12] JELLINEK, K. and WOLFF, J.; Z. anorg. alleg. chem. 1925 **146** 329. [13] DROSSBACH, P.; *loc. cit.* p. 117. [14] British Patent 586194. [15] British Patent 652227; U.S. Patent 2452914. [16] German Patent 140737/1901. [17] BICHOWSKI and ROSSINI; Thermochemistry of Chemical Substances. Rheinhold, New York 1936. [18] SAUERWALD, F.; Z. anorg. chem. 1949 **258** (3) 296; (5) 306. [19] POTVIN, R. and FARNHAM, G. S.; Trans. Canad. Inst. Min. Met. 1946 **49** 516. [20] British Patent 652224: U.S. Patent 2497529. [21] NEUMANN, B. and RICHTER, H.; Z. Elektrochem. 1925 **31** 287. [22] CAMBI, L. and DEVOTO, G.; Giorn. Chim. ind. applic. 1927 **8** 303. [23] RINCK, E.; Annales de Chim., 10th Series 1932 **18** 395. [24] JELLINEK, K. and WOLFF, J.; Z. anorg. alleg. Chem. 1925 **146** 329. [25] JELLINEK, K. and CZERWINKI, J.; Z. Phys. Chem. 1924 **110** 192. [26] JELLINEK, K. and CZERWINKI, J.; Z. anorg. alleg. chem. 1924 **139** 233. [27] JELLINEK, K. and TOMOFF, G.; Z. phys. Chem. 1924 **111** 234. [28] ENGELHARDT, V.; Handbuch der Technischen Elektrochemie. Leipzig, 1934 **3** 100. [29] KROLL, W. J.; Metal Ind. 1948 **73** 265. [30] EMLEY, E. F.; Ph. D. *Thesis* 1950 (London). [31] TREADWELL, W. D., AMMANN, A. and ZÜRRER, I.; Helv. Chim, Acta 1936 **19** 1255. [32] LORENZ, R.; Z. anorg. alleg. chem. 1929 **183** 81. [33] ZHURIN, A. I.; Trans. Len. Inst. Sect. Met. 1940 (4) 6074. [34] GROTHE, H. and SAVELSBERG, W.; Z. Elektrochem. 1940 **46** (6) 336. [35] BECKE, A.; Technology of Magnesium and its Alloys (F. A. Hughes) p. 317. London 1940. [36] MARANDE, R. F.; Materials and Methods 1946 **23** 418. [37] British Patent 652235; U.S. Patent 2497540. [38] TROMBE, F. and MAHN, F.; Annal de Chimie, 11th Series, 1944 **19** 345. [39] FOX, F. A.; J. Inst. Metals 1946 **73** (4) 223. [40] PLOTNIKOV, V. A. and KERICHENKO E. I.; Mem. Inst. Chem. Ukrain, Acad. Sci. 1939 **6** (1) 3. [41] HAISSINSKY, M.; J. Chem. Soc. 1950 (Sup. 2) S.241. [42] RICHARDSON, F. D. and JEFFES, J. H. E.; J. Iron and Steel Inst. 1948 **160** (3) 261. [43] OSBORN,

C. J.; Trans. Amer. Inst. Min. Met. Eng. 1950 **188** 600. [44] KELLOGG, H. H.; J. of Metals 1950 **188** (6) 862. [45] BREWER, L., BROMLEY, L. A., GILLES, P. W. and LOFGREN, N. L.; The Chemistry and Metallurgy of Miscellaneous Materials: Thermodynamics. McGraw Hill, New York and London 1950. [46] FROST, P. D$_1$, JACKSON, J. H., LOONAM, A. C. and LORIG, C. H.; Trans. A.I.M.E. 1950 **188** 1171. [47] BOCKRIS, J. O'M., KITCHENER, J. A., IGNATOWICZ, S. and TOMLINSON, J. W.; Discuss. Farad. Soc., 1948 (4) 265. [48] SACKUR, O.; Z. Phys. Chem. 1912 **78** 550. [49] LEWIS, G. N. and RANDALL, M.; Thermodynamics. McGraw Hill, New York 1923, p. 219. [50] EMLEY, E. F.; J. Inst. Metals 1949 **75** (6) 431. [51] EMLEY, E. F.; J. Inst. Metals 1948/49 **75** (13) 1113. [52] KRAUSE, I. K. and BERGMANN, H. E.; Compt. rend. Acad. Sci. U.R.S.S. 1942 **35** (1) 20. [53] RUFF, O. and BUSCH, W.; Z. anorg. Chem. 1925 **146** 87. [54] VILLA, H.; J. Soc. Chem. Ind. 1950 **69** (Sup. 1) S9. [55] KELLOGG, H. H.; Trans. A.I.M.E. 1951 **191** 139. [56] WENNER, R. W.; Thermochemical Calculations. McGraw Hill, New York 1941. [57] TREADWELL, W. D. and MAUDERLI, B.; Helv. Chim. Acta 1944 **27** 567. [58] GLASSTONE, S.; Textbook of Physical Chemistry, p. 141. Macmillan, London 1943. [59] WESTRUM, E. F. and PITZER, K. S.; J. Amer. Chem. Soc. 1949 **71** 1940. [60] GROSS, P.; Discuss. Faraday Soc. 1948 (4) 213. [61] British Patent 597206. [62] TODD, S. S.; J. Amer. Chem. Soc. 1949 **71** 4115; **72** 2914. [63] LATIMER, W. M.; J. Amer. Chem. Soc. 1921 **43** 818. [64] SMITHELLS, C. J.; Metals Reference Book. Butterworth, London 1949. [65] CLUSIUS, K., GOLDMAN, J. and PERLICK, A.; Z. Naturforsch. 1949 **4a** 424. [66] WEST, E. G.; Quarterly Trans. Inst. Welding 1940 **3** (2) 93. [67] KAYE, G. W. C. and LABY, T. H.; Tables of Physical and Chemical Constants. London 1948. [68] International Critical Tables. McGraw Hill, New York and London 1928 **4** 63. [69] BOMMER, H. and HOHMANN, E.; Z. anorg. Chem. 1941 **248** 373. [70] ZIMM, B. H. and MAYER, J. E.; J. Chem. Phys. 1944 **12** 362. [71] KELLEY, K. K.; Bull. U.S. Bur. Mines, 1941 No. 434. [72] KELLEY, K. K. and MOORE, G. E.; J. Amer. Chem. Soc. 1943 **65** 1264. [73] ROTH and BÜCHNER; Z. Elektrochem. 1934 **40** 89. [74] KELLEY, K. K.; Bull U. S. Bur. Mines, XI Entropy of Inorg. substances (1948). [75] MOORE, G. E.; J. Amer. Chem. Soc. 1943 **65** 1701. [76] EYRING, L. and WESTRUM, E. F.; J. Amer. Chem. Soc. 1950 **72** 5555. [77] JOHNSTONE, H. L. and BAUER, T. W.; J. Amer. Chem. Soc. 1951 **73** 1119. [78] OSBORN, C. J., Trans. AIME 1950 **188** 1388.

VOL. 1 1952